Aus dem Institut für Transfusionsmedizin
der Medizinischen Fakultät Charité – Universitätsmedizin Berlin

DISSERTATION

Hemoglobin-Based Oxygen Carriers:
in vitro Hemocompatibility and Functionality

zur Erlangung des akademischen Grades

Doctor rerum medicinalium (Dr. rer. medic.)

vorgelegt der Medizinischen Fakultät
Charité – Universitätsmedizin Berlin

von

Kathrin Smuda

aus Berlin

Datum der Promotion: 26. Juni 2022

Content

Content

Abstract (German)

Hämoglobinmikropartikel (HbMP) stellen als künstliche Sauerstoffträger eine vielversprechende Alternative zur allogenen Bluttransfusion dar. Die hantelförmigen HbMP haben eine typische Größe von etwa 700 nm in der Längsachse und 400 nm in der Querachse. Für die Zulassung klinischer Studien ist es jedoch notwendig sowohl ihre physikalischen Eigenschaften als auch ihre Funktion, Pharmakokinetik und Toxizität zunächst *in vitro* zu charakterisieren. Von essenzieller Bedeutung für eine Anwendung der Suspensionen der HbMP als Blutersatzstoff sind überdies Untersuchungen zur Hämokompatibilität.

Im Rahmen der Arbeit wurden durch Ko-Präzipitation, Vernetzung und Auflösung (co-precipitation-crosslinking-dissolution, CCD) HbMP mit unterschiedlichen Vernetzern hergestellt, ihre Funktionalität durch spektrale Extinktionsmessungen bestimmt und die Hämokompatibilität untersucht.

Die CCD-Technik erlaubt die Herstellung von Biopolymerpartikeln mit bioaktiven Bestandteilen. Relevante Parameter wie Größe, Form und Einschlusseffizienz können durch die Variation der mineralischen Matrizen und Reagenzien optimiert werden. Nutzt man $MnCl_2$ und Na_2CO_3 für die Präzipitation, weisen die Teilchen eine Hantelform auf und die Effizienz des Proteineinbaus erreicht nahezu 100 %. Hyaluronsäure hat keinen Einfluss auf die erreichte Einschlusseffizienz von Hämoglobin. Das Verfahren zur funktionellen Charakterisierung der HbMP basiert auf spektralen Extinktionsmessungen im Wellenlängenbereich von etwa 300 nm bis 850 nm. Der angegebene Wellenlängenbereich schließt die Absorptionsbanden der verschiedenen Hämoglobinvarianten von oxygeniertem bzw. deoxygeniertem Hämoglobin und Methämoglobin ein, so dass diese bei bekannter HbMP-Konzentration quantifiziert werden können.

HbMP, die mit oxidiertem Dextran als Vernetzer hergestellt wurden, weisen eine gute Hämokompatibilität auf, so dass dieser Ansatz auch zukünftig verfolgt werden sollte. Als Methoden wurden dabei Tests zur Bestimmung der Hämolyse und der Plättchenaktivierung verwendet. Außerdem wurde ein indirekter Phagozytosetest entwickelt, um die Auswirkungen auf die angeborene Immunantwort zu ermitteln.

Abstract (English)

Hemoglobin microparticles (HbMP) present a promising alternative for allogenic blood transfusions. The peanut shaped HbMP show an average size of about 400 nm x 700 nm. However, it is necessary to thoroughly characterize such artificial blood substitute for clinical approval. Physical properties of HbMP must be determined. The HbMP must be investigated *in vitro* regarding their function, pharmacokinetics and toxicity. Additionally, it is essential to evaluate the hemocompatibility of the particles.

In this study, HbMP were fabricated by the co-precipitation, crosslinking and dissolution (CCD) technique using two different crosslinking agents. The functionality was determined by spectral extinction measurements and hemocompatibility was investigated.

The CCD technique allows the fabrication of biopolymer particles with bioactive components. Relevant parameter – such as size, shape and entrapment efficiency – were optimized by varying the minerals used as templates. Particles prepared with $MnCl_2$ and Na_2CO_3 exhibit a protein entrapment efficiency of nearly 100 %. Hyaluronic acid could not influence entrapment efficiency, morphology and size of HbMP.

The procedure to investigate the functionality of HbMP is based on spectral extinction measurements between 300 nm and 850 nm. The optical setup features a white light source collimated to obtain a low divergence. In contrast to commercial devices, this setup allows rapid measurements within 10 s and the detection of collimated spectral transmittance under defined conditions. The observed wavelength range includes absorption bands for the important hemoglobin variants necessary to determine the functionality of the particles. Due to the differences of the three absorption bands of oxygenated and deoxygenated hemoglobin as well as methemoglobin, the quantities of these three variants are accessible at a known HbMP concentration. Hence, the functionality of the particles was determined.

A modified CCD technique using oxidized dextran as crosslinker was applied to fabricate HbMP with a good hemocompatibility, which was investigated by testing hemolysis and platelet activation. An indirect phagocytosis test was established in order to determine the innate immunological response to HbMP.

Introduction

Transfusions of blood cells, mainly erythrocytes and platelets, are among the most frequently performed therapies in the clinic. Annually, more than 80 million units of red blood cells are transfused worldwide [1] showing an increasing tendency. However, blood transfusions include several risks and limitations. Standards are principally high and compliance is extremely important. A particular high health hazard arises from mismatched transfusions and transmissible diseases [2]. Furthermore, the logistics of blood products are highly demanding as storage time and temperature must be respected. In addition, there are always shortages due to a lack of donors. Obviously, this represents the need for an artificial blood substitute which is able to carry and release oxygen.

Research in transfusion medicine focuses on the search for such an artificial blood substitute for more than three decades. Hemoglobin-based oxygen carriers (HBOC) present a very promising candidate [3]. However, to ensure patients' health safety, the requirements for clinical applications are high. Free hemoglobin (Hb) cannot be administered as it leads to strong vasoconstriction and hypertension [4]. Therefore, research concentrates on modified hemoglobin such as intra- or intermolecular crosslinking or encapsulation of hemoglobin. Diaspirin crosslinked hemoglobin (DCHb) or polymerized bovine hemoglobin seemed promising. However, pulmonary hypertension and cardiac depression were observed in surgical patients in clinical trials [5]. A low oxygen binding affinity might have led to an oxygen oversupply [6]. The described side effects might have been caused by scavenging of nitric oxide (NO). Stroma-free hemoglobin is able to pass the endothelial gaps of the capillary walls and bind NO. However, homeostatic vascular function is maintained by the bioavailability of NO. It controls direct and indirect vasodilation and has anti-thrombotic, anti-inflammatory and anti-proliferative effects [7]. Consequences of NO scavenging can be vasoconstriction, thrombosis, inflammation, vascular hypertrophy and stenosis. Thus, the size requirements for HBOC are above 100 nm so penetration of endothelial gaps is disabled [8]. Moreover, HBOC should not initiate an immune response. To avoid the innate immune response by phagocytes, HBOC must be smaller than 1 μm [9] suggesting size requirements in the submicron range.

One method describes the encapsulation of hemoglobin into liposomes [3]. Another promising approach are hemoglobin microparticles (HbMP) fabricated by co-precipitation,

crosslinking and dissolution (CCD) [8,10,11]. Inorganic salts like manganese chloride ($MnCl_2$) and sodium carbonate (Na_2CO_3) are able to entrap proteins such as hemoglobin during precipitation. The hemoglobin containing template is covered with human serum albumin (HSA) for stabilization and surface adsorption. Glutaraldehyde is used to subsequently crosslink hemoglobin and HSA molecules. Template dissolution with ethylenediaminetetraacetic acid (EDTA) results in HbMP. The average length of the long axis is about 700 nm showing a narrow size distribution and a peanut-shaped morphology. These particles bind and release oxygen [10] and do not initiate platelet activation and aggregation. Immunogenicity is low and no vasoconstriction on afferent arterioles of mouse kidney glomeruli could be observed [11].

Moreover, the CCD technique can be further modified by replacing the crosslinker glutaraldehyde by a macromolecular crosslinker like periodate-oxidized dextran (Odex, with a molecular weight of 40 kDa and 70 kDa). Hence, the co-precipitation and crosslinking step can be combined. Consequently, Odex and proteins were incorporated into the $MnCO_3$ template. Dissolution of the inorganic template by EDTA leads to deformable hemoglobin microparticles (HbMP) in the submicron range. An entrapment efficiency of 60 % to 70 % was observed. HbMP show an average size between 800 and 1000 nm, a uniform morphology and negative zeta-potential [12].

Extensive characterizations regarding toxicology and biocompatibility are required prior animal testing and (pre-)clinical studies. Additionally, the physical, physicochemical and morphological properties must be determined and functionality must be ensured. The relative and total amounts of the methemoglobin (metHb), oxygenated hemoglobin (oxyHb), deoxygenated hemoglobin (deoxyHb) need to be verified. Furthermore, the ability to bind and release oxygen and the corresponding kinetics are crucial factors.

The aim of this study was to investigate the functionality and hemocompatibility of HbMP as candidate for an artificial blood substitute.

This thesis presents the fabrication and characterization of HBOC prepared by the classical CCD technique. The produced particles were characterized regarding their functionality and methemoglobin content. Standardized photometric measurements applied in medical laboratories cannot be used to determine the amounts of metHb, oxyHb and deoxyHb as light scattering has disturbing effects inhibiting quantitative analysis. Furthermore, oxygen release measurements are time consuming, only reveal

the quantity of oxyHb and give only indirect access to the content of non-functional hemoglobin. Presently, the content of deoxyHb cannot be determined. For the characterization of the HbMP, an optical setup for spectral extinction measurements was developed. Both, the divergence of the incident light beam and the solid angle used for observation, are well characterized allowing analysis of the spectral extinction of the HbMP applying Mie theory. For validation of the optical setup and the analysis of the measurements by Mie theory, polystyrene microspheres were examined. In addition, we investigated oxygenated erythrocytes to derive their complex refractive index, which is associated with the intracellular oxyHb concentration [13]. In this way, the method allows the determination of the important hemoglobin variants necessary to verify the functionality of the particles.

Furthermore, hemocompatibility of HbMP was investigated detecting hemolysis rate and the impact on platelet activation. An indirect test was developed to investigate phagocytosis rates.

Materials and Methods

Materials

The following tables provide information about substances, materials and instruments.

Table 1: Substances and supplier

Substance	Abbreviation	Supplier
acetated Ringer's solution	RAc	Serumwerk Bernburg AG, Bernburg, Germany
Alexa Fluor® 488 anti-human CD62P (P-Selectin)		BioLegend, San Diego, USA
alkaline haematin D-575	AHD reagent	Sigma-Aldrich, Munich, Germany
APC anti-human CD42b (GPIbα)		BioLegend, San Diego, USA
arachidonic acid	AA	möLab GmbH, Langenfeld, Germany
argon 5.0	Ar	Linde GmbH, Pullach Germany
BD Vacutainer 0.129 M Na_3-Citrate		Becton & Dickinson GmbH, Heidelberg, Germany
BD Vacutainer 17 IU/mL LiHeparin		Becton & Dickinson GmbH, Heidelberg, Germany
bovine hemoglobin	Hb	hypertonic hemolysis [14]
bovine whole blood		Biophyll GmbH, Dietersburg, Germany
collagen	Coll	möLab GmbH, Langenfeld, Germany
dextran from *Leuconostoc mesenteroides*, 40 kDa, 70 kDa		AppliChem GmbH, Darmstadt, Germany
epinephrine	Epi	möLab GmbH, Langenfeld, Germany
ethylenediaminetetraacetic acid	EDTA	Fluka, Seelze, Germany
glutaraldehyde	GA	Sigma-Aldrich, Munich, Germany
human serum albumin solution, 20 %	HSA	Grifols Deutschland GmbH, Frankfurt am Main, Germany
manganese chloride tetrahydrate	$MnCl_2$	Sigma-Aldrich, Munich, Germany
meta periodate		Sigma-Aldrich, Munich, Germany
Phagoburst™		Glycotope GmbH, Berlin, Germany
Phagotest™		Glycotope GmbH, Berlin, Germany
phosphate-buffered saline pH 7.4	PBS	Sigma-Aldrich, Munich, Germany
poly-L-ornithine	PLO	Sigma-Aldrich, Munich, Germany
potassium ferricyanide	$K_3[Fe(CN)_6]$	Sigma-Aldrich, Munich, Germany

Pronase		Sigma-Aldrich Chemie GmbH, Munich, Germany
sodium carbonate	Na_2CO_3	Sigma-Aldrich, Munich, Germany
sodium chloride solution, sterile, 0.9 %	NaCl	Fresenius Kabi Deutschland GmbH, Bad Homburg, Germany
sodium dithionite	$Na_2S_2O_4$	Fluka, Seelze, Germany
sodium hydroxide	NaOH	Carl Roth, Karlsruhe, Germany
sodium nitrite	$NaNO_2$	Sigma-Aldrich, Munich, Germany
water, Ampuwa, sterile	H_2O	Fresenius Kabi Deutschland GmbH, Bad Homburg, Germany

Table 2: Instruments and suppliers

Instrument	Supplier
ABX Micros 60 haematology analyser	HORIBA Europe GmbH, Potsdam, Germany
BD FACS Canto™ II Flowcytometer	Becton & Dickinson GmbH, Heidelberg, Germany
BD FACS Canto™ II Flowcytometer	Becton & Dickinson GmbH, Heidelberg, Germany
Cary 5000i spectrophotometer	Agilent Technologies, Waldbronn, Germany
Cytation™ 3 Cell Imaging Multi-Mode Reader	BioTek Instruments GmbH, Bad Friedrichshall, Germany
inverted microscope	Carl Zeiss Microscopy GmbH, Oberkochen, Germany
Leo Supra 35 VP microscope	Carl Zeiss Microscopy GmbH, Oberkochen, Germany
LSM 510 meta	Carl Zeiss Microscopy GmbH, Jena, Germany
Maya2000 Pro spectrometer with xenon light source HPX-2000	Ocean Optics, Incorparated, Dunedin, Florida, USA
NanoWizard 4 microscope	JPK BioAFM, Bruker Nano GmbH, Berlin, Germany
oxygen meter Microx 4 with microsensor NTH-PSt7	PreSens–Precision Sensing GmbH, Regensburg, Germany
PowerWave 340	BioTek Instruments GmbH, Bad Friedrichshall, Germany

Methods

Preparation of HbMP

Fresh bovine whole blood was provided by Biophyll GmbH (Dietersburg, Germany). Hemoglobin used for the production of the hemoglobin microparticles particles (HbMP) was prepared by hypertonic hemolysis [14].

HbMP were prepared by the classical CCD technique as previously described [11]. The production scheme of HbMP is visualized in Figure 1.
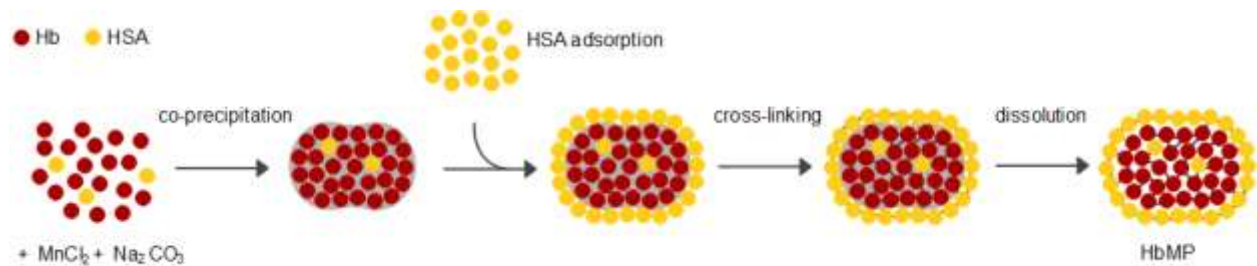

Figure 1: Production process of HbMP, modified from [15]

Briefly, bovine hemoglobin ($2.5 - 15$ mg mL^{-1}) was entrapped by co-precipitation of 0.25 M manganese chloride ($MnCl_2$) or Calcium chloride ($CaCl_2$) and 0.25 M sodium carbonate (Na_2CO_3). Subsequently, the raw particles are covered with human serum albumin (HSA). Hemoglobin and albumin molecules were crosslinked by glutaraldehyde with a final concentration of 0.04 %. Dissolution of the salt template by 0.18 M EDTA results in the final HbMP. Prepared HbMP suspensions were stored in Ringer's acetate (RAc) under sterile conditions at 4 °C in aliquots of 15 mL. For storage, the packed particle volume (PPV) was 19.9 %. Sample collection for the various measurements was taken under sterile conditions.

Furthermore, protein particles crosslinked with oxidized dextran (Odex) were prepared as previously described [16]. Briefly, dextran was oxidized by periodate. Subsequently, double aldehyde groups were formed. These groups are able to react with amino groups. Odex can therefore be used as crosslinker for biopolymers.

The CCD technique was modified to co-precipitate and crosslink in one step. Solution A (consisting of $MnCl_2$ and hemoglobin) was rapidly mixed with solution B (consisting of Na_2CO_3 and Odex) resulting in Odex-crosslinked hemoglobin microparticles (odex-

HbMP). Subsequently, HSA was added for surface adsorption. $MnCO_3$ template was dissolved by EDTA. Lastly, the odex-HbMP were washed and stored in a sterile physiological sodium chloride solution.

Preparation of oxyHbMP, deoxyHbMP and metHbMP

For verification of experimental data, three variations of HbMP were prepared and analyzed. HbMP exposed to air are saturated with oxygen and therefore identified as oxygenated HbMP (oxyHbMP). Suspensions containing deoxygenated hemoglobin were identified as deoxyHbMP. DeoxyHbMP were either prepared with 2 mg mL^{-1} sodium dithionite ($Na_2S_2O_4$) or by flushing with argon. 10 mM $NaNO_2$ was used to prepare HbMP containing methemoglobin (metHbMP).

Entrapment efficiency

To obtain entrapment efficiency (EE), hemoglobin concentrations were detected in the supernatant after co-precipitation and after each washing step (PAf). The difference of the hemoglobin amount applied (PAt) and the hemoglobin amount in the supernatants was determined. EE % was calculated as follows:

$$EE\,\% = \frac{(PAt - PAf) \cdot 100}{PAt} \quad [15].$$

A microplate reader (PowerWave 340) was used to measure hemoglobin concentrations (Wavelength 415 nm).

Morphology

To compare morphology and size of the particles, confocal laser scanning microscopy (CLSM) was used.

The influence of the fabrication procedure on morphology and size of the particles was observed by a confocal microscope LSM 510 meta equipped with a 100 fold oil-immersion objective with a numerical aperture of 1.3 in transmission mode.

In order to reveal the morphology of the particles with higher resolution, further microscopic analyses were carried out by scanning electron microscopy (SEM) and atomic force microscopy (AFM).

A Leo supra 35 VP microscope was used for scanning electron microscopy. A pre-diluted HbMP suspension (PPV of 2 %) was rigorously mixed with a tube roller for 5 minutes and

subsequently treated in an ultrasonic bath at 35 kHz and 130 kHz for 15 minutes and 5 minutes, respectively. HbMP were pipetted on a plate and left for drying overnight. Thereafter, the samples were sputtered with platinum leading to a platinum layer of 2 nm. An Inlens SE detector operated at an acceleration voltage of 5 kV with a working distance of 5.2 mm was used to record scanning electron micrographs of the dried samples.

AFM images of HbMP in suspension were obtained by a NanoWizard 4 instrument, mounted on an inverted microscope. To allow proper adhesion of HbMP, the microscopic slides were coated by 2 mg mL^{-1} poly-L-ornithine (PLO). HbMP suspension was rigorously mixed and diluted with RAc (1:500). 50 µL of the diluted sample were pipetted on a coated slide and incubated in a humid chamber for particle adhesion. Atomic force micrographs were obtained with 10 nm spatial resolution and a USC 0.3 cantilever with a spring constant of 0.61 N m^{-1}.

Hemoglobin determination

Total hemoglobin

AHD method was used to determine the total hemoglobin concentration [17,18]. A HbMP aliquot was rigorously vortexed for 10 minutes to homogenize the suspension. As hemoglobin and albumin molecules are crosslinked and therefore entrapped, the particles were enzymatically digested to completely degrade the HbMP. Pronase solution (10 mg mL^{-1}) and HbMP suspension with a 1:1 mass ratio were incubated for 30 minutes at 50 °C. The resulting hemoglobin solution was diluted in series with volume fractions between 0.116 and 0.215 for absorption measurements using a Cary 5000i spectrophotometer. An additional dilution series containing Pronase solution only served as reference solution. The reference samples were filled in an identical quartz cuvette and positioned in the reference beam of the spectrophotometer. Thus, the contribution of the digested HbMP is represented by the absorption spectra. The spectral absorbance $A(\lambda)$ at 574 nm is determined for the different dilutions φ_i and the mass concentration can be calculated according to

$$\beta_{\mathrm{Hb}}^{sus} = \frac{A(\lambda)\, M\big(\mathrm{Hb(Fe)}\big)}{\ell\; \varepsilon(\lambda)\; \varphi_i} \quad [19].$$

The molar mass $M\big(Hb(Fe)\big)$ of the monomeric $Hb(Fe)$ is 16114.5 g mol^{-1}, the absorption lengths of the quartz cuvette was d = 10 mm and the molar extinction coefficient is $\varepsilon\,(\lambda=574nm)$ = 6945 L mol^{-1} cm^{-1} [19]. The total hemoglobin concentration was defined as

the weighted average of the different dilutions. The procedure was repeated several times at various days to estimate the uncertainty.

Spectral extinction measurements

A previously developed optical setup was used for the measurement of collimated transmittance spectra to quantify oxyHb, deoxyHb and metHb in the HbMP [13].
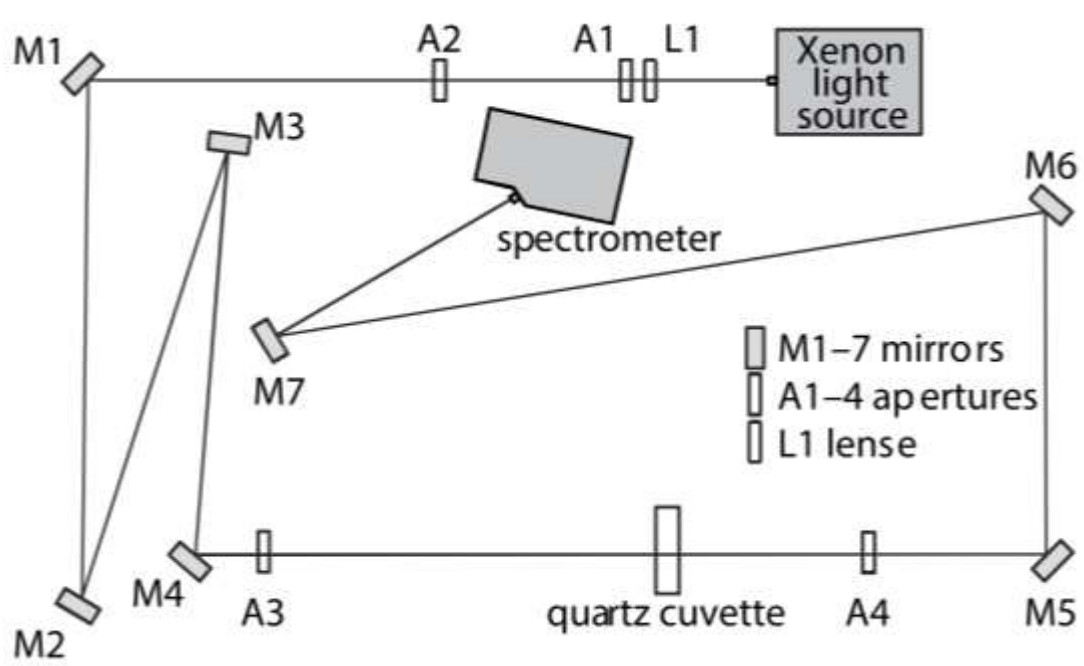

Figure 2: Optical setup to measure collimated transmittance spectra. Light path length was increased with mirrors. Divergence of the incident and detected beams were kept low by apertures [13].

Spectral extinction measurements were carried out as described before [19]. Briefly, oxyHbMP or metHbMP suspensions were diluted in water (1:100). A quartz cuvette was positioned in the holder of the optical setup. 2.2 mL of water were filled into cuvette. Volumes between 10 µL and 670 µL of the pre-diluted HbMP suspension were pipetted and mixed by carefully pipetting up and down. Dilutions were chosen to gain transmittances ranging from T (300 nm) $\approx$ 92 % and T (800 nm) > 99.5 % for the lowest volume fraction to T (300 nm) = 1.6 % and T (800 nm) > 65 % for the highest volume fraction (670 µL sample). Argon was flushed through the suspension with T (800 nm) $\approx$ 65 % for an hour to purge oxygen from hemoglobin to obtain deoxyHbMP. Flushing was stopped for recording the measurement. For re-oxygenation, the

suspension was flushed with air for a minute. The flushing was stopped prior recording the spectra.

In this approach, calculations are independent from particle concentrations. The packed particles volume (PPV) was determined with a higher accuracy than particle concentration which differed widely in dependence on the method applied. PPV was 19.9 % [19]. Moreover, the mean particle size has a little impact [19]. Furthermore, there is a negligible influence on the extinction spectra due to the non-spherical shape of HbMP [20].

Oxygen release experiments

A ferricyanide-induced release of hemoglobin-bound oxygen [21,22] was used to determine the mass concentration of functional, i.e. oxyHb, in HbMP. The chemically released oxygen of the three different HbMP suspensions (oxyHbMP, deoxyHbMP, metHbMP) was measured by a miniaturized optical needle type NTH-PSt7 oxygen microsensor which was connected to a Microx 4 oxygen meter. 1 mL of HbMP suspensions was left for equilibration for 10 minutes under stirring to allow oxygen saturation. Subsequently, up to 100 µL of 10 % ferricyanide ($K_3[Fe(CN)_6]$) were added to induce oxygen release. The concentration change of dissolved oxygen with an acquisition rate of one data point per second was detected until a stable value was reached. Aqua destillata served as control where no oxygen release could be detected. A hemoglobin concentration dependent change in pO_2 was observed. It is assumed that all released oxygen was previously bound to hemoglobin. Hence, the difference of final and initial pO_2 corresponds to the amount of previously bound oxygen. A standard curve for hemoglobin concentration versus change of pO_2 was generated and used to obtain the mass concentration of functional hemoglobin in the HbMP. The same procedure was used to determine the mass concentration of functional hemoglobin in different HbMP (oxyHbMP, deoxyHbMP, metHbMP).

Hemocompatibility

For hemocompatibility assays, venous blood was collected from healthy volunteers. Blood withdrawal was carried out according to the transfusion law of Germany. The ethics committee of Charité – Universitätsmedizin Berlin (# EA1/137/14) approved the use of donor blood samples for scientific purposes. All assays were carried out within two hours

after blood collection. Odex-crosslinked particles consisting of pure HSA served as control and were compared with odex-HbMP.

Hemolysis

Hemolysis describes the release of hemoglobin from damaged erythrocytes. Hemolysis rate of any artificial blood substitute must be as low as possible. Three individual hemolytic tests were performed as previously described [16]. Briefly, human heparinized erythrocytes were washed and mixed with odex-HbMP mimicking a blood exchange rate of 50 %. Water served as positive control, whereas phosphate-buffered saline (PBS) served as negative control. After 3 hours of incubation at 37 °C, samples were centrifuged and the supernatant was collected. Absorbance was measured at 545 nm by a Cytation™ 3 microplate reader. Hemolysis rate was calculated as follows:

$$hemolytic\ rate\ [\%] = \frac{OD_{sample} - OD_{NC}}{OD_{PC} - OD_{NC}} \cdot 100 \quad [16].$$

Mean ± SD [23] values were calculated whereas the value of the positive control was regarded as 100 % hemolysis [16].

Phagocytosis

Odex-HbMP exhibit no fluorescence disabling the use of the commercially available Phagotest™. Therefore, phagocytosis rates of granulocytes and monocytes were determined by an indirect phagotest which allows the detection of phagocytic activity for non-fluorescent particles in heparinized whole blood. All components are taken from the Phagoburst™ and Phagotest™. 50 µL of whole blood were used to pre-fed the phagocytes with 10 µL of $2 \cdot 10^{11}$ mL^{-1} odex-HbMP at 37 °C for 0, 10, 30, 60 and 120 minutes. 10 µL of $2 \cdot 10^9$ mL^{-1} non-fluorescent *Escherichia coli* (*E. coli*) and PBS, respectively, served as positive and negative control. Subsequently, 10 µL of $2 \cdot 10^9$ mL^{-1} fluorescein isothiocyanate (FITC) labelled *E. coli* were pipetted to each sample and incubated at 37 °C for further 10 minutes. After quenching non-phagocyted bacteria, erythrocytes were lysed, leucocytes fixed and the nuclei stained with propidium iodide. All samples were measured within 30 minutes with a BD FACS Canto II™. The higher the phagocytosis (saturation) rate of non-fluorescent particles, the lower is the phagocytosis rate of FITC-*E. coli*. Thus, a high phagocytosis rate of FITC-*E. coli* indicates a low phagocytic activity to the non-fluorescent bacteria or particles.

Platelet activation

The impact of odex-HbMP on the activation and aggregation of human platelets was determined in platelet rich plasma (PRP). Therefore, PRP was prepared from citrated human whole blood by centrifugation at room temperature at 150 g for 15 minutes. Platelet concentration was detected by a hematology analyzer ABX Micros 60. PRP (45 µL) and particles (5 µL) were carefully mixed with a platelet to particle ratio of 1:10 and incubated at 37 °C for 30 minutes under gentle agitation. PBS served as negative control. After this pre-incubation step, arachidonic acid (0.5 mg mL^{-1}), collagen (0.2 mg mL^{-1}) and epinephrine (0.01 mM) where added to initiate platelet activation and aggregation. After a further incubation for 30 minutes at 37 °C, platelets were fixed with formaldehyde (0.5 % in PBS). All platelets were labelled with APC anti-human CD42b (GPIbα) antibody whereas activated platelets were stained with Alexa Fluor® 488 anti-human CD62P (P-Selectin) antibody. This allows the distinction between resting (single stained) and activated (double stained) platelets [24,25]. All samples were measured within 30 minutes with a BD FACS Canto II™.

Results

Entrapment efficiency

Entrapment efficiency (EE) depends on the initial hemoglobin concentration and on the salts used to form the template. Hemoglobin EE was between 13 % and 38 % when $CaCl_2$ and Na_2CO_3 were used to form the template whereas co-precipitation with $MnCl_2$ and Na_2CO_3 led to an EE of 54 % and 99.6 %. The absolute entrapped amount of hemoglobin (in gram per mol carbonate) depended on the initial hemoglobin concentration. The higher the initial hemoglobin concentration the more hemoglobin was captured in the particles. However, the use of $MnCl_2$ was much more effective regarding EE [15].

Morphology and size

Figure 3 A-C shows that the mixing speed during co-precipitation has a clear impact on size and shape when $CaCl_2$ and Na_2CO_3 were used to form the template.
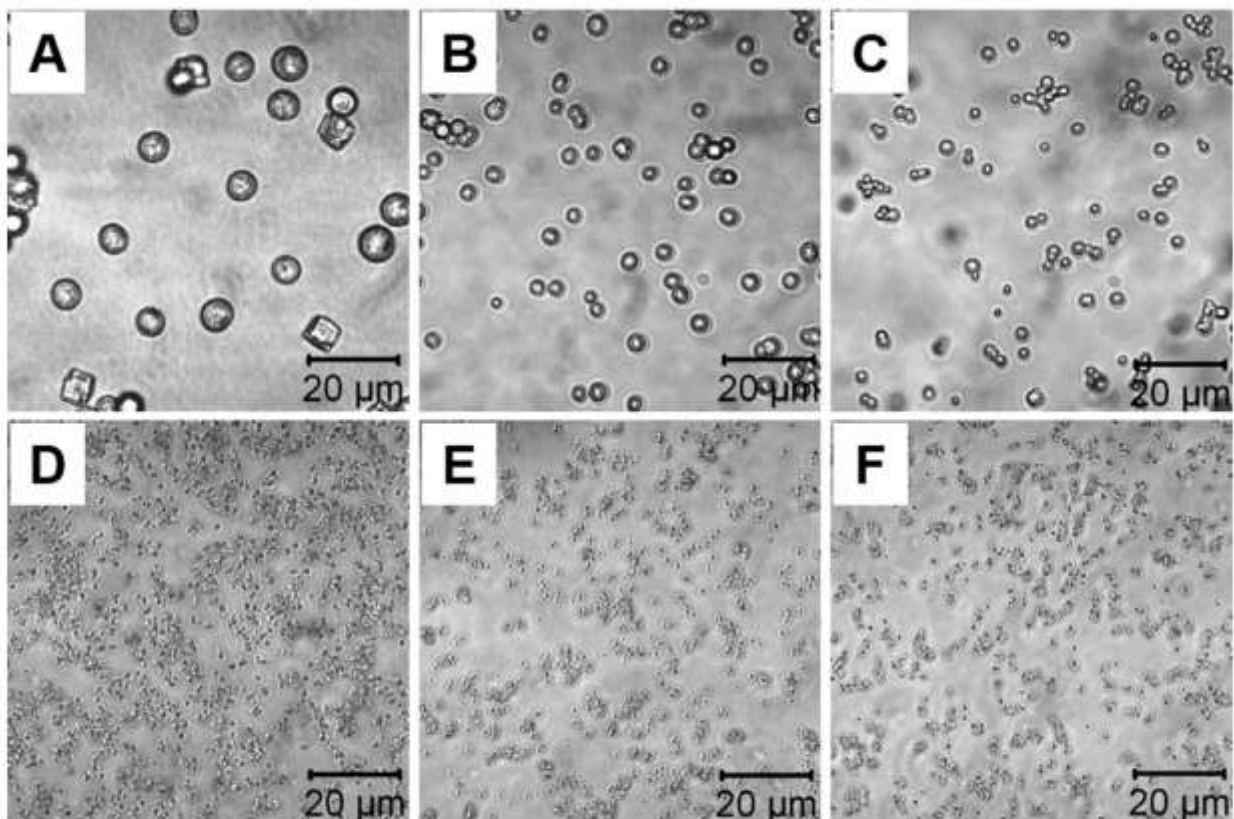

Figure 3: CLSM images of HbMP co-precipitated with $CaCl_2$ and Na_2CO_3 (A-C) and $MnCl_2$ and Na_2CO_3 (D-F). Stirring speed in rounds per minute (rpm) during precipitation increases from left to right: 200 rpm (A, D), 400 rpm (B, E) and 600 rpm (C, F) [15].

Particle size decreases with increasing stirring speed. The micrographs show a size between 2 and 10 µm (Figure 3 A-C). In contrast, the particles templated by $MnCl_2$ and Na_2CO_3 reveal a constant size in the submicron range and narrow size distribution independent from the stirring speed during co-precipitation (Figure 3 D-F). Further fabrications used a stirring speed of 600 rpm [15].

After detailed investigations comparing and varying mineral templates, additives and preparation conditions such as the mixing speed, further characterizations focused on the particles based on $MnCl_2$ and Na_2CO_3 and are consequently declared as HbMP.

Further SEM and AFM reveal the morphology and structure of the particles. The micrographs show their peanut like shape.

SEM images in Figure 4 show a particle length of approximately 800 nm and a width of about 400 nm. Additionally, the fine structures of the surface in the range of 20 nm to 30 nm are clearly visible.
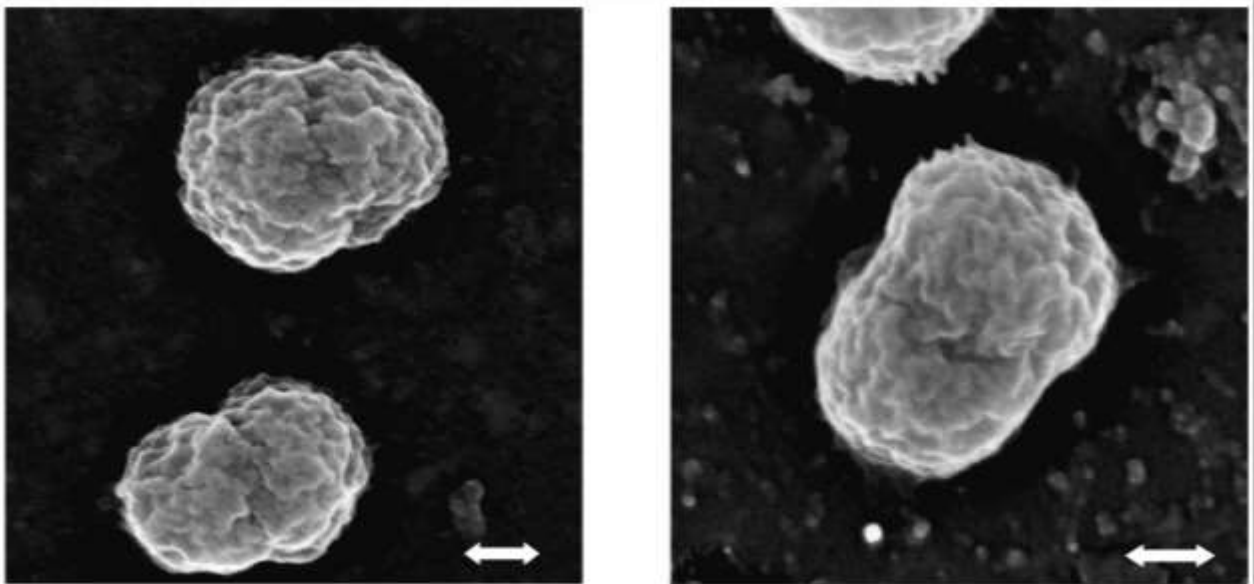

Figure 4: SEM images of HbMP. The scale arrows are 200 nm. [19]

Atomic force micrographs in Figure 5 are encoded in false colors depicting HbMP in two different orientations. The particle in Figure 5a was fixed with its long axis parallel to the slide. Whereas the particle in Figure 5b oriented perpendicular to the surface of the microscopic slide. The height scale on the right indicates a particle height of

approximately 450 nm (Figure 5a) and 950 nm (Figure 5b), respectively. In Figure 5a an artefact (brownish) due to interactions of the cantilever at the border of the particle can be seen.
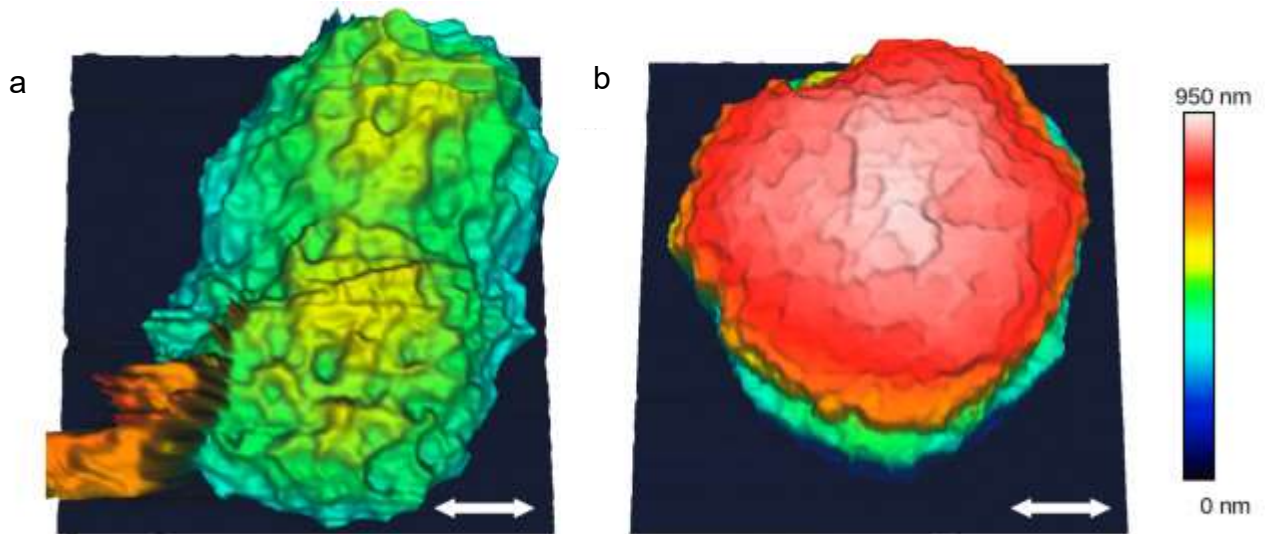

Figure 5: AFM images. Scale arrows are 200 nm. Height scale on the right for size determination. [19]

In principle, microscopy reveals the size of the particles. Due to the poor statistic and preparation involved, the data may not be representative. Alternatively, dynamic light scattering (DLS) and analytical centrifugation (AC) were used yielding ensemble values for the particle size and size distribution. However, it is well known that particle size determination in the range from 10 nm to 1000 nm is complex [26] and method specific differences are observed. HbMP present a non-spherical and polydisperse suspension being sensitive to method specific differences. Elastic properties, porosity and orientation of the HbMP will further affect the determination of size and size distribution. Therefore, the results depend on the method applied. The median particle diameter and the relative distribution width differ for DLS and AC measurements. As previously shown the median diameter derived from DLS is 760 nm ± 54 nm. The median diameter derived from AC is 996 nm ± 26 nm [19]. The method specific effects are more evident in AC measurements. Hence, DLS results are used for further calculations and analysis of spectral extinction measurements.

Functionality of HbMP

Determination of functional hemoglobin and methemoglobin

An optical setup was developed to measure the collimated transmittance spectra of different HbMP suspensions [13]. Calculations revealed the percentage of functional hemoglobin in HbMP with a PPV of 19.9 % [19]. Oxygen release measurements as well as x-ray fluorescence measurements were used to validate the derived data.

The following Figure 6 shows simulations and experimental results of spectral extinction measurements. HbMP suspensions completely converted to metHbMP served as control. The simulated curve for 100 % metHbMP is in agreement with the curve derived from experimental data and was used for calibration [19]. The measured spectra are in accordance to simulations for a metHb fraction of 35 % and an oxyHb fraction of 65 % (Figure 6a). Calculated extinction spectra for various metHb fractions are compared to measured extinction spectra for oxyHbMP (Figure 6b). $\overline{C}_{ext}(\lambda)/\overline{V}$ represents the volume-specific extinction cross section.
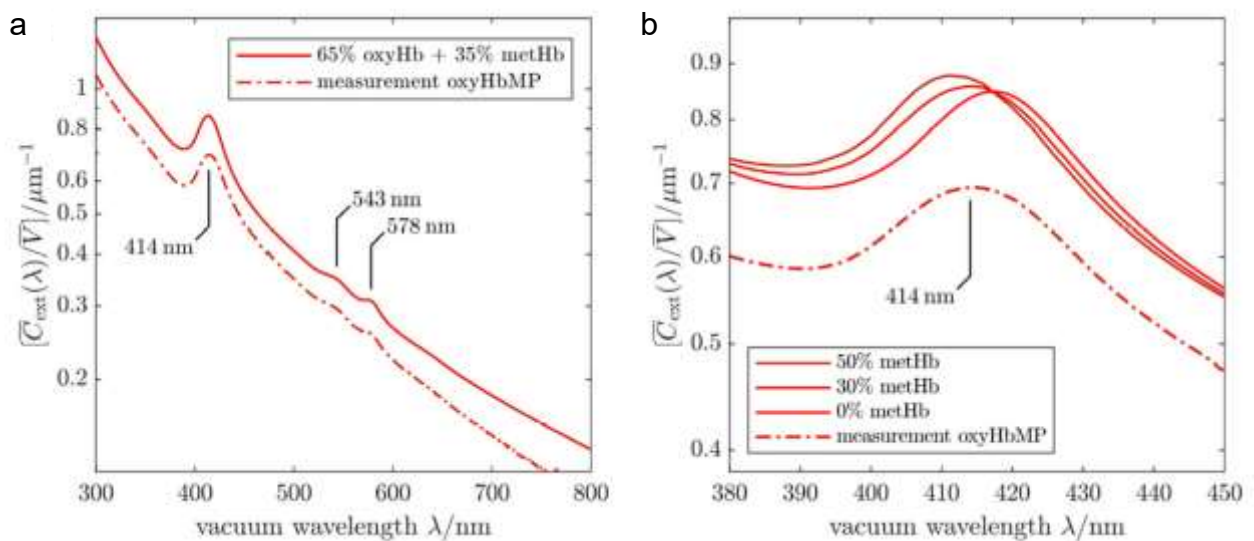

Figure 6: Spectral extinction measurements and simulations. (a) Measurement of volume-specific spectral extinction cross section $(\overline{C}_{ext}(\lambda)/\overline{V})$ for oxyHbMP (dot-dashed red line) and calculations (red line) using a 35 % fraction of metHb and 65 % fraction of oxyHb. (b) Measured spectral cross section in the Soret band compared with simulations of cross sections for various metHb fractions. [19]

Additionally, as demonstrated by the results depicted in Figure 7, HbMP are able to carry and release oxygen.
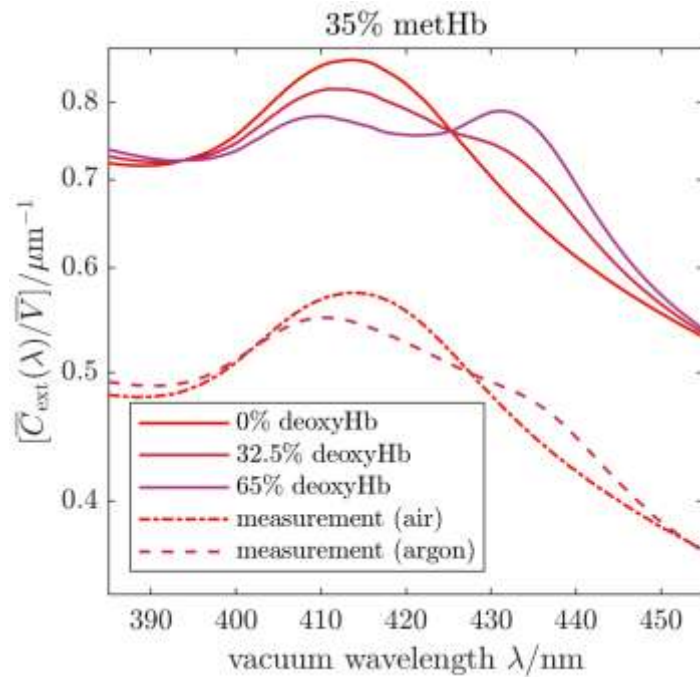
Figure 7: Measured volume-specific spectral extinction cross sections $\left(\overline{C}_{ext}(\lambda)/\overline{V}\right)$ of oxyHbMP (air, dash-dotted) and deoxyHbMP (argon, dashed) compared to calculated volume-specific spectral extinction cross sections (solid lines). [19]

Argon was used to deoxygenate hemoglobin in oxyHbMP. Figure 7 shows measured volume-specific spectral extinction measurements for oxyHbMP (dash-dotted line) and for deoxyHbMP (dashed line). The Soret band characteristic for oxyHb can be seen as well as an absorbance signal at about 430 nm attributed to deoxyHb. To illustrate the change from oxygenation to deoxygenation, calculated volume-specific spectral extinction measurements for different oxygenation states are included. MetHb content was kept at 35 % for these calculations. The measurement corresponds best to a deoxygenation of 32.5 % indicating that half of the oxygenated hemoglobin could be deoxygenated by argon. Deoxygenation by argon is challenging and time-consuming. Therefore, only partial deoxygenation could be achieved.

Different HbMP suspensions were investigated and different methods were compared (Table 3). Suspensions exposed to air and therefore saturated with oxygen are regarded as oxygenated HbMP (oxyHbMP). MetHbMP suspensions are prepared by treatment with sodium nitrite ($NaNO_2$). Deoxygenated HbMP (deoxyHbMP) were prepared by treatment with sodium dithionite ($Na_2S_2O_4$). Mass and relative concentrations of functional hemoglobin in different HbMP suspensions (19.9 % PPV) are listed in the table below.

Results

Table 3 shows an overview of the results obtained by different methods applied to determine the functionality and metHb content of HbMP.

Table 3: Mass and relative concentrations of functional Hb and relative concentrations of metHb in different HbMP suspensions. * X-ray fluorescence measurements are sensitive to Fe(II) and Fe(III) but not deoxygenated hemoglobin.** Value was set to 100 % for validation. [19]

| | Mass concentration of functional Hb | Relative concentration of non-functional Hb / metHb | | |
Method	Oxygen release	Oxygen release	Spectral extinction measurement	X-ray fluorescence
	g L^{-1}	%	%	%
oxyHbMP	11.8 ± 0.7	54 ± 3	35 ± 5	35 ± 5
deoxyHbMP	4.8 ± 0.9	81 ± 3	-*	-*
metHbMP	2.8 ± 0.4	89 ± 1	100 **	100 **

Spectrophotometric absorbance measurements were carried out to determine total hemoglobin concentration. After enzymatic digestion, the alkaline haematin and detergent (AHD) conversion procedure revealed a total hemoglobin concentration of 25.5 ± 0.5 g L^{-1} [17–19]. Hemoglobin concentration in the supernatant was 2.0 ± 0.2 g L^{-1} [19].

Oxygen release measurements provide absolute values for functional hemoglobin. Due to the measured total hemoglobin concentration, total mass and relative oxyHb concentrations are available. Mass concentration of functional hemoglobin for oxyHb measured by oxygen release was 11.8 ± 0.7 g L^{-1}. Concentrations of 4.8 ± 0.9 g L^{-1} and 2.8 ± 0.4 g L^{-1} could be observed for deoxyHbMP and metHbMP, respectively, implying that hemoglobin was not converted completely into deoxygenated hemoglobin and methemoglobin, respectively. Relative values for non-functional hemoglobin are indirectly available from oxygen release measurements and total hemoglobin determination revealing a fraction of 54 ± 3 % of non-functional hemoglobin, presumably methemoglobin [19].

Values for metHb are directly accessible from spectral extinction and x-ray fluorescence measurements. Both methods are in agreement revealing a content of methemoglobin in

HbMP of 35 ± 5 %. MetHbMP suspensions were used to validate spectral extinction and x-ray fluorescence measurements.

The oxygen release measurements reveal a significantly larger concentration of the non-functional hemoglobin. Non-functional hemoglobin might not only be methemoglobin. The discrepancy can also be explained by an impeded confirmation change of hemoglobin when immobilized in the salt matrix and crosslinked. This might lead to an increased time constant for oxygen binding and release. In contrast, the optical method allows the distinction between metHb and oxyHb due to different refractive indices. On the other hand, X-ray spectroscopy is sensitive against Fe(II) and Fe(III).

Hemocompatibility of odex-HbMP

Hemolysis

Hemolysis describes the release of hemoglobin from erythrocytes caused by a damaged cell membrane. The biosafety of artificial blood substitutes can be determined, among other things, by the hemolytic rate which should be less than 5 %. Hemolytic rates of different odex-HbMP were determined. PBS and water served as negative and positive control. The hemolytic rates were between 1 % and 2 % meaning that there is no significant damage caused to the cell membrane when whole blood is incubated with odex-HbMP [16].

Phagocytosis

Phagocytosis rates of granulocytes and monocytes can be determined in heparinized human whole blood with the commercially available Phagotest™. However, to directly detect phagocytic granulocytes and monocytes, ingested bacteria or particles must be fluorescently labelled. As odex-HbMP do not show any fluorescence [16], an indirect assay was developed. Therefore, phagocytes were pre-fed with different odex-HbMP, non-fluorescent bacteria (positive control) and PBS (negative control) for 10 to 120 minutes to reach maximum phagocytic saturation. Subsequently, FITC-labelled bacteria were fed to the phagocytes. This step allows the uptake of FITC-labelled bacteria by those granulocytes and monocytes which did not ingest the non-labelled particles. High phagocytosis rates of FITC-labelled bacteria indicate low phagocytosis rates of non-fluorescent particles.

Figure 8 shows time dependent results from the indirect phagotest. Phagocytosis rates of human granulocytes (Figure 8a) and monocytes (Figure 8b) for odex-HbMP, non-labelled *E. coli* and PBS for a time span of 10 to 120 minutes are shown.

Phagocytes pre-incubated with non-labelled *E coli* (solid squares) are mainly saturated leading to a reduced uptake of labelled *E. coli*. Phagocytes pre-incubated with the negative control (PBS, solid circles) and all types of odex-HbMP (triangle, inversed triangle, diamond, hexagon) show a high phagocytosis rate of labelled *E. coli* suggesting that there was no phagocytic activity during pre-incubation [16].
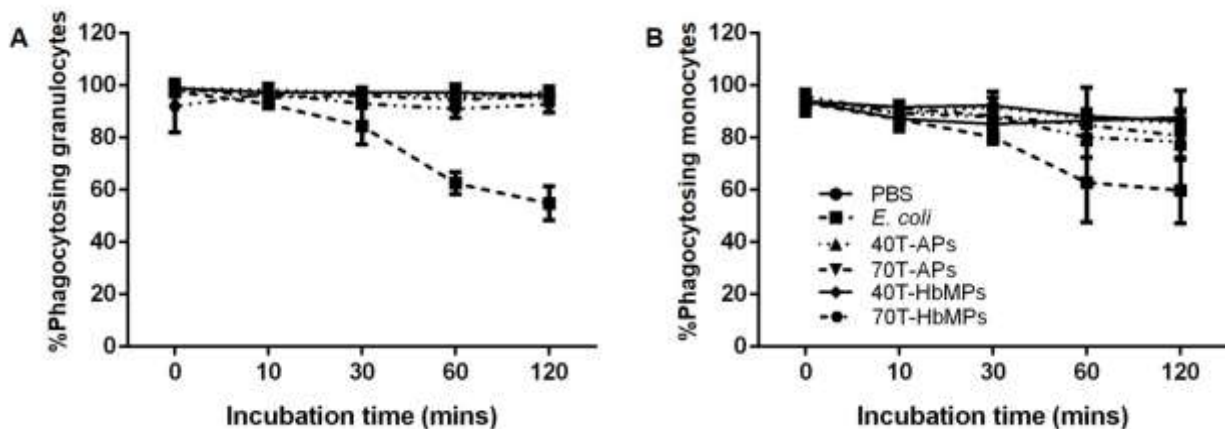

Figure 8: Indirect phagotest. Time dependent phagocytosis rates of human (a) granulocytes and (b) monocytes for odex-HbMP*, non-labelled *E. coli* and PBS. The longer phagocytes are pre-incubated with non-labelled *E. coli*, the less phagocytosis of labelled *E. coli* could be observed. In contrast, duration of pre-incubation has no impact on the phagocytosis rates of odex-HbMP and PBS. Here, constantly high phagocytosis rates of labelled *E. coli* could be observed. Mean ± SD is presented (n = 3). [16]

*40T-APs and 70T-APs indicate Odex-crosslinked particles consisting of HSA. 40T-HbMPs and 70T-HbMPs indicate Odex-crosslinked particles consisting of hemoglobin and HSA. 40T and 70T (40 kDa and 70 kDa, respectively) refer to the molecular weight of dextran used to prepare Odex.

Platelet activation

A platelet activation assay was used to evaluate the impact of odex-HbMP on the homeostatic system. Therefore, platelet rich plasma was incubated with odex-HbMP and PBS (negative control). Subsequently, activation ability by different agonists was determined by selective antibodies and flowcytometric analysis. CD42b (GPIbα) is a surface protein present on all platelets. APC anti-human CD42b (GPIbα) antibodies bind to all platelets whereas Alexa Fluor® 488 anti-human CD62P (P-Selectin) antibodies specifically bind to activated platelets only as CD62P (P-Selectin) is only expressed by

activated platelets. Thus, inactive platelets can be distinguished from activated platelets. The percentage of activated platelets could therefore be calculated. Platelet to particle ratio was 1:10. A sample set without particles served as control.

Figure 9 presents an overview of the platelet activation assay. All types of odex-HbMP do not activate platelets. Activation rates of platelets in the presence and absence of odex-HbMP are identical. The presence of different odex-HbMP does not interfere with the process of platelet activation leading to the assumption that the particles will not have any negative impact on the hemostasis system [16].
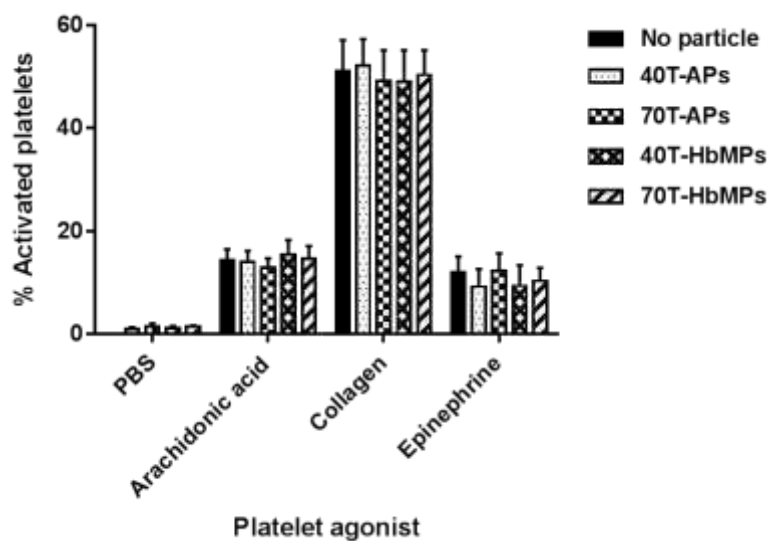

Figure 9: Impact of odex-HbMP on platelet activation by different agonists. Mean ± SD is presented (n = 3). [16]

*40T-APs and 70T-APs indicate Odex-crosslinked particles consisting of HSA. 40T-HbMPs and 70T-HbMPs indicate Odex-crosslinked particles consisting of hemoglobin and HSA. 40T and 70T refer to the molecular weight of dextran (40 kDa and 70 kDa, respectively) used to prepare Odex.

Discussion

The CCD technique is of special interest as it allows the fabrication of particles consisting of a variety of biopolymers (including proteins) in an easy manner. Size, morphology and entrapment efficiency are controllable and adjustable by the choice of inorganic salts and preparational conditions [8,10,11,15].

Particles consisting of hemoglobin present an interesting research subject as they are suitable as artificial blood substitute.

The simple CCD technique allows the fabrication of HbMP. HbMP fabricated with $MnCl_2$ and Na_2CO_3 reveal robust particles in a nearly uniform peanut shape in the submicron size range. The strong affinity of Mn^{2+} to proteins leads to a high entrapment efficiency.

Blood substitute candidates must be characterized extensively regarding their haemoglobin composition, function, pharmacokinetics, toxicity and hemocompatibility. However, a standard cyanomethemoglobin method to determine the metHb content uses a highly toxic agent disabling routine measurements [27]. Additionally, the characterization regarding haemoglobin composition and functionality is problematic due to the scattering of particles. Commercial devices which are presently available are not suited since the contribution of light scattering to the measured extinction cannot be quantified.

Spectral extinction measurements allow the determination of the functionality of HbMP. The developed optical layout offers a fast and robust method to monitor and optimize the production process of microparticles and sub-microparticles. Relative concentrations of oxyHb, deoxyHb as well as metHb are directly accessible. Appropriate dilutions ensure that multiple scattering signals are negligible. In our investigated samples, values of approximately 65 % oxyHb and 35 % metHb were obtained. X-ray fluorescence measurements were applied to validate the ratio of oxyHb and metHb and confirmed these findings. However, x-ray fluorescence measurements are very complex and demanding. The operation and data analysis require trained specialists. X-ray fluorescence instruments are not part of routine laboratories, whereas the optical setup is easily accessible and can be built quickly. Its operation and data analysis are easy and robust.

Hitherto, documentation of deoxygenation was achieved by irreversibly converting oxyHbMP chemically into deoxyHbMP [8,10,11]. Spectral extinction measurements allow to investigate the reversible deoxygenation process in the HbMP. Here, it could be shown that roughly the half of oxyHb can be converted to deoxyHb by flushing with argon. The partial pressure to achieve 50 % saturation (p50) of hemoglobin in erythrocytes is much higher than for hemoglobin in HbMP [11] indicating that oxygen affinity in HbMP is much higher as in erythrocytes. Furthermore, diffusion of oxygen and argon, respectively, is slower. These factors influence the deoxygenation process.

Furthermore, spectral extinction measurements exhibit a significant advantage towards oxygen release measurements. Procedures to chemically release oxygen from hemoglobin are time consuming and do not allow the distinction between hemoglobin in the particles and the surrounding media. Moreover, it is a method that needs the detection of total hemoglobin to reveal the ratio of functional and non-functional hemoglobin. Concentrations of non-functional hemoglobin (presumably methemoglobin) are only indirectly accessible.

Here, spectral extinction measurements were used to specify the function of HbMP prepared by the classical CCD technique. However, this method is also available for other HBOC.

Additionally, the spectral extinction measurements will be further modified and improved by the addition of a flow-through system containing a gas exchanger. Kinetic studies as well as reversible oxygenation and deoxygenation studies could be used for quality control for hemoglobin-based oxygen carriers.

Moreover, the biosafety of potential artificial blood substitutes must be evaluated prior animal testing and (pre-)clinical studies. It is central to rule out any interaction with blood cells and to determine the hemocompatibility of the particles. Hemolysis assays revealed a hemolytic rate less than 2 % suggesting that the particles do not cause disruption to the erythrocyte membrane. Therefore, no release of hemoglobin into the plasma is expected. Any innate or adaptive immune response must be avoided to inhibit clearance by the immune system. An indirect phagocytosis assay showed no change regarding the phagocytic activity of granulocytes and monocytes after incubation with odex-HbMP for up to two hours. Glutaraldehyde-crosslinked HbMP were investigated with a direct phagocytosis assay after fluorescence labelling with FITC. Low phagocytosis rates of

3 – 5 % were measured. However, FITC-labelling is influencing the innate immune response of phagocytes and a direct comparison is not possible. It is expected that both types of HbMP will not be recognized and cleared by phagocyting cells. Furthermore, odex-HbMP and HbMP do not initiate platelet activation and aggregation. Additionally, the presence of odex-HbMP does not alter the agonist mediated platelet activation.

Future research will focus on a more thorough characterization and detailed comparison of HbMP and odex-HbMP. As previously described, both candidates – HbMP and odex-HbMP – meet crucial criteria for an artificial blood substitute. In conclusion, HbMP as well as odex-HbMP exhibit a very good hemocompatibility and represent a highly promising carrier for medical use.

References

1. Carson JL, Grossman BJ, Kleinman S, Tinmouth AT, Marques MB, Fung MK, Holcomb JB, Illoh O, Kaplan LJ, Katz LM, Rao S V., Roback JD, Shander A, Tobian AAR, Weinstein R, McLaughlin LGS, Djulbegovic B. Red blood cell transfusion: A Clinical practice guideline from the AABB. Annals of Internal Medicine. 2012. 10.7326/0003-4819-157-1-201206190-00429

2. Klein HG. How safe is blood, really? Biologicals. 2010; 10.1016/j.biologicals.2009.10.008

3. Sen Gupta A. Hemoglobin-based oxygen carriers: Current state-of-the-art and novel molecules. Shock. 2019. 10.1097/SHK.0000000000001009

4. Thompson A, McGarry AE, Valeri CR, Lieberthal W. Stroma-free hemoglobin increases blood pressure and GFR in the hypotensive rat: role of nitric oxide. J Appl Physiol [Internet]. 1994;77(5):2348–54.

5. Chen JY, Scerbo M, Kramer G. A review of blood substitutes: Examining the history, clinical trial results, and ethics of hemoglobin-based oxygen carriers [Internet]. Vol. 64, Clinics. Clinics (Sao Paulo); 2009. p. 803–13. 10.1590/S1807-59322009000800016

6. Winslow RM. Current status of blood substitute research: Towards a new paradigm. In: Journal of Internal Medicine. 2003. 10.1046/j.1365-2796.2003.01150.x

7. Ignarro LJ, Buga GM, Wood KS, Byrns RE, Chaudhuri G. Endothelium-derived relaxing factor produced and released from artery and vein is nitric oxide. Proc Natl Acad Sci U S A [Internet]. 1987;84(24):9265–9. 10.1073/pnas.84.24.9265

8. Bäumler H, Xiong Y, Liu ZZ, Patzak A, Georgieva R. Novel hemoglobin particles-promising new-generation hemoglobin-based oxygen carriers. Artif Organs. 2014; 10.1111/aor.12331

9. Montel L, Pinon L, Fattaccioli J. A Multiparametric and High-Throughput Assay to Quantify the Influence of Target Size on Phagocytosis. Biophys J [Internet]. 2019 Aug 6;117(3):408–19. 10.1016/j.bpj.2019.06.021

10. Xiong Y, Steffen A, Andreas K, Müller S, Sternberg N, Georgieva R, Bäumler H. Hemoglobin-based oxygen carrier microparticles: Synthesis, properties, and in vitro and in vivo investigations. Biomacromolecules. 2012;13(10):3292–300. 10.1021/bm301085x

11. Xiong Y, Liu ZZ, Georgieva R, Smuda K, Steffen A, Sendeski M, Voigt A, Patzak A, Bäumler H. Nonvasoconstrictive hemoglobin particles as oxygen carriers. ACS Nano. 2013;7(9):7454–61. 10.1021/nn402073n

12. Kloypan C, Prapan A, Suwannasom N, Chaiwaree S, Kaewprayoon W, Steffen A, Xiong Y, Baisaeng N, Georgieva R, Bäumler H. Improved oxygen storage capacity of haemoglobin submicron particles by one-pot formulation. Artif Cells,

Nanomedicine Biotechnol. 2018 Nov 12;46(sup3):S964–72. 10.1080/21691401.2018.1521819

13. Gienger J, Smuda K, Müller R, Bär M, Neukammer J. Refractive index of human red blood cells between 290 nm and 1100 nm determined by optical extinction measurements. Sci Rep. 2019; 10.1038/s41598-019-38767-5

14. Haney CR, Buehler PW, Gulati A. Purification and chemical modifications of hemoglobin in developing hemoglobin based oxygen carriers. Adv Drug Deliv Rev. 2000; 10.1016/S0169-409X(99)00047-2

15. Xiong Y, Georgieva R, Steffen A, Smuda K, Bäumler H. Structure and properties of hybrid biopolymer particles fabricated by co-precipitation cross-linking dissolution procedure. J Colloid Interface Sci. 2018; 10.1016/j.jcis.2017.12.030

16. Kloypan C, Suwannasom N, Chaiwaree S, Prapan A, Smuda K, Baisaeng N, Pruß A, Georgieva R, Bäumler H. In-vitro haemocompatibility of dextran-protein submicron particles. Artif Cells, Nanomedicine Biotechnol. 2019; 10.1080/21691401.2018.1548476

17. Zander R, Lang W, Wolf HU. Alkaline haematin D-575, a new tool for the determination of haemoglobin as an alternative to the cyanhaemiglobin method. I. description of the method. Clin Chim Acta. 1984; 10.1016/0009-8981(84)90250-X

18. Wolf HU, Lang W, Zander R. Alkaline haematin D-575, a new tool for the determination of haemoglobin as an alternative to the cyanhaemiglobin method. II. Standardisation of the method using pure chlorohaemin. Clin Chim Acta. 1984; 10.1016/0009-8981(84)90251-1

19. Smuda K, Gienger J, Hönicke P, Neukammer J. Function of Hemoglobin-Based Oxygen Carriers: Determination of Methemoglobin Content by Spectral Extinction Measurements. Int J Mol Sci [Internet]. 2021 Feb 10;22(4):1753. 10.3390/ijms22041753

20. Gienger JC. Determination of optical and geometrical properties of blood cells and microparticles from light scattering measurements. PhD thesis, Tech Univ Berlin, Ger. 2019;

21. Haldane J. The ferricyanide method of determining the oxygen capacity of blood. J Physiol. 1900; 10.1113/jphysiol.1900.sp000797

22. Cook SF. The action of potassium cyanide and potassium ferricyanide on certain respiratory pigments. J Gen Physiol. 1928; 10.1085/jgp.11.4.339

23. Lu M, Zhao C, Wang Q, You G, Wang Y, Deng H, Chen G, Xia S, zhao J, Wang B, Li X, Shao L, Wu Y, Zhao L, Zhou H. Preparation, characterization and in vivo investigation of blood-compatible hemoglobin-loaded nanoparticles as oxygen carriers. Colloids Surfaces B Biointerfaces [Internet]. 2016 Mar 1;139:171–9. 10.1016/j.colsurfb.2015.12.012

24. Braune S, Walter M, Schulze F, Lendlein A, Jung F. Changes in platelet morphology and function during 24 hours of storage. Clin Hemorheol Microcirc [Internet].

2014;58(1):159–70. 10.3233/CH-141876

25. De Cuyper IM, Meinders M, Van De Vijver E, De Korte D, Porcelijn L, De Haas M, Eble JA, Seeger K, Rutella S, Pagliara D, Kuijpers TW, Verhoeven AJ, Van Den Berg TK, Gutíerrez L. A novel flow cytometry-based platelet aggregation assay. Blood [Internet]. 2013 Mar 7;121(10). 10.1182/blood-2012-06-437723

26. Babick F, Mielke J, Wohlleben W, Weigel S, Hodoroaba VD. How reliably can a material be classified as a nanomaterial? Available particle-sizing techniques at work. J Nanoparticle Res [Internet]. 2016 Jun 1;18(6):158. 10.1007/s11051-016-3461-7

27. Zijlstra WG, Buursma A. Spectrophotometry of hemoglobin: Absorption spectra of bovine oxyhemoglobin, deoxyhemoglobin, carboxyhemoglobin, and methemoglobin. Comp Biochem Physiol - B Biochem Mol Biol. 1997; 10.1016/S0305-0491(97)00230-7

Affidavit / Eidesstattliche Versicherung

„Ich, Kathrin Smuda, versichere an Eides statt durch meine eigenhändige Unterschrift, dass ich die vorgelegte Dissertation mit dem Thema: *Hemoglobin-Based Oxygen Carriers:*

in vitro Hemocompatibility and Functionality / Sauerstoffträger auf Hemoglobinbasis: in vitro Hämkompatibilität und Funktionalität selbstständig und ohne nicht offengelegte Hilfe Dritter verfasst und keine anderen als die angegebenen Quellen und Hilfsmittel genutzt habe.

Alle Stellen, die wörtlich oder dem Sinne nach auf Publikationen oder Vorträgen anderer Autoren/innen beruhen, sind als solche in korrekter Zitierung kenntlich gemacht. Die Abschnitte zu Methodik (insbesondere praktische Arbeiten, Laborbestimmungen, statistische Aufarbeitung) und Resultaten (insbesondere Abbildungen, Graphiken und Tabellen) werden von mir verantwortet.

Meine Anteile an etwaigen Publikationen zu dieser Dissertation entsprechen denen, die in der untenstehenden gemeinsamen Erklärung mit dem/der Erstbetreuer/in, angegeben sind. Für sämtliche im Rahmen der Dissertation entstandenen Publikationen wurden die Richtlinien des ICMJE (International Committee of Medical Journal Editors; www.icmje.org) zur Autorenschaft eingehalten. Ich erkläre ferner, dass ich mich zur Einhaltung der Satzung der Charité – Universitätsmedizin Berlin zur Sicherung Guter Wissenschaftlicher Praxis verpflichte.

Weiterhin versichere ich, dass ich diese Dissertation weder in gleicher noch in ähnlicher Form bereits an einer anderen Fakultät eingereicht habe.

Die Bedeutung dieser eidesstattlichen Versicherung und die strafrechtlichen Folgen einer unwahren eidesstattlichen Versicherung (§§156, 161 des Strafgesetzbuches) sind mir bekannt und bewusst.

Datum   Unterschrift

_____   _____

Declaration of contribution to the submitted publications / Anteilserklärung

Publikation 1: Smuda K, Gienger J, Hönicke P, Neukammer, Function of Hemoglobin-Based Oxygen Carriers: Determination of Methemoglobin Content by Spectral Extinction Measurements., International Journal of Molecular Sciences, 2021, IF-5.923 (2020)

Beitrag im Einzelnen: 80 %, Spectral extinction measurements, oxygen release measurements, total hemoglobin determination; analyzed, interpreted the data and performed statistical analysis together with the co-authors, wrote the concept and the final version of the manuscript. (Figure 1, Figure 4, Figure 5, Figure 6, Figure 7, Table 3)

Publikation 2: Kloypan C, Suwannasom N, Chaiwaree S, Prapan A, Smuda K, Baisaeng N, Pruß A, Georgieva R, Bäumler H., In-vitro haemocompatibility of dextran-protein submicron particles., Artificial Cells, Nanomedicine and Biotechnology, 2019, **IF-3.343**

Beitrag im Einzelnen: 15 %, Design, measurements, data analysis (Figure 8, Figure 9)

Publikation 3: Xiong Y, Georgieva R, Steffen A, Smuda K, Bäumler H., Structure and properties of hybrid biopolymer particles fabricated by co-precipitation cross-linking dissolution procedure., Journal of Colloid and Interface Science, 2018, IF-6.361

Beitrag im Einzelnen: 30 %, Fabrication and characterization of particles (Figure 3)

_____

Unterschrift, Datum und Stempel des/der erstbetreuenden Hochschullehrers/in

_____

Unterschrift des Doktoranden/der Doktorandin

Selected Publications / Ausgewählte Publikationen

Smuda K, Gienger J, Hönicke P, Neukammer

Function of Hemoglobin-Based Oxygen Carriers: Determination of Methemoglobin Content by Spectral Extinction Measurements.

J. Int J Mol Sci. 2021 Feb 10;22(4):1753. doi: 10.3390/ijms22041753. PMID: 33578723, **IF-5.923 (2020)**

Kloypan C, Suwannasom N, Chaiwaree S, Prapan A, **Smuda K**, Baisaeng N, Pruß A, Georgieva R, Bäumler H.

In-vitro haemocompatibility of dextran-protein submicron particles.

Artif Cells Nanomed Biotechnol. 2019 Dec;47(1):241-249. Doi:10.1080/21691401.2018.1548476. PMID: 30663396, **IF-3.343**

Xiong Y, Georgieva R, Steffen A, **Smuda K**, Bäumler H.

Structure and properties of hybrid biopolymer particles fabricated by co-precipitation cross-linking dissolution procedure.

J Colloid Interface Sci. 2018 Mar 15;514:156-164. doi: 10.1016/j.jcis.2017.12.030. Epub 2017 Dec 12., **IF-6.361**

Publication 1 / Publikation 1

International Journal of
Molecular Sciences

MDPI

Article

Function of Hemoglobin-Based Oxygen Carriers: Determination of Methemoglobin Content by Spectral Extinction Measurements

Kathrin Smuda [1,2,*], Jonas Gienger [2], Philipp Hönicke [2] and Jörg Neukammer [2,*]

[1] Institute of Transfusion Medicine, Charité-Universitätsmedizin Berlin, 10117 Berlin, Germany
[2] Physikalisch-Technische Bundesanstalt, 10587 Berlin, Germany; jonas.gienger@ptb.de (J.G.); philipp.hoenicke@ptb.de (P.H.)
* Correspondence: kathrin.smuda@charite.de (K.S.); j.neukammer@gmx.net (J.N.)

Abstract: Suspensions of hemoglobin microparticles (HbMPs) are promising tools as oxygen therapeutics. For the approval of clinical studies extensive characterization of these HbMPs with a size of about 750 nm is required regarding physical properties, function, pharmaco-kinetics and toxicology. The standard absorbance measurements in blood gas analyzers require dissolution of red blood cells which does not work for HbMP. Therefore, we have developed a robust and rapid optical method for the quality and functionality control of HbMPs. It allows simultaneous determination of the portion of the two states of hemoglobin oxygenated hemoglobin (oxyHb) and deoxygenated hemoglobin (deoxyHb) as well as the content of methemoglobin (metHb). Based on the measurement of collimated transmission spectra between 300 nm and 800 nm, the average extinction cross section of HbMPs is derived. A numerical method is applied to determine the composition of the HbMPs based on their wavelength-dependent refractive index (RI), which is a superposition of the three different states of Hb. Thus, light-scattering properties, including extinction cross sections can be simulated for different compositions and sizes. By comparison to measured spectra, the relative concentrations of oxyHb, deoxyHb, metHb are accessible. For validation of the optically determined composition of the HbMPs, we used X-ray fluorescence spectrometry for the ratio of Fe(II) (oxyHb/deoxyHb) and Fe(III) (metHb). High accuracy density measurements served to access heme-free proteins, size was determined by dynamic light scattering and analytical centrifugation and the shape of the HbMPs was visualized by electron and atomic force microscopy.

Keywords: hemoglobin-based oxygen carrier; artificial blood substitute; HbMP; methemoglobin determination; spectral extinction; spectral refractive index; sub-micrometer particle characterization; light scattering

check for updates

1. Introduction

Worldwide, about 85 million units of red blood cells are transfused annually [1] and an increasing need for blood is observed. However, the transfusion of red blood cells holds risks and limitations. Mismatched transfusions as well as transmissible infections present a major health hazard [2]. Additionally, the storage time of red blood cells is limited, cold chain principles must be respected and the logistics are highly demanding. Clearly, there is a highly and fast growing demand for an artificial oxygen carrier which is able to carry and deliver oxygen at the sites of need.

The search for an artificial blood substitute based on oxygen carriers has presented a great challenge in transfusion medicine for more than three decades. In the focus of research are hemoglobin-based oxygen carriers (HBOCs) [3]. However, clinical applications of such agents in humans is not yet possible due to several issues which need to be solved to ensure the patients' safety. As free hemoglobin (Hb) induces strong vasoconstriction and

hypertension [4], modified hemoglobin has been intensely investigated. Several modifications were based on intra- or intermolecular cross-linking or encapsulation. Diaspirin cross-linked hemoglobin (DCHb) or polymerized bovine hemoglobin showed potential for surgical patients in clinical trials, but also limitations caused by severe side effects like pulmonary hypertension and cardiac depression [5]. Oxygen oversupply due to low oxygen binding affinity and scavenging of nitric oxide (NO), respectively, might be the reasons [6]. Stroma-free hemoglobin passes the endothelial gaps of the capillary walls leading to nitric oxide binding. The bioavailability of NO is crucial to maintain homeostatic vascular function. It enables direct and indirect vasodilation and can be responsible for anti-thrombotic, anti-inflammatory and anti-proliferative effects [7]. Scavenging of NO can lead to vasoconstriction, thrombosis, inflammation, vascular hypertrophy and stenosis. Therefore, hemoglobin-based oxygen carriers should not be able to penetrate the endothelial gaps requiring that all their dimensions should exceed 100 nm [8]. Furthermore, clearance by phagocytes must be avoided. Hence, the dimensions of particles in a blood substitute must be smaller than 1 µm. It follows that particles in the submicron size range are the most promising approach.

Besides encapsulated Hb, loaded into lipid microvesicles [3], a promising method for fabrication of such hemoglobin particles is the co-precipitation–cross-linking–dissolution technique [8–10]. This method allows the entrapment of hemoglobin by co-precipitation with inorganic salts like manganese chloride ($MnCl_2$) and sodium carbonate (Na_2CO_3) forming the Hb-containing template followed by a coverage with human serum albumin (HSA). Subsequently, hemoglobin and albumin molecules are cross-linked with glutaraldehyde. The dissolution of the template with ethylenediaminetetraacetic acid (EDTA) results in hemoglobin microparticles (HbMPs) with an average diameter of 700 nm with a narrow size distribution and a nearly uniform peanut-shaped morphology. The particles are able to bind and release oxygen. They show a low immunogenicity and no vasoconstrictive effects on afferent arterioles of mouse kidney glomeruli [10].

The approval of HBOCs for animal experiments and (pre-) clinical studies requires, besides investigations of toxicology and biocompatibility, also the characterization of the physical and physicochemical properties of the respective material. Morphological features of the particles, i.e. size, shape, density as well as the methemoglobin (metHb), oxyhemoglobin (oxyHb), deoxyhemoglobin (deoxyHb) amounts and the oxygen binding capacity need to be determined. It is important that these quantities are accessible for quality control by a rapid and reliable method. This demand cannot be met by standard procedures applied in laboratory medicine. In particular, HbMPs cannot be lysed like erythrocytes, photometric measurements are disturbed by light scattering, oxygen release measurements are time consuming and the deoxyHb content cannot be determined at present. To address this gap and to establish a rapid and reliable characterization of suspensions of HbMPs, we apply spectral transmission measurement and data analysis and present results in this paper. Our method, designated as spectral extinction measurement in particle suspensions and analysis (SEMPA) was recently demonstrated to allow the determination of size and refractive index of sphered erythrocytes [11]. By selecting the appropriate model for light scattering, i.e. Lorenz-Mie theory [12] for spherical particles or the T-matrix [13] method for small non-spherical particles with high symmetries, the ensemble averaged spectral extinction cross section of the particles is calculated. This measurand, i.e. the quantity to be measured [14], sensitively depends on the complex refractive index (RI) [15] and hence on the composition of the particles investigated. In our work, we analyze spectral extinction cross sections to determine the content of metHb, oxyHb as well as heme-free globins (Gl)/human serum albumin (HSA) of a specific batch of HbMPs.

For the validation of our spectral extinction measurements, we applied near edge X-ray absorption fine structure (NEXAFS) fluorescence measurements, being sensitive to the ratio of Fe(II) and Fe(III) thus allowing the determination of the relative concentrations of functional sum of oxyHb and deoxyHb and metHb. Alternatively, as demonstrated

recently, the metHb fraction of the total Hb content and the total Hb concentration are accessible by NMR relaxometry [16].

Our investigations were complemented to support the analyses of spectral extinction measurements and interpretation of results. For this purpose, we applied scanning electron microscopy (SEM), atomic force microscopy (AFM), dynamic light scattering (DLS), analytical centrifugation (AC), flow cytometric measurements (FCM), high accuracy density measurement and spectrophotometric determination of the hemoglobin concentration after previous enzymatic digestion. In addition, the packed particle volume (PPV) was determined accounting for the elastic deformability of the HbMP.

The fundamental advantage of our approach is that intact microparticles are analyzed in suspension by extinction measurements. The straightforward access to the essential features of the particle ensemble stands in contrast to presently applied indirect methods. In particular, the ratio of oxyHb/deoxyHb as well as the content of metHb are not accessible by such indirect measurements, but can now be determined by SEMPA, since oxygenation and deoxygenation can be reversibly carried out.

We expect that our method can be used for the quantification of the function of various particles based HBOCs and possibly contribute to the optimization of their fabrication thus facilitating the initiation of pre-clinical studies.

2. Results and Discussion

2.1. Fabrication of Hemoglobin Microparticles

Hemoglobin microparticles particles (HbMPs) were fabricated as described previously [10], a schematic of the production process is illustrated in Figure 1a. Briefly, bovine hemoglobin (10 mg/mL) was entrapped by co-precipitation of 0.25 mol L^{-1} manganese chloride ($MnCl_2$) and 0.25 mol L^{-1} sodium carbonate (Na_2CO_3) and the resulting particles are covered with human serum albumin (HSA). Hemoglobin and albumin molecules were cross-linked by glutaraldehyde with a final concentration of 0.04%, and the salt templates were dissolved by 0.18 mol L^{-1} EDTA resulting in the final HbMPs.
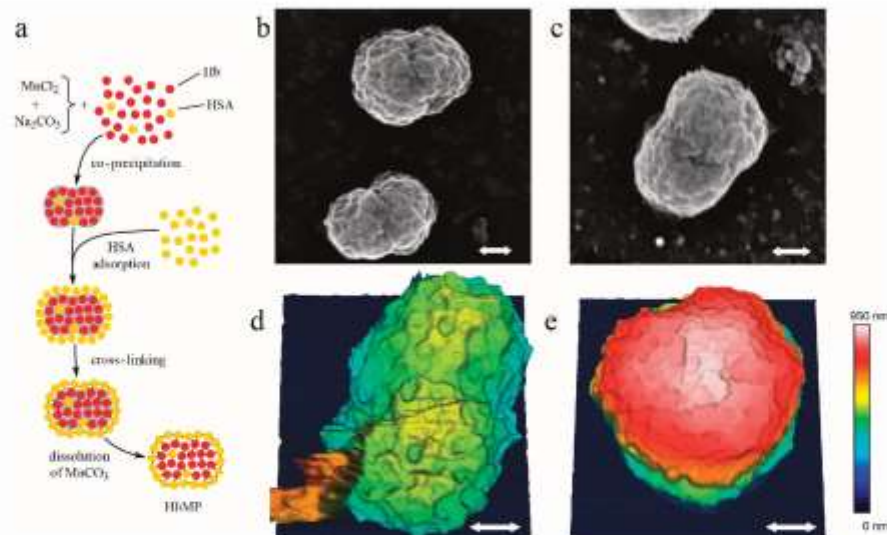
Figure 1. (a) Production scheme of HbMPs by co-precipitation and cross linking. (b,c) Images of HbMPs taken by scanning electron microscopy. (d,e) Atomic force microscopy of HbMPs attached with two different orientations to the surface. The white arrows correspond to a length of 200 nm in each image.

2.2. Morphology of Hemoglobin Microparticles

To obtain access to the shape of the particles and to estimate the size, we applied scanning electron microscopy (SEM) and atomic force microscopy (AFM). As is evident from Figure 1b–e the particles exhibit a non-spherical, peanut like shape with a ratio between the short and long axes of approximately 1:1.5. Inspection of SEM and AFM images yields a range between 600 nm and 1100 nm for the long axis of the particles. Our observations show that the size of the particles derived from SEM is smaller compared to AFM, which is explained by the different preparation procedures. For SEM, the samples must be dried and the particles are covered by a thin platinum layer. Hence, due to dehumidification shrinking of the HbMPs might be induced [17]. On the other hand, AFM images are taken in solution approximately matching the biological environment for the intended application. The particles in Figure 1d,e, imaged by AFM, were oriented differently, one with its long axis parallel (Figure 1d) and the other with the particle's long axis upright (Figure 1e) with respect to the surface. Due to their different orientation, the maximum heights (encoded in false colors) of the particles relative to the surface, are approximately 600 nm and 900 nm, respectively. In SEM and AFM images, the waist of the particles is visible. Furthermore, both methods reveal the fine structure of the surface, which is associated with the $MnCO_3$ scaffold used to incorporate the proteins and which is finally removed when producing the HbMPs.

2.3. Optical Determination of metHb in Hemoglobin Microparticles

To measure collimated transmittance spectra of diluted HbMP suspensions, we used a dedicated optical setup [11] (Figure S1), described in more detail in the Materials and Methods section. Regular spectrophotometers are intended for purely absorbing samples but unsuitable for the quantitative analysis of light-scattering samples. In contrast, our setup allows the quantitative determination of the spectral extinction cross section of the HbMPs in suspension, since unwanted contributions from light scattered in non-forward directions are negligible due to the small divergence of the incident light beam and a low angle of detection for the transmitted light.

We derived from the measured spectral transmittance $T(\lambda)$ of the particle ensemble the average spectral extinction cross section $\overline{C}_{ext}(\lambda)$ according to:

$$\overline{C}_{ext}(\lambda) = \frac{-1}{\ell \, C_0 \, \varphi} \ln T(\lambda) \qquad (1)$$

where C_0 denotes the concentration of HbMPs in the stock suspension, φ the volume fraction of the stock suspension in the measurement suspension and ℓ the absorption length of the cuvette.

In order to avoid the influence of large uncertainties associated with the direct flow cytometric measurement of the concentration C_0 and the values derived from particle size and the packed particle volume (PPV) (see Section 2.5. Physical Properties of HbMPs), for quantitative comparison we consider the quantity:

$$Z(\lambda) = \frac{\overline{C}_{ext}(\lambda)}{\overline{V}} = \frac{-1}{\ell \, PPV \, \varphi} \ln T(\lambda) \qquad (2)$$

being the volume-specific extinction cross section (VSECS). The symbol $\overline{V}$ is the mean volume of the HbMPs and PPV, i.e. packed particle volume denotes the solid fraction of particles in the stock solution. The advantage of our approach is that the PPV is known to higher accuracy than the particle concentration in the stock suspension. Furthermore, compared to $\overline{C}_{ext}(\lambda)$, $Z(\lambda)$ changes only moderately with the mean particle size (Figures S2 and S3), while being equally sensitive to the relative Hb composition.

Experimental results and calculated extinction spectra are compared for three differently treated samples: (a) exposed to air and hence saturated with oxygen, (b) treated with sodium nitrite ($NaNO_2$) to convert all Hb components to metHb and (c) purged with argon

to obtain deoxygenated Hb. These preparations are referred to in Figure 2 and in the following as (a) oxyHbMP and (b) metHbMP. The case (c) is shown in Figure 3 as "measurement (argon)". Calculations are based on the Lorenz-Mie theory [12,15] taking into account the known optical properties of the individual proteins in the HbMPs (see Section 3.6. Model for optical properties). Lorenz-Mie theory refers to the exact mathematical solution for the scattering and absorption of light by a homogeneous spherical particle. Its use is justified here because the influence of the HbMPs' non-spherical shape on the extinction spectra was proven to be negligible [18].
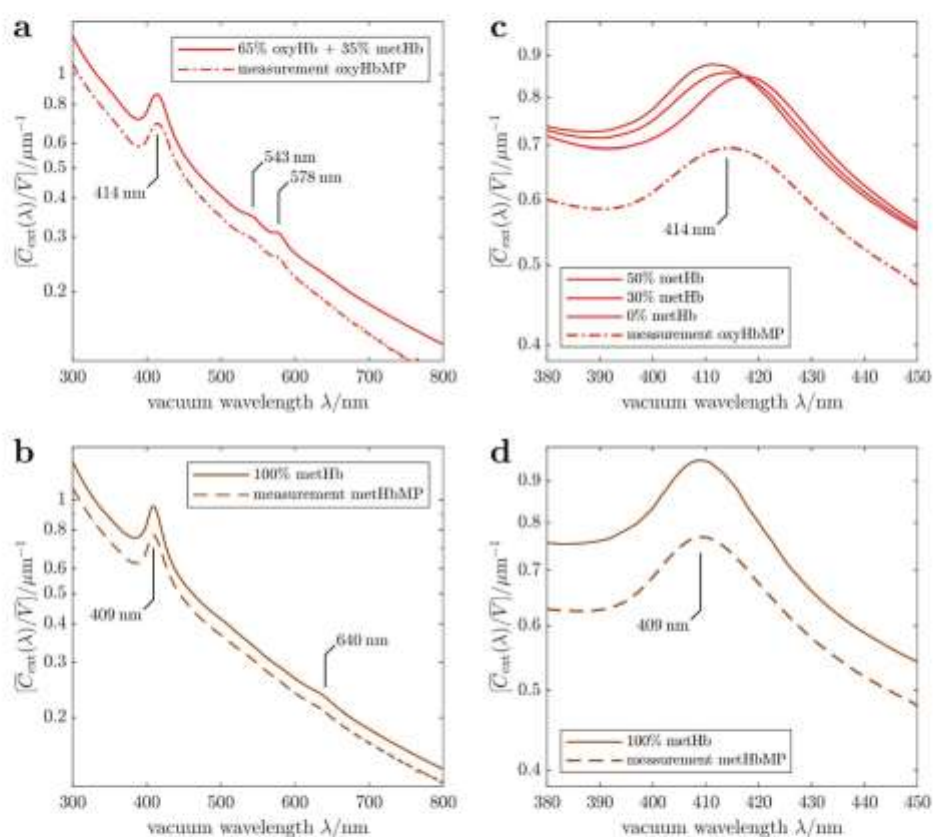
Figure 2. Results of spectral extinction measurements and simulations. (**a**) Volume-specific spectral extinction cross sections measured for oxyHbMP (dot-dashed red line) and calculated (red line) using 35% fraction of metHb and 65% oxyHb. (**b**) Volume-specific spectral extinction cross sections measured for metHbMP (dashed brown line) and calculated for 100% metHbMP (brown line). (**c**) Comparison of the measured spectral cross section in the Soret band and cross sections calculated for various metHb fractions. (**d**) Reduced wavelength range to show the Soret band of the measured and calculated extinction spectra.
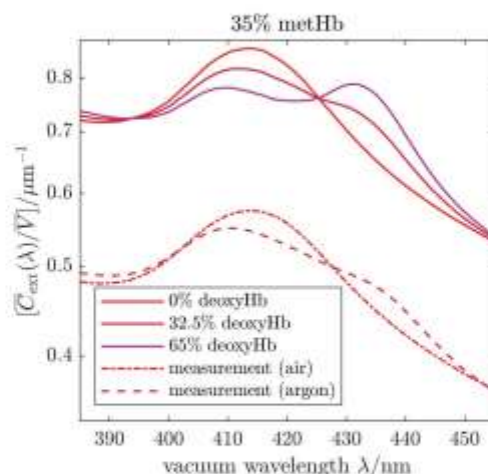
Figure 3. Volume-specific spectral extinction cross sections measured (dash-dotted and dashed lines) in air and using argon for deoxygenation. Calculated, volume-specific spectral extinction cross sections (solid lines) are included to illustrate the change of oxygenation of the HbMPs.

In Figure 2a, the measured extinction cross section of oxyHbMP reveals the decrease of the cross section with increasing wavelength, caused by light scattering as well as the absorption bands of hemoglobin centered at about 413 nm (Soret band), 543 nm and 578 nm (Q-band). The corresponding calculated cross section was varied with respect to the ratio of oxyHb and metHb and compared to measured spectra. The resulting simulated curve in Figure 2a, obtained for 35% metHb abundance relative to the total Hb, does reflect the same behavior as the measured one, except the shift to higher values of the volume-specific cross section $Z(\lambda)$. We attribute this deviation in the smaller measured cross sections, which were observed in all measurements, to systematic uncertainties caused: (i) by particle loss due to adhesion when pipetting, (ii) by agglomeration, (iii) or by trapped volume leading to a systematic increase in the PPV value. However, the observed spectral characteristic is well reproduced by our simulations. In addition, based on our simulations we estimated an accuracy for the determination of the metHb fraction to be 5 percentage points, i.e. the uncertainty is given by $u(\phi_{metHb}) = 0.05$, where ϕ_{metHb} is the mass fraction of metHb relative to the total Hb. The spectrum measured for 100% metHb and the related calculated spectral cross section are shown in Figure 2b. For calibration purposes, the Hb in the HbMP suspension was completely converted to metHb by $NaNO_2$. Compared to the oxygenated sample, the Soret band is slightly shifted from 413 nm to about 409 nm and its width is somewhat reduced. In addition, the Q bands characteristic for oxyHb are missing and a small metHb specific peak appears at approximately 640 nm. Again, the observed spectral features are reproduced by the cross section simulated for 100% metHb portion. In Figure 2c,d an enlarged view for the wavelength region of the Soret bands is shown. We include in Figure 2c results for calculated cross sections assuming different metHb fraction, i.e. 0%, 30% and 50%. The simulated curve for 100% metHb is shown in Figure 2d for comparison with the experiment. It is obvious from our simulations and measurements that the increase of the metHb portion results in a shift of the Soret band towards smaller wavelengths. The best agreement between measured oxygen saturated HbMP suspensions was obtained for a metHb fraction of 35% and 65% oxyHb.

Besides the samples of HbMPs saturated with oxygen and converted to metHbMP, we studied the transition between oxygenated HbMPs and partially deoxygenated HbMPs. Starting with the fully oxygenated sample as shown in Figure 2a,c, i.e. the fractions correspond to 65% oxyHb, 35% metHb and 0% deoxyHb, the cuvette was flushed with

argon for about 60 min. As can be seen from Figure 3 the experimental cross section changes when the sample is exposed to argon. Besides the Soret band characteristic for oxyHb, we observe a superposition with the absorbance of deoxyHb, the maximum of which is located at about 430 nm. Deoxygenation using argon is difficult and complete release of oxygen requires an unrealistically long treatment of the sample. Hence, only partial deoxygenation was reached in our experiment and the agreement with the simulation result is best for 32.5% deoxyHb, 32.5% oxyHb and 35% metHb. To illustrate the change of the line shape, we include also calculations for 0% deoxyHb and 65% deoxyHb in Figure 2e. In particular, for 0% deoxyHb the combination of the metHb and oxyHb bands leads to a slight shift and a broadening of the measured absorption band. On the other hand, for 65% deoxyHb both Soret bands for the respective Hb variants, i.e. metHb and deoxyHb, are clearly discernable.

2.4. MetHb Detection by X-ray Fluorescence

Near edge X-ray absorption fine structure (NEXAFS) is sensitive for the chemical state of the targeted element. Hence, due to the different oxidation states of iron Fe(II) and Fe(III) in oxyHb/deoxyHb and metHb, both variants are distinguishable in the HbMP suspension by scanning the photon energy of the exciting radiation across the L_2 and L_3 absorption edges of iron. The scanning range between 698 to 736 eV corresponds to a range of vacuum wavelengths between 1.776 to 1.685 nm.

In Figure 4a NEXAFS fluorescence spectra of two HbMP suspensions are shown, exposed to air (dot-dashed red curve, oxyHbMP) or treated with sodium nitrite ($NaNO_2$) to convert all Hb variants to metHb (dashed brown trace). For metHbMP, apart from a small shoulder at the low energy edge, the spectrum is dominated by the peak caused by the Fe(III) absorbance. Hence, approximately all Hb variants are converted to metHb. We used this measurement for normalization at 100% metHb content. The spectrum of the oxyHbMP shows a broad absorbance feature between 705 eV and 715 eV with the indication of two superposed maxima. It is evident that these maxima in the oxyHbMP spectrum coincide with the peaks of the Fe(II) and Fe(III) absorbance in the reference spectra [19]. To guide the eye, we include vertical lines at the corresponding energies. These two contributions to the measured oxyHbMP fluorescence spectrum are illustrated in Figure 4b. To prove the consistency with results of optical extinction measurements, the measured metHbMP spectrum was scaled according to the 35% metHb content in the oxyHbMP sample (the result is included as brown trace). The resulting difference spectrum (red line) between the measured oxyHbMP fluorescence and the scaled metHbMP exhibits a single Fe(II) peak only, thus being in agreement with the Fe(II) and confirming that the X-ray fluorescence spectra are in accordance with results derived by optical transmission measurements.

2.5. Physical Properties of Hemoglobin Microparticles

To set the size distribution for the analysis of the spectral extinction measurements, we characterized the HbMP sample with respect to the (sphere-equivalent) particle volume, the particle size distribution and the packed particle volume (PPV). In addition, the particle concentration in the stock suspension was determined directly by flow cytometry and derived from the measurements of the particle size and the PPV. Densities of the HbMP stock suspension and the supernatant were measured and used to calculate the density of the HbMP. Densities of reagents used for sample dilution and preparation, i.e. acetated Ringer's solution and Pronase solution were determined. All values and estimated uncertainties are listed in Table 1 together with density increments of heme-free globins/HSA and bovine Hb, needed to calculate the density of the HbMP. Details of the different methods applied for the characterization of the HbMP are given in the corresponding paragraphs in Section Materials and Methods, i.e. dynamic light scattering (DLS), analytical centrifugation (AC), determination of the PPV, flow cytometry and density measurements.
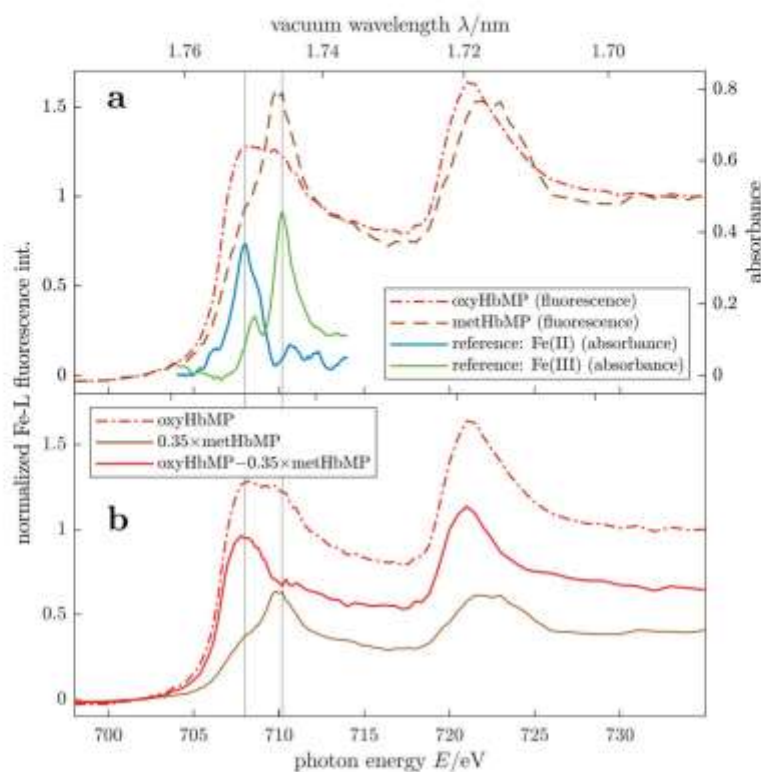
Figure 4. (a) NEXAFS fluorescence spectra of an oxygenated HbMP suspension (dot-dashed red trace) and metHbMP (dashed brown graph). For comparison, the absorbance of reference spectra for Fe(II) and Fe(III) [18] are included as blue and green lines, respectively. (b) Analysis of the oxygenated HbMPs (dot-dashed red curve) spectra as superposition of HbMPs containing 35% metHb and 65% oxyHb.

Table 1. Summary of results for the characterization of the HbMP suspension. Besides the (sphere equivalent) median particle diameter and the particle distribution width, the packed particle volume, the concentration and densities relevant for our analysis are listed.

Quantity	Symbol	Value		Uncertainty	Unit	Relative Uncertainty		Measurement Method
Median diameter (Intensity Weighted Distribution)	$D_{median} =$	760	$\pm$	54	nm	7.2	%	DLS
Distribution Width (16–84%)	$w(D) =$	395	$\pm$	94	nm	23.8	%	
Relative Distribution Width	$w_{rel}(D) =$	52	$\pm$	12	%	23.8	%	
Median Diameter (Intensity Weighted Distribution)	$D_{median} =$	996	$\pm$	26	nm	2.6	%	Analytical Centrifugation (AC)
Distribution Width (16–84%)	$w(D) =$	300	$\pm$	20	nm	6.7	%	
Relative Distribution Width	$w_{rel}(D) =$	30	$\pm$	2	%	6.7	%	
Packed Particle Volume of HbMP Stock Suspension	PPV =	0.1992	$\pm$	0.0003				Centrifugation
Particle Concentration of HbMP Stock Suspension	$C_0 =$	866	$\begin{matrix}+\\-\end{matrix}$	259 / 162	pL^{-1}			PPV, Particle Volume Determined by DLS
	$C_0 =$	385	$\begin{matrix}+\\-\end{matrix}$	190 / 180	pL^{-1}			PPV, Particle Volume Determined by AC
	$C_0 =$	293	$\pm$	30	pL^{-1}			Flow Cytometry

Table 1. *Cont.*

Quantity	Symbol	Value	Uncertainty		Unit	Relative Uncertainty	Measurement Method
Densities ρ at 23 °C							
HbMP Stock Suspension	$\rho^{stt} =$	1.01639	±	0.00010	g mL⁻¹		
Supernatant of HbMP Stock Suspension	$\rho^{sup} =$	1.00422	±	0.00010	g mL⁻¹		Mechanical Oscillator Device
Acetated Ringer's Solution	$\rho^{RAc} =$	1.00320	±	0.00010	g mL⁻¹		
Pronase Solution	$\rho^{Pro} =$	1.00101	±	0.00009	g mL⁻¹		
H₂O	$\rho^{water} =$	0.99749	±	0.00003	g mL⁻¹		
HbMP	$\rho^{HbMP} =$	1.0653	±	0.0006	g mL⁻¹		Mechanical Oscillator Device, PPV
Density Increment Gl/HSA	DI $_{Gl/HSA}$ =	0.2505	±	0.0056			Literature Value
Density Increment Hb	DI $_{Hb}$ =	0.2450	±	0.0010			Bovine Hb, Literature Value

The results for the median particle diameter and the relative distribution width differ for the DLS and AC methods. As previously discussed [20], the determination of particle size in the 10 to 1000 nm range is complex and the results strongly depend on the specific method used. In particular, polydisperse samples like the HbMPs are sensitive to such method specific differences. In addition, elastic properties, porosity and orientation of the HbMPs will influence the determination of size and size distribution. Taking into account that these effects are more pronounced in AC measurements due to the high centrifugation forces, for our analysis of spectral extinction measurements, we rely on the DLS results.

In order to calculate the concentration of the particles in the HbMP stock suspension, the total Hb concentration in the HbMPs and their density, we measured the packed particle volume. The details of the calculations and the PPV measurement are given in the section Materials and Methods. In principle, the PPV is determined similar to hematocrit measurements in blood samples. However, due to the smaller size and lower density of the HbMPs compared to erythrocytes [21], we increased the relative centrifugal force and the centrifugation time to assure complete sedimentation. To account for the elastic deformability of the HbMPs, the boundary between the solid fraction and the supernatant was read out several times to obtain the final value after about 100 h when relaxation of the particles was complete (Figure S4). We observed a change of the PPV value of 4%, the end point is given in Table 1. In our analyses, volume of fluid trapped between the solid phase particle is neglected, hence the value given corresponds to an upper limit.

The particle concentration is calculated using the PPV and the sphere-equivalent volumes determined by DLS and AC. Since the different–method specific–sizes result in correspondingly different concentrations, we used flow cytometry to directly measure the concentration of HbMPs in the stock suspension. However, flow cytometry yields the lowest concentration associated with particle loss due to adhesion on tube and container walls during preparation and measurement and agglomeration of the HbMPs. Taking into account the respective uncertainties, it follows from our observations that at present only a concentration range of $260 \, \text{pL}^{-1} \leq C_0 \leq 1125 \, \text{pL}^{-1}$ can be reliably given. As consequence, we introduce the volume-specific extinction cross section $Z(\lambda)$, defined in Equation (2), which does not explicitly depend on the concentration and only slightly changes with particle size.

In our analysis of the optical extinction spectra, we noted that the experimental data are not well reproduced by the simulations, if the HbMPs are modeled using only the three Hb components for the complex RI. The simulated cross sections are too low under this assumption. Instead, a significant content of heme-free proteins had to be included in the model. Such proteins do not exhibit significant absorption features in the spectral range under consideration, but increase the real part of the RI and hence influence the light-scattering properties, including extinction cross sections. While a certain content of HSA in the HbMPs ($\leq$10% of the total protein content) is expected from the production, the apparent concentration of heme-free proteins is much higher. We attribute this to Hb molecules that lose their heme group during production or storage of the particles, i.e.,

globin molecules. Throughout the text, the heme-free proteins in the HbMP are referred to as a globin/human serum albumin mixture (Gl/HSA). Their content was assessed by means of high accuracy density measurements.

The densities of the stock suspension of HbMPs and the supernatant were measured by means of an instrument based on a mechanical oscillator method [22]. In addition, the densities of acetated Ringer's solution used for diluting the stock suspension for AC measurements and Pronase solution for the enzymatic digestions in context with the spectrophotometric total Hb determination are listed in Table 1. The value for ultrapure water that served for validation is also included. The uncertainties of typically 10^{-4} g mL^{-1} represent standard deviations for ≥ 10 repeat measurements. In analogy with the determination of the density of erythrocytes [20], we obtain the ensemble averaged density of the HbMPs from the measured densities of the HbMP stock suspension ρ^{sus} and the supernatant ρ^{sup} in combination with the PPV value (see Section 3.12. Density of HbMPs) according to:

$$\rho^{HbMP} = \frac{1}{\text{PPV}} \left(\rho^{sus} - \rho^{sup} \right) + \rho^{sup} \tag{3}$$

As described in the Hb Concentration in HbMPs subsection, the density difference $\rho^{sus} - \rho^{RAc}$ derived from these measurements is compared to calculated values based on the linear superposition of the mass concentrations β^{sus}_{Hb} of Hb and β^{sus}_{Hb} of heme-free globin/HSA (Table 2), weighted by the corresponding density increments DI (see Table 1):

$$\rho^{sus} - \rho^{RAc} = \text{DI}_{Hb}\ \beta^{sus}_{Hb} + \text{DI}_{Gl/HSA}\ \beta^{sus}_{Gl/HSA} \tag{4}$$

Table 2. (a) Total hemoglobin concentrations in the various components of the HbMP suspension and total concentration of heme-free globin/HSA. (b) Concentrations of functional Hb and relative concentrations of metHb. * The HbMP suspension with all Hb variants converted to metHb was used for validation of the spectral extinction measurements and the X-ray fluorescence by setting the value to 100%.

a	Mass Concentrations			
	Total Hb in Stock Suspension	Hb in Supernatant of Stock Suspension	Heme-Free Globin/HSA in Stock Suspension	HbMP
Results for PPV = 19.9%	β^{sus}_{Hb}	β^{sup}_{Hb}	$\beta^{sus}_{Gl/HSA}$	β^{HbMP}_{Hb}
Method	Enzymatic Digestion, AHD Conversion and Spectrophotometry	Results for Total Hb, Density Measurements by Mechanical Oscillator Device and PPV		
Sample Preparation oxyHbMP, deoxyHbMP, metHbMP	g L^{-1} 25.5 ± 0.5	g L^{-1} 2.0 ± 0.2	g L^{-1} 27.7 ± 0.9	g L^{-1} 120.1 ± 2.7
b	Mass Concentration of Functional Hb	Relative Concentration of Non-functional Hb/metHb		
Results for PPV = 19.9%				
Method	Oxygen Release	Oxygen Release	Spectral Extinction Measurements	X-ray Fluorescence
Sample Preparation	g L^{-1}	%	%	%
oxyHbMP	11.8 ± 0.7	54 ± 3	35 ± 5	35 ± 5
deoxyHbMP	4.8 ± 0.9	81 ± 3	—	—
metHbMP	2.8 ± 0.4	89 ± 1	100 *	100 *

— value not determined by Spectral Extinction Measurements, X-ray Fluorescence not sensitive to deoxyHb.

This comparison reveals that the density difference $\rho^{sus} - \rho^{RAc}$ cannot be explained by a particle consisting of predominantly hemoglobin and small HSA contributions. A significant mass of heme-free globin must be present. It follows from the absolute mass concentrations given in Table 2 that the suspension–and most likely also the HbMPs – contains 48% hemoglobin and 52% heme-free globin/HSA. These results derived from the high accuracy density measurement explain the low Hb concentrations in the particle suspension and in the HbMPs.

2.6. MetHb and Functional Hb in Hemoglobin Microparticles

Results for the metHb fraction in HbMPs obtained by spectral extinction measurements and NEXAFS are compared to measurements based on oxygen release [23–25], details of which are given in Materials and Methods section. The absolute mass concentrations for the functional Hb components determined by the oxygen release procedure are related to the total Hb concentrations of the stock suspension, listed in Table 2a. The total Hb concentration was obtained by spectrophotometric absorbance measurements. Briefly, HbMPs were enzymatically digested followed by the alkaline haematin and detergent (AHD) conversion procedure [26,27]. In addition, in Table 2a the values for the Hb mass concentrations in the supernatant of the HbMP stock solution and in the HbMP are given as well as the concentration of heme-free proteins and HSA. As described in Materials and Methods, these values are derived from the measured total Hb mass concentration, high accuracy density measurements and the packed particle volume (PPV), i.e. the solid fraction in the HbMP stock suspension (see Table 1). The total mass concentrations summarized in Table 1a elucidate that about 8% of the hemoglobin is not incorporated in the particles or is released during production or storage into the supernatant. The amount of heme-free globins/HSA slightly exceeds 50%.

The part of functional Hb is listed in Table 2b for the three different preparations of the sample referred to as oxyHbMP for the suspension exposed to air and thus saturated with oxygen, as metHbMP when treated with sodium nitrite ($NaNO_2$) and deoxyHbMP when using sodium dithionite ($Na_2S_2O_4$). The oxygen release method allows the determination of absolute values for the functional hemoglobin, for the air-equilibrated suspension the mass concentration is 11.8 g L^{-1}. As can be seen from the first column in Table 2b, for the deoxygenated sample as well as for the metHbMP suspension, we still observe a significant oxygen release, indicating that the conversions were not complete. The absolute values were related to the total hemoglobin concentration in the sample (Table 2a) and we obtain the relative concentrations of non-functional hemoglobin and metHb. In this work, we focus on the comparison of the relative concentrations of the non-functional component for oxygenated samples (Table 2b, yellow row). The metHbMP suspensions were used for the validation of the spectral extinction and X-ray fluorescence methods, as indicated by the value set to 100%.

It is apparent that the concentration of metHb determined by the oxygen release procedure as difference between the total Hb concentration and the oxyHb concentration is significantly larger compared to the results obtained using spectral extinction and X-ray fluorescence measurements. This discrepancy is attributed to the hindered confirmation change of hemoglobin when embedded in the salt matrix and cross-linked, which results in increased time constants for oxygen intake and release and change in the reaction equilibrium. On the other hand, the optical method distinguishes metHb and oxyHb on the basis of different refractive indices and X-ray spectroscopy is sensitive against Fe(II) and Fe(III), independent on the localization of the two Hb components. The value of 35% determined for the relative metHb concentration corresponds to an absolute value of $0.65 \times (120.1)$ g L$^{-1} \approx 78$ g L^{-1} of functional hemoglobin in the particles. Taking into account the ratio of Hb and heme-free globin/HSA in the stock suspension of 1.086, we obtain a total protein concentration of $(120.1 + 130.5)$ g L^{-1} for the particles, which results in a fraction of about 31% of functional Hb in the particles. This value obtained for the specific batch investigated indicates that it is absolutely necessary to control the production process

in order to improve the oxygen transport capacity and to allow reproducible fabrication of the HbMPs.

3. Materials and Methods

3.1. Experimental Designs

The objective of this work was to develop a robust and reliable method with a low turnaround time to determine the biological function of HbMPs as promising candidate for artificial blood substitute. The function of HbMPs is defined by a sufficiently high hemoglobin component capable for transport of oxygen, while the methemoglobin component is required to be as low as possible. To quantify the abundance of oxyHb, deoxyHb and metHb in the HbMPs, we used a dedicated optical setup (Figure S1) [11] to measure collimated transmittance spectra of diluted HbMP suspensions. In contrast to a regular spectrophotometer, intended for purely absorbing samples but unsuitable for the quantitative analysis of light-scattering samples, our setup, described in Subsection Optical Setup, features a very low angle of detection for the transmitted light. This allows the quantitative determination of the spectral extinction of the HbMPs in suspension without unwanted contributions from light scattered in non-forward directions. The results of the optical extinction measurements were validated by comparison with other methods sensitive to the composition and function of the HbMPs, i.e. high accuracy density determination, NEXAFS fluorescence and oxygen release determination.

To validate our measurements and analyses, three different modifications of hemoglobin microparticles were prepared. Particle suspensions, exposed to filtrated air when preparing the suitable dilution for the respective measurement are saturated with oxygen and hence identified as oxyHbMP. Samples containing deoxygenated particles, marked as deoxyHbMP, were generated with a solution containing 2 mg/mL sodium dithionite ($Na_2S_2O_4$). Extinction spectra (Figure 3) of deoxyHbMP were obtained by flushing the diluted measurement suspension with argon. Hemoglobin in the HbMPs was converted into metHb by sodium nitrite ($NaNO_2$) with final concentrations of 10 mM $NaNO_2$ and 10% HbMPs, the samples were labelled as metHbMP.

3.2. Materials

Bovine hemoglobin, derived from fresh whole blood (Biophyll GmbH, Dietersburg, Germany) by hypertonic hemolysis [28] was used for the production of the HbMPs. Glutaraldehyde, manganese chloride ($MnCl_2$) tetrahydrate, sodium carbonate (Na_2CO_3), sodium nitrite ($NaNO_2$), phosphate-buffered saline pH 7.4 were purchased from Sigma-Aldrich (Munich, Germany). EDTA and sodium dithionite ($Na_2S_2O_4$) were provided by Fluka (Seelze, Germany) and sodium hydroxide (NaOH) by Carl Roth (Karlsruhe, Germany). Ampuwa and sterile 0.9% NaCl solution were purchased from Fresenius Kabi Deutschland GmbH (Bad Homburg, Germany). Human serum albumin solution 20% was obtained from Grifols Deutschland GmbH (Frankfurt am Main, Germany) and Pronase purchased from Sigma-Aldrich Chemie GmbH (Munich, Germany). The fabricated suspension of HbMPs was aliquoted in 15 mL vials under sterile conditions and stored at 4 °C. The volumes required for the various measurements were also taken under sterile conditions.

3.3. Morphology of Hemoglobin Microparticles

The shape of the particles was determined by scanning electron microscopy (SEM) and atomic force microscopy (AFM). Whereas for SEM extensive preparation is required and dry samples are examined, HbMPs in suspension are investigated by AFM.

For scanning electron microscopy, a Leo Supra 35 VP microscope (Zeiss, Oberkochen, Germany) was used. The suspension was pre-diluted to a PPV of 2% and mixed for about 5 min using a tube roller, thereafter treated in an ultrasonic bath at 35 kHz and 130 kHz for 15 min and 5 min, respectively. First investigations were based on positioning the HbMPs on a grid and recording images by observing (i) transmitted electrons or secondary, low energy electrons emerging from the surface (SE2). The later are either (ii) detected by an

Everhardt-Thomley-SE2-detector oriented laterally with respect to the incident electron beam or (iii) using an Inlens SE detector, sensitive against SE2 electrons emerging in a small solid angle symmetric to the backward direction. However, due to the properties of the biological particles none of the techniques is suited to obtain high contrast sharp images of the HbMP. Consequently, to record high contrast images, HbMPs were deposited on a plate and the sample was coated by sputtering platinum, resulting in a layer of 2 nm thickness. Besides contrast enhancement, charging is inhibited by the platinum coating. The SEM images shown in Figure 1b,c were recorded with the Inlens SE detector, which was operated at an acceleration voltage of 5 kV and a working distance of 5.2 mm.

AFM images were acquired with a NanoWizard 4 instrument (JPK BioAFM Business, Bruker Nano Surfaces, Berlin, Germany), mounted on a Zeiss inverted microscope. Since the HbMPs do not sufficiently adhere to glass surfaces, the microscopic slides were coated by a 50 µL drop of poly-L-ornithine (PLO). After incubation with PLO for 20 min the slides were washed twice with ultrapure water and blown dry with nitrogen flow. The HbMP suspension was prepared using a vortex mixer (5 min), a roll mixer (5 min) and an ultrasonic bath (5 min) to reduce agglomeration. Subsequently, the HbMP suspension was diluted 1:500 in acetated Ringer's solution, 50 µL were pipetted on the coated slide and incubated in a humid chamber to allow particles to adhere. The AFM images were acquired with spatial resolution of 10 nm using a USC 0.3 cantilever, the calibration of which yielded a spring constant of 0.61 N m^{-1}. In Figure 1d,e two HbMPs are shown with the height at 400 pN encoded in false colors. The long axis of the particle in Figure 1d is oriented parallel to the surface of the slide, while the particle in Figure 1e is fixated perpendicular to the surface of the slide. We observed that about 20% of the particles are oriented perpendicular. The electrostatic adhesion forces between the PLO coated slide and the particles immobilize the HbMPs with their respective orientation at the initial contact.

Both methods reveal the "peanut shape" of the HbMP with a long axis of approximately 800 nm and a waist of 400 nm. In addition, the surface exhibits fine structures in the range of 20–30 nm resulting from the $MnCO_3$ salt template, which was dissolved in the final step when preparing the HbMPs.

3.4. Optical Setup

The optical setup for the measurement of collimated transmittance spectra is described by Gienger et al. [11] and is shown in Figure S1 of the Supplementary Materials. A high-power, continuous xenon light source (HPX-2000, Ocean Optics, Inc., Dunedin, FL, USA) irradiates the sample. Data were acquired in the spectral range between 200 nm and 1100 nm by a Maya2000 Pro spectrometer (Ocean Optics, Inc., Dunedin, FL, USA). In total, 7 Mirrors M1–M7 are used to provide a path length of approximately 1.5 m for the incident light beam and a distance of 1.5 m between the sample cuvette and the entrance aperture of the spectrometer (Figure S1). The lens L1 is used for collimation, i.e. to obtain an approximately parallel light beam. The apertures A1–A3 serve to reduce the divergence of the beam to about 0.01° (half angle), ensuring a plane-wave illumination from a single, well-defined direction. The samples are filled in a quartz cuvette (Hellma Analytics, Müllheim, Germany) with $\ell = (10 \pm 0.01)$ mm optical path length. Aperture A4 blocks the light scattered in the non-forward direction by the sample. The spectrometer receives light from an observation angle as small as 0.02° (half angle). In contrast to a normal spectrophotometer, this serves to effectively suppress any light scattered at an angle to the incident beam. Hence, one can neglect unwanted contributions to the directed transmittance when analyzing the measurements. With the 50 µm entrance slit of the spectrometer, the spectral resolution is approximately 1.9 nm and spectra are sampled at about 0.45 nm per pixel on the CCD chip. Typically, spectra are generated within 10 s, thus the method allows rapid characterization of suspensions of HbMPs.

3.5. Protocol for Spectral Extinction Measurements

The HbMP stock suspension was pre-diluted 100-fold with water. The quartz cuvette with inner dimensions 10 mm × 10 mm was placed in the holder and filled with 2.2 mL of water. A dilution series was measured by subsequently pipetting volumes between 10 μL and 670 μL (in total) of the pre-diluted HbMP suspension into the cuvette, without touching it. This eliminates changes in reflections at the optical interfaces that would otherwise cause artifacts in the measured signals. Mixing of the fluids was achieved by pipetting back and forth into the cuvette several times. Six dilutions per sample were measured in this manner with transmittances ranging from T (300 nm) ≈ 92% and T (800 nm) > 99.5% for the lowest volume fraction (10 μL sample) down to T (300 nm) = 1.6% and T (800 nm) > 65% for the highest volume fraction (670 μL sample). The low-concentration high-transmittance measurements are prone to noise and measurement errors. On the other hand, the high-concentration measurements may show unwanted multiple-scattering effects. This was assessed by comparing the curves for $Z(\lambda)$ or $\bar{C}_{ext}(\lambda)$ obtained from the different dilutions. They agree well with each other as long as the transmittance is $T(\lambda) \geq 30\%$. That is to say, they differ by no more than an up- or downward shift on a logarithmic y-scale, i.e. by a re-scaling of the curve (due to volume errors of the pipette, compare Equations (1) and (2)). We used the highest concentration that shows no multiple-scattering effects for further analysis, due to the favorable signal-to-noise ratio. This corresponds to a sample volume of 130 μL and transmittances T (300 nm) = 30%, T (800 nm) > 89% for the curves in Figures 2 and 3.

The extinction spectra of oxygenated/functional HbMPs and metHbMP were measured as described above. For deoxygenation of the HbMPs, argon gas was bubbled through the suspension to purge oxygen from the particles and liquid. The argon gas was fed into the cuvette through a metal capillary which remained in place during the recording of transmittance spectra. Foaming of the sample suspension did occur in this process, leading to a noticeable decrease in the particle concentration (or, equivalently to a reduced PPV) and hence to a systematic decrease in the determined extinction cross section. Since the VSECS is inversely proportional to the PPV, this error was corrected for by re-scaling the $Z(\lambda)$ data of the deoxygenated HbMPs by 1.626 to match the data of oxygenated HbMPs, measured before bubbling, in a least-squares sense over the whole wavelength range between 300 to 800 nm. Non-rescaled spectra are provided in Figure S5 of the Supplementary Materials. The argon was applied for approximately 60 min and then turned off before recording the spectrum of the deoxygenated HbMPs. After deoxygenation, the sample was bubbled with air to re-oxygenate the particles within less than one minute.

3.6. Model for Optical Properties of Hemoglobin Microparticles

Complex RI data for the constituents of the HbMPs are required for the numerical simulation of extinction spectra. The light-scattering properties of a single spherical particle are determined by its diameter D and its complex refractive index (RI). For the light scattering simulations, the RI of the HbMPs was modelled by:

$$n(\lambda) + i\kappa(\lambda) = n_{H_2O}(\lambda) + \beta_{Hb}^{HbMP} \left[a_{Hb}(\lambda) + i\,\gamma_{Hb}(\lambda) \right] + \beta_{Gl/HSA}^{HbMP} \left[a_{HSA}(\lambda) + i\,\gamma_{HSA}(\lambda) \right] \tag{5}$$

which is the complex RI of an aqueous protein solution [11] containing a total hemoglobin mass concentration β_{Hb} and a heme-free globins (Gl)/HSA mixture at mass concentration $\beta_{Gl/HSA}$ [29,30]. The optical properties of HSA alone are used here to model both, HSA and (heme-free) globin. This approximation is justified, because the increments of the real and imaginary parts $a(\lambda)$ and $\gamma(\lambda)$ for globin are unknown but expected to be very similar due to the absence of a heme group and the similar molecular mass of the two globular proteins. The imaginary part of the respective RI increment, $\gamma_y(\lambda)$ with y = Hb, Gl/HSA, corresponds to the absorption spectrum of an aqueous protein solu-

tion. For hemoglobin, this imaginary RI increment contains contributions from the three hemoglobin components:

$$\gamma_{Hb}(\lambda) = \phi_{oxyHb} \; \gamma_{oxyHb}(\lambda) + \phi_{deoxyHb} \; \gamma_{deoxyHb}(\lambda) + \phi_{metHb} \; \gamma_{metHb}(\lambda) \qquad (6)$$

where ϕ_{oxyHb}, $\phi_{deoxyHb}$ and ϕ_{metHb} are the mass fractions of oxygenated, deoxygenated and methemoglobin, respectively. Similarly, the real RI increment of the hemoglobin component contains three contributions:

$$\alpha_{Hb}(\lambda) = \phi_{oxyHb} \; \alpha_{oxyHb}(\lambda) + \phi_{deoxyHb} \; \alpha_{deoxyHb}(\lambda) + \phi_{metHb} \; \alpha_{metHb}(\lambda) \qquad (7)$$

In Figure 5, the real and imaginary RI increments used in the simulations are shown. This enables us to simulate spectral extinction cross sections $C_{ext}(\lambda)$ of single particles by Lorenz-Mie theory for any possible composition by changing β_{Hb}^{HbMP}, $\beta_{Gl/HSA}^{HbMP}$, ϕ_{oxyHb}, $\phi_{deoxyHb}$, ϕ_{metHb} and thus $n(\lambda) + ix(\lambda)$ as well as the particle diameter D. Finally, VSECS spectra $Z(\lambda)$ are obtained by integration over the particle size distribution (PSD).
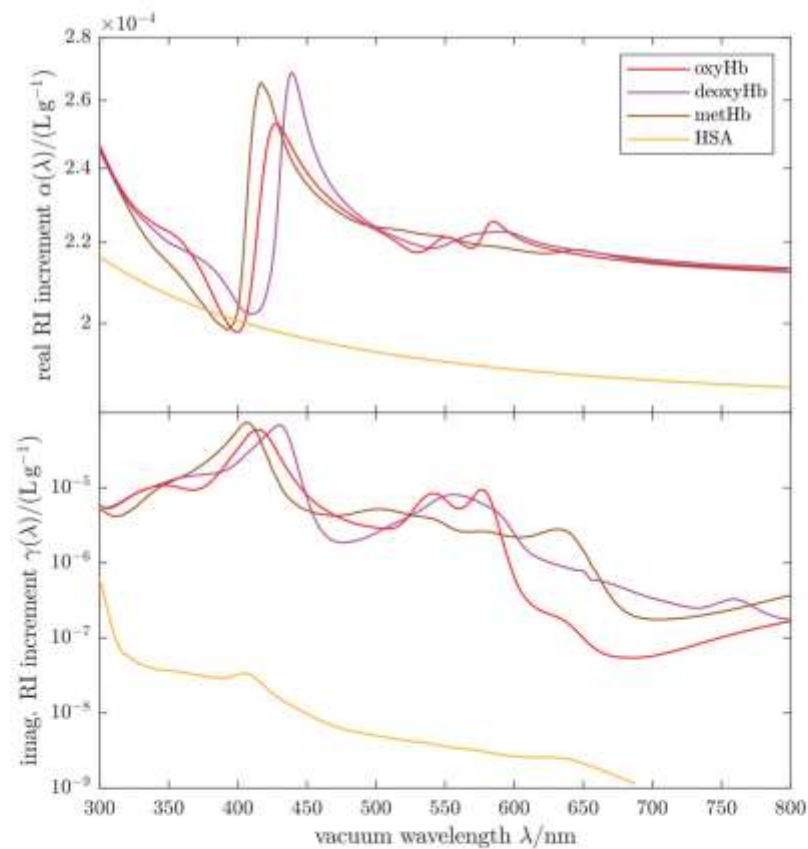
Figure 5. Complex refractive index increments of the Hb components and HSA used in our calculations of the extinction cross sections of HbMPs.

50

3.7. Calculation of Extinction Cross Sections

The imaginary RI increments of the respective Hb components are linked to their molar extinction coefficients $\epsilon_x(\lambda)$ by:

$$\gamma_x(\lambda) = \frac{\ln 10}{4\pi} \frac{\epsilon_x(\lambda)}{4 \, M(\text{Hb(Fe)})} \lambda \tag{8}$$

where $x = \text{oxyHb}$, deoxyHb or metHb and $M(\text{Hb(Fe)})$ is the molar mass of the hemoglobin monomer. An analogous relation holds true for $\gamma_{\text{HSA}}(\lambda)$, the imaginary part of the RI increment of GI/HSA. In the simulations, we used the absorption spectra reported by Friebel and Meinke [31] for human oxyHb and deoxyHb and those reported by Zijlstra et al. [32] for human metHb. While such absorption spectra (i.e., $\gamma(\lambda)$ data) are available for bovine Hb as used in the HbMPs, too, quantitative data for the real RI increment (i.e., $\alpha(\lambda)$ data) are only available for human Hb.

We use values for $\alpha_{\text{oxyHb}}(\lambda)$ that were obtained from measurements of the extinction spectra of sphered oxygenated human erythrocytes [11]. For $\alpha_{\text{deoxyHb}}(\lambda)$ and $\alpha_{\text{metHb}}(\lambda)$ we use values that are consistent with the $\alpha_{\text{oxyHb}}(\lambda)$ data and that were computed from the absorption spectra $\gamma_{\text{deoxyHb}}(\lambda)$ and $\gamma_{\text{metHb}}(\lambda)$ for human hemoglobin using Kramers-Kronig relations, i.e. a fundamental causality principle in physics [18,31]. The absorption spectra of human and bovine hemoglobin are known to differ very little [32] and consequently the real parts of the RI differ very little, too. Hence the error made by assuming the optical properties of human Hb even though the HbMPs contain bovine Hb is small. The values for $\alpha_{\text{HSA}}(\lambda)$, used to model the globin/HSA mixture in the HbMPs, were determined from extinction spectroscopy with well-characterized quasi-monodisperse polystyrene beads suspended in the HSA solution. The $\gamma_{\text{HSA}}(\lambda)$ spectra were obtained by standard spectrophotometry. The details of the RI determination of HSA are described in the corresponding section of the Supplementary Materials.

To compute the complex RI of the HbMPs for light scattering simulations, the intra-particle protein concentrations were set to $\beta_{\text{Hb}} = 120\text{g L}^{-1}$ and $\beta_{\text{GI/HSA}} = 130\text{g L}^{-1}$, corresponding to the results of the density and PPV measurements. For our analysis we use the RI of pure water [33] for the host medium surrounding the particles in accordance with the measurement conditions, i.e. the HbMP suspension was diluted in pure water. The increase of the RI due to dissolved proteins from the storage solution of the HbMPs is negligible due to the high dilution (>1000-fold) of the sample in the extinction measurements.

In general, the dependence of $C_{\text{ext}}(\lambda)$ for a single particle on both, the complex RI $n(\lambda) + ix(\lambda)$ and the diameter D is highly nonlinear, thus requiring to repeat the computations for every composition and size. For a given particle size distribution (PSD), labeled by the symbol $p(D)$, the ensemble-averages are computed as:

$$\overline{C}_{\text{ext}}(\lambda) = \int_{D_{\min}}^{D_{\max}} C_{\text{ext}}(\lambda; D) \, p(D) \, dD \quad \wedge \quad \overline{V} = \int_{D_{\min}}^{D_{\max}} \frac{\pi}{6} D^3 \, p(D) \, dD \tag{9}$$

to obtain $Z(\lambda) = \overline{C}_{\text{ext}}(\lambda)/\overline{V}$. The PSD is assumed to be a log-normal distribution:

$$p(D) = \frac{1}{\sqrt{2\pi}\,\sigma_D} \frac{1}{D} \exp\left[\frac{-\ln(D/\mu_D)^2}{2\sigma_D^2}\right] \tag{10}$$

which fits the DLS and AC results well. The parameter μ_D coincides with the median diameter and σ_D is a measure for the relative distribution width. Note that the distribution width $w(D)$ defined for the measured PSDs correlates with but is not identical to the parameter σ_D. Using the quantiles Q of the PSD, which can be expressed in terms of μ_D and σ_D, the distribution width is given as $w(D) = Q(84\%) - Q(16\%)$. For the simulations, we used those parameter values that yield the same median and absolute distribution width $w(D)$ as the DLS measurements, i.e. $\mu_D = 760 \, \mu\text{m}$ and $\sigma_D = 25.8\%$. Simulations using

the AC distribution parameters, i.e. $\mu_D = 996$ μm and $\sigma_D = 15.1\%$ as well as other sets of parameters are provided in Figures S2 and S3 of the Supplementary Materials. Ideally the integration limits used with a log-normal PSD would be $D_{min} = 0$, $D_{max} = \infty$. In practice, we used numerical integration with bounds $D_{min} \leq Q(0.1\%)$, $D_{max} \geq Q(99.9\%)$ and a step width ≤ 20 nm.

3.8. Soft X-ray Fluorescence

The NEXAFS experiments were carried out at the plane grating monochromator (PGM) beamline [34] for undulator radiation in the PTB laboratory of the BESSY II electron storage ring in Berlin (Germany). This beamline provides soft X-ray radiation of high photon flux and spectral purity in the photon energy range of 78 eV–1860 V (15.7–0.659 nm) and allows for dedicated experiments on light elements such as carbon, nitrogen, or oxygen. A UHV chamber [35], which is equipped with a scanning table for sample alignment, photo diodes for normalization and a silicon drift detector (SDD) for detection of the emitted fluorescence radiation from the sample. The SDD detector is equipped with a thin Be-window in order to improve the ratio between the detected Fe-L and the intense oxygen (O-Kα) fluorescence radiation originating from the water-based solution containing the HbMPs. The liquid must be transferred into the UHV in order to avoid the strong attenuation of soft x-rays in all kinds of media. In this work, the hemoglobin microparticle suspensions are probed using a liquid sample cell with an ultra-thin entrance window (thickness 100 nm) made from Si_3N_4 as an appropriate separator between liquid and vacuum [36]. The liquid cell was directly mounted into the UHV chamber and has a total sample volume of about 0.4 mL. The actual interaction volume, defined by the excitation beam and the solid angle of observation (cylindrical with diameter 4 mm and depth 3 mm) behind the window amounts to about 40 μL.

In Figure 4a, two X-ray fluorescence spectra of HbMP suspensions (dot-dashed red and dashed brown traces) are shown, recorded by scanning the excitation energies between 698 to 736 eV (1.776–1.685 nm). The HbMP stock solution was enriched to about a PPV of 60% to ensure that the exciting X-ray beam is absorbed by the HbMPs. The spectra shown are averaged over three repeat measurements each, conducted on the same sample to prove that influences due to sedimentation, irradiation induced effects or sample degradation were not relevant. Besides the spectra for oxyHbMP (dot-dashed red line) and the metHbMP (dashed brown trace), we include absorbance reference spectra [18] for Fe(II) and Fe(III) as blue and green lines.

3.9. Packed Particle Volume

Centrifugation with a standard hematocrit centrifuge (Hettich EBA 12, Andreas Hettich GmbH, Tuttlingen, Germany) was used to determine the solid fraction or packed particle volume (PPV), i.e. the ratio of the volume occupied by particles to the total volume in the suspension of hemoglobin microparticles. The suspension of HbMPs was filled into 10 BRAND® micro hematocrit capillary (BRAND GmbH + Co KG, Wertheim, Germany), typically the height amounts to 55 mm. The protocol usually applied to determine the hematocrit value in whole blood samples, described in the standard DIN 58933-1 [37], had to be modified since sedimentation of HbMPs was observed to be incomplete. To ensure that the end point is reached, the relative centrifugation force was increased from 5000 to 6250 g, g = 9.8 m s^{-2} being the terrestrial gravitational acceleration, and the centrifugation time was increased to 21 min compared to 16 min. For readout of the hematocrit tubes, an electronic scale (Peak Optics, La Quinta, CA, USA) with a 100 μm resolution was used. We observed that the HbMPs are flexible and the corresponding compression results in a lower PPV if measured directly after centrifugation. To account for this effect, we measured the PPV of the 10 capillaries as a function of time and determined the mean value and standard deviation. To avoid systematic deviations, three persons were involved, characterized by different symbols (circle, diamond, cross) in Figure S4 of the Supplementary Materials. The

data were modeled by a dose response function yielding a value of PPV = 0.1992(3) (see Table 1), the expansion of the PPV amounts to 0.0084 corresponding to about 4%.

3.10. Dynamic Light Scatter

Particle size was determined by dynamic light scattering (DLS) employing a Litesizer™ 500 (Anton Paar GmbH, Graz, Austria) instrument. To prove that the instrument was operated in its specified transmittance range a series of six dilutions was prepared for DLS measurements covering particle concentrations $50 \times 10^3 \, \text{nL}^{-1} \geq C \geq 103 \, \text{nL}^{-1}$. The resulting transmittance values range from 0.01 to 60%. For suspensions with low particle concentrations the Litesizer™ was operated in the side scatter mode (red symbols in Figure S6) while for high particle concentrations backscatter was measured (blue symbols in Figure S6). The result, i.e. the median diameter of the intensity weighted distribution, is listed in Table 1. For consistency the median value is given, since we analyzed our extinction measurements taking the median of the size distribution. The uncertainty $u(D_{median})$ was estimated accounting for the standard deviation of the six measurements of the dilution series. It should be noted that the particle size distributions, derived from the measured temporal autocorrelation function, can be described to a good approximation by logarithmic normal distributions. Results for such fits agree well with the averaged value for the width $w(D)$ (Table 1) obtained by numerical analysis of the distributions for the 16% to 84% summarized intensities.

3.11. Analytical Centrifugation

Besides DLS, we applied analytical centrifugation (AC) to derive the particle size distribution, characterized by median and width. The type of centrifugation used is based on cuvettes containing the diluted samples and transmission measurements and generally abbreviated as cAC-turb [38]. For simplification, we use the abbreviation AC in this paper. Two different suspensions were prepared from the HbMP stock suspension by adding acetated Ringer's solution (Serumwerk Bernburg AG, Bernburg, Germany) to obtain dilutions of 1:40 and 1:75. These dilutions were selected to meet the requirements of the LUMiSizer centrifuge (LUM GmbH, Berlin, Germany), i.e. the initial transmittance should be between 30% and 50%. Each suspension was pipetted to 3 disposable cuvettes of 2 mm path length. The centrifugation force was increased in several steps to cover a large size range from 100 nm to several micrometer. Total measurement time amounted to about 18 min. Since for the 1:40 dilution the initial transmittance amounted to 40% and for the 1:75 dilution to 55%, the median diameter given in Table 1 is determined from the measurements of the 1:40 dilution only. As observed with DLS, the particle size distributions measured by AC, derived from the time dependence of the interface between the suspension and the transparent supernatant, is well described by logarithmic normal distributions. To estimate the uncertainty contribution due to the uncertainty of the density, the AC measurements were analyzed using different particle densities and the solvent's density, i.e. acetated Ringer's solution. In Figure S7, we plotted the result for the median sphere equivalent particle diameter versus the particle density in the vicinity of the values derived by the density measurements. Hence, the uncertainty in Table 1 for the sphere equivalent diameter determined by AC accounts for the standard deviation from the results obtained for the 3 cuvettes of the 1:40 dilution and the uncertainty of the density measurements.

3.12. Concentration of Hemoglobin Microparticles

The concentration of HbMPs in the stock suspension was measured directly by flow cytometry and calculated according to:

$$C_0 = \frac{PPV}{(4/3) \, \pi \, (D_{median}/2)^3} \tag{11}$$

taking into account the median particle diameters derived by DLS and AC. Flow cytometric measurements were performed with a CyFlow Cube 8 instrument (Sysmex Partec, Görlitz, Germany), configured with a 50 mW 488 nm solid state laser and observation channels for forward light scatter (FSC), side scatter (SSC) and three fluorescence channels. This system offers volumetric counting by start stop electrodes and a computer controlled pump for high accuracy syringes. The stock solution of the HbMPs was diluted by about a factor 1:106 to adjust the count rate in the range between 1 kHz and 5 kHz. Whereas autofluorescence of HbMPs could not be detected, in the FSC versus SSC diagram HbMPs (Figure S8a) can be discerned from the background and the debris. To assess the sensitivity, we include a scatter diagram of a mixture of polystyrene microspheres with diameters of 220 nm and 500 nm (Figure S8b). The clusters of these two populations are clearly visible, additional populations at higher signal intensities are caused by particle agglomerates. The events localized close to the trigger level are due to electronic noise or contaminating particles in the sheath fluid. Gating the cluster representing the HbMPs in the FSC versus SSC dot plot, we obtain the pulse height distribution of the SSC intensities, depicted in the histogram in Figure S8c. The same gate was used for the polystyrene particles, the corresponding histogram is included in Figure S3c for comparison. It is evident that the maximum of the HbMP distribution is located at lower side scatter intensity compared to the 220 nm polystyrene particles, although their sphere equivalent diameter is approximately 4 times and their volume 40 times larger. The difference in light scattering intensity is caused by the different polarizability of the particles, i.e. their refractive indices, being 1.605 for polystyrene and $(1.390 + 3.6 \times 10^{-4} i)$ for the oxyHbMP at 488 nm. Hence, for flow cytometric detection of HbMPs the sensitivity of the flow cytometer should be sufficient to detect 100 nm polystyrene micro spheres. The measurement time amounted to 30 s, 44,000 HbMPs out of 70,000 total events were delineated by setting the gate as illustrated in Figure S8a. Taking into account the volume fraction (7.5×10^{-7}) of the HbMP suspension in the measurements sample and the measurement volume (200 µL), we obtain the concentration of HbMPs given in Table 1, i.e. (293 ± 30) pL^{-1}. Compared to the values derived from the measurements of the particles' volume by DLS and AC this value is the smallest, possibly caused by adhesion loss on container and tube walls or agglomerates of HbMPs, detected as single event. However, because of the relatively large range for the concentrations measured with different methods, as described in the Section Physical Properties of HbMPs, we introduce the quantity $Z(\lambda)$, independent on the concentration, to analyze the extinction spectra. Hence, uncertainties due to the concentration are avoided.

3.13. Density of Hemoglobin Microparticles

The densities of the stock suspension of HbMPs, the supernatant and reagents involved in the various preparations were measured by a mechanical oscillator device [28]. We used a prototype model µDMA (Hans Stabinger GmbH, Graz, Austria) which was developed to allow density determination for sample volumes of typically 100 µL with an accuracy of about 10^{-4} g mL^{-1}. The densities of the HbMP suspension and the various reagents in Table 1 are directly determined with the µDMA instrument from up to 10 repeated measurements. As uncertainty, the standard deviation is reported. The density of water was measured to validate the calibration of the instrument. As already stated in the Results and Discussion (Section 2.5. Physical properties of HbMPs), the density of the HbMPs is calculated from the PPV and the densities of the HbMP suspension and the supernatant according to:

$$\rho^{HbMP} = \frac{1}{PPV} \left(\rho^{sus} - \rho^{sup} \right) + \rho^{sup} \tag{12}$$

This procedure was applied to determine the densities of erythrocytes as function of the mean corpuscular hemoglobin concentration (MCHC) [21]. The high accuracy density determination of the HbMPs allows to model the composition of the HbMPs, since besides Hb, heme-free globin (Gl) and human serum albumin (HSA) are incorporated

in the particles, as discussed in the Results section. In this context, we use the values in Table 1 for the density increments DI_{Hb} of bovine hemoglobin and $DI_{Gl/HSA}$ and of a 1:1 mixture of Hb (in lack of a value for heme-free globin) and HSA. The density increment of a solution in a given solvent is defined as $DI_{solute} = \left(\partial \rho_{solution} / \partial \beta_{solute} \right)$. A higher uncertainty is assumed for $DI_{Gl/HSA}$ to account for the possibility of Gl to HSA ratios other than 1:1.

3.14. Total Hemoglobin Concentration

The total Hb concentration in the suspension of HbMPs was determined by spectrophotometry using the AHD method [26,27], which was demonstrated to allow high accuracy reference measurements of the total hemoglobin concentration in whole blood samples by comparison with the hemiglobincyanide (HiCN) procedure [39,40]. An aliquot of the HbMP stock suspension was vortexed for 10 min for homogenization. Due to the cross-linking of the hemoglobin and albumin molecules, an enzymatic digestion is required to completely degrade the HbMP. For this purpose, a Pronase solution with a concentration of about 10 mg mL^{-1} was used. A mixture containing Pronase solution and HbMP suspension with a 1:1 mass ratio was incubated for 30 min at 50 °C. The resulting Hb solution was used to prepare a dilution series with volume fractions between 0.116 and 0.215 for absorption measurements using a Cary 5000i spectrophotometer (Agilent Technologies, Waldbronn, Germany). A second "reference" solution was prepared just containing Pronase with the same concentration as in the Hb-solution. A corresponding dilution series was prepared, filled in an identical quartz cuvette, which was positioned in the reference beam of the spectrophotometer. Hence, the absorption spectra (Figure S9) represent the contribution caused by the digested HbMPs. From the spectra, the spectral absorbance $A(\lambda)$ at 574 nm is determined for the different dilutions φ_i and the mass concentration is calculated according to:

$$\beta_{Hb}^{sus} = \frac{A(\lambda)\ M(Hb(Fe))}{\ell\ \varepsilon(\lambda)\ \varphi_i} \tag{13}$$

The molar mass $M(Hb(Fe))$ of the monomeric Hb(Fe) amounts to 16114.5 g mol^{-1}, the absorption lengths for the quartz cuvettes were d = 10 mm and the molar extinction coefficient is given by ε (λ = 574 nm) = 6945 L mol^{-1} cm^{-1}. Finally, the total Hb concentration (Table 2a) is determined as the weighted average of the different dilutions. The uncertainty given in the table is estimated by repeating the procedure several times at various days.

3.15. Hemoglobin Concentration in Hemoglobin Microparticles

To determine the content of hemoglobin as well as heme-free globin and HSA, we calculate the density difference between the HbMP suspension and acetated Ringer's solution according to:

$$\rho^{sus} - \rho^{RAc} = DI_{Hb}\ \beta_{Hb}^{sus} + DI_{Gl/HSA}\ \beta_{Gl/HSA}^{sus} \tag{14}$$

Each of these two components contributes according to its mass concentration β and its density increment given in Tables 1 and 2. For aqueous protein solutions it was found that the density increments are almost constant over a wide range of concentrations [41]. The values in Table 1 were taken from this Reference and converted from water or phosphate buffer to RAc and extrapolated to 23 °C. Rearrangement of Equation (14) allows the calculation of the concentration of heme-free globin/HSA in the suspension by:

$$\beta_{Gl/HSA}^{sus} = \frac{\rho^{sus} - \rho^{RAc} - DI_{Hb}\ \beta_{Hb}^{sus}}{DI_{Gl/HSA}} \tag{15}$$

The resulting concentration $\beta_{Gl/HSA}^{sus}$ = 27.7 g L^{-1} (Table 2a) corresponds to a ratio between non-heme proteins and hemoglobin or relative concentration of $\left(\beta_{Gl/HSA}^{sus} / \beta_{Hb}^{sus} \right)$

= 1.0868. In the production process of the HbMPs, only a small fraction of the HSA is used for coating or in washings steps and the majority of HSA is co-precipitated and cross-linked together with the Hb. Hence, we will assume that the HSA to Hb ratio is the same in the supernatant as in the particles. This means that the mass concentration of hemoglobin in the supernatant β_{Hb} follows in analogy to Equation (14) from the density difference between the supernatant and Ringer's solution:

$$\rho^{sup} - \rho^{RAc} = DI_{Hb} \ \beta_{Hb}^{sup} + DI_{Gl/HSA} \ \beta_{Gl/HSA}^{sup} \tag{16}$$

Replacing the mass concentration of the Gl/HSA proteins $\beta_{Gl/HSA}$ by the product of the ratio in the suspension and the mass concentration β_{Hb}^{sup} of Hb in the supernatant and rearranging Equation (16) the mass concentration of Hb in the supernatant is given by:

$$\beta_{Hb}^{sup} = \frac{\left(\rho^{sup} - \rho^{RAc} \right)}{DI_{Hb} \ + \ DI_{Gl/HSA} \ \left(\frac{\beta_{Gl/HSA}^{sus}}{\beta_{Hb}^{sus}} \right)} \tag{17}$$

Finally, the mass concentration of Hb proteins β_{Hb}^{HbMP} in the HbMP is calculated taking into account that the total Hb concentration in the suspension is the sum of the concentrations in the HbMP according to

$$\beta_{Hb}^{sus} = PPV \ \beta_{Hb}^{HbMP} + (1 - PPV) \ \beta_{Hb}^{sup} \tag{18}$$

with the contributions weighted by the packed volume fraction PPV = 0.1992(3). Hence, the mass concentration of Hb in the HbMPs follows as

$$\beta_{Hb}^{HbMP} = \frac{1}{PPV} \left\{ \beta_{Hb}^{sus} - (1 - PPV) \ \beta_{Hb}^{sup} \right\} \tag{19}$$

The results for these quantities are summarized in Table 2a.

3.16. Oxygen Release Measurements

To determine the mass concentration of functional, i.e. oxyhemoglobin in HbMPs, we measured the ferricyanide-induced release of hemoglobin-bound oxygen into the surrounding medium [23,24]. The dissolved oxygen of the three different HbMP suspensions (oxyHbMP, deoxyHbMP, metHbMP) was measured by a miniaturized optical needle type oxygen sensor (oxygen microsensor NTH-PSt7, PreSens–Precision Sensing GmbH, Regensburg, Germany) connected to an oxygen meter with data logging (Microx 4, PreSens—Precision Sensing GmbH). For saturation with oxygen, 1 mL of HbMP suspensions and hemoglobin solutions were left for equilibration for 10 min under stirring. Thereafter, 50 μL to 100 μL of 10% ferricyanide ($K_3[Fe(CN)_6]$) were added to detect the concentration change of dissolved oxygen with an acquisition rate of one data point per second. When a stable value was reached, the measurement was stopped. Further adding of ferricyanide did not lead to a pO_2 increase. While there was no increase of dissolved oxygen when ferricyanide was added to the control (aqua dest.), a hemoglobin concentration dependent change in pO_2 was observed. Taking into account the difference of final and initial pO_2 and assuming that all released oxygen was previously bound to hemoglobin, a standard curve for the hemoglobin concentration versus change of pO_2 was generated and used to derive the mass concentration of the functional hemoglobin in the HbMPs. Apart from the different preparation to generate deoxyHb and metHb (see 3.1. Experimental Designs), the same protocol was applied to determine the dissolved oxygen in suspensions of deoxyHbMP and metHbMP.

4. Conclusions

We have demonstrated that spectral optical extinction measurements of hemoglobin microparticles and analysis (SEMPA) is a valuable tool to monitor and optimize the produc-

tion of microparticles and sub-micrometer particles and to evaluate the effect of relevant influencing factors. Extinction data were analyzed by Lorenz-Mie theory to yield the relative concentrations of metHb, oxyHb and deoxyHb and thus the functionality of microparticle based artificial blood substitutes. In particular, by ensuring that multiple scattering events are negligible, the—ensemble averaged—particle properties are easily accessible. This is a significant advantage with respect to the oxygen release measurements as the usually applied technique, which cannot distinguish between Hb inside and outside the microparticles. We applied the SEMPA technique to specify hemoglobin microparticles, fabricated by the co-precipitation—cross-linking—dissolution technique. For validation of the determined ratio of functional Hb/metHb, we applied NEXAFS fluorescence measurements as complementary method and observed good agreement between these results. The observed spectral extinction cross sections cannot be described by calculations assuming that the HbMPs are composed of the three component oxyHb, deoxyHb and metHb solely. Our results prove that a considerable portion of heme-free globin/HSA of about 50% of the total protein is present in the investigated particles, a value which was confirmed by high accuracy density measurements.

The SEMPA method could potentially replace the elaborate oxygen release analysis by adding a flow-through system. Integration of a gas exchanger would allow the reversible oxygenation and deoxygenation of the sample including kinetic studies.

5. Patents

On behalf of J.G. and J.N. the Physikalisch-Technische Bundesanstalt has filed a patent application (DE 10 2017 121 587 A1) describing the optical procedure for the simultaneous determination of particle properties and particle measuring device. Issues related to intellectual properties will be managed by the Innovation and Technology Transfer Department at the Physikalisch-Technische Bundesanstalt.

Supplementary Materials: The following are available online at https://www.mdpi.com/1422-0067/22/4/1753/s1, List of abbreviations; List of symbols; Figure S1: Optical Setup for collimated transmittance measurements; Figure S2: Influence of median particle size on the volume-specific extinction cross section for HbMPs of given relative size distribution width $\sigma_D = 25.8\%$ and composition; Figure S3: Influence of distribution width parameter σ_D of the log-normal particle size distribution on the volume-specific extinction cross section of HbMPs at fixed median $D_{median} = 760$ nm; Figure S4: Packed particle volume (PPV) or solid fraction of the HbMP stock suspension as function of time; Figure S5: Oxygenation—deoxygenation and effect of particle loss; Paragraph "RI determination of HSA"; Figure S6: Particle diameter of HbMP measured by DLS for different concentrations; Figure S7: Correlation of the results for the particle size determined from sedimentation measurements and the density of the HbMP; Figure S8. Flow cytometric measurements of HbMP and polystyrene microspheres; Figure S9: Absorption spectra of the HbMP suspension resulting from different dilutions.

Author Contributions: Conceptualization, K.S. and J.N.; methodology, K.S., J.G., P.H., and J.N.; software, J.G.; validation, K.S., J.G., P.H., and J.N.; formal analysis, J.G. and J.N.; investigation, K.S., P.H., and J.N.; resources, K.S.; data curation, J.G. and J.N.; writing—original draft preparation, J.G., and J.N.; writing—review and editing, K.S., J.G., P.H. and J.N.; visualization, J.G. and J.N.; supervision, J.N.; project administration, J.N.; funding acquisition, J.N. All authors have read and agreed to the published version of the manuscript.

Institutional Review Board Statement: Not applicable.

Informed Consent Statement: Not applicable.

Data Availability Statement: All data is contained within the article or supplementary material as Figure or Table. The numerical data represented in the Figures are available on request from the corresponding author.

References

1. Carson, J.L.; Grossman, B.J.; Kleinman, S.; Tinmouth, A.T.; Marques, M.B.; Fung, M.K.; Holcomb, J.B.; Illoh, O.; Kaplan, L.J.; Katz, L.M.; et al. Red blood cell transfusion: A Clinical practice guideline from the AABB. *Ann. Intern. Med.* **2012**, *157*, 49–58. [CrossRef]
2. Klein, H.G. How safe is blood, really? *Biologicals* **2010**, *38*, 100–104. [CrossRef]
3. Gupta, A.S. Hemoglobin-based oxygen carriers: Current state-of-the-art and novel molecules. *Shock* **2019**, *52*, 70–83. [CrossRef] [PubMed]
4. Thompson, A.; McGarry, A.E.; Valeri, C.R.; Lieberthal, W. Stroma-free hemoglobin increases blood pressure and GFR in the hypotensive rat: Role of nitric oxide. *J. Appl. Physiol.* **1994**, *77*, 2348–2354. [CrossRef]
5. Chen, J.Y.; Scerbo, M.; Kramer, G. A review of blood substitutes: Examining the history, clinical trial results, and ethics of hemoglobin-based oxygen carriers. *Clinics* **2009**, *64*, 803–813. [CrossRef] [PubMed]
6. Winslow, R.M. Current status of blood substitute research: Towards a new paradigm. *J. Intern. Med.* **2003**, *253*, 508–517. [CrossRef] [PubMed]
7. Ignarro, L.J.; Buga, G.M.; Wood, K.S.; Byrns, R.E.; Chaudhuri, G. Endothelium-derived relaxing factor produced and released from artery and vein is nitric oxide. *Proc. Natl. Acad. Sci. USA* **1987**, *84*, 9265–9269. [CrossRef]
8. Bäumler, H.; Xiong, Y.; Liu, Z.Z.; Patzak, A.; Georgieva, R. Novel hemoglobin particles-promising new-generation hemoglobin-based oxygen carriers. *Artif. Organs* **2014**, *38*, 708–714. [CrossRef]
9. Xiong, Y.; Steffen, A.; Andreas, K.; Müller, S.; Sternberg, N.; Georgieva, R.; Bäumler, H. Hemoglobin-based oxygen carrier microparticles: Synthesis, properties, and in vitro and in vivo investigations. *Biomacromolecules* **2012**, *13*, 3292–3300. [CrossRef]
10. Xiong, Y.; Liu, Z.Z.; Georgieva, R.; Smuda, K.; Steffen, A.; Sendeski, M.; Voigt, A.; Patzak, A.; Bäumler, H. Nonvasoconstrictive hemoglobin particles as oxygen carriers. *ACS Nano* **2013**, *7*, 7454–7461. [CrossRef]
11. Gienger, J.; Smuda, K.; Müller, R.; Bär, M.; Neukammer, J. Refractive index of human red blood cells between 290 nm and 1100 nm determined by optical extinction measurements. *Sci. Rep.* **2019**, *9*, 4623. [CrossRef] [PubMed]
12. Mie, G. Beiträge zur Optik trüber Medien, speziell kolloidaler Metallösungen. *Ann. Phys.* **1908**, *330*, 377–445. [CrossRef]
13. Waterman, P.C. Matrix Formulation of Electromagnetic Scattering. *Proc. IEEE* **1965**, *53*, 805–812. [CrossRef]
14. International Organization for Standardization. *ISO-ISO/IEC Guide 99: International Vocabulary of Metrology—Basic and General Concepts and Associated Terms (VIM)*, 3rd ed.; International Organization for Standardization: Geneva, Switzerland, 2007. Available online: https://www.bipm.org/utils/common/documents/jcgm/JCGM_200_2012.pdf (accessed on 2 January 2021).
15. Bohren, C.F.; Huffman, D.R. *Absorption and Scattering of Light by Small Particles*; Wiley: New York, NY, USA, 1983; pp. 83–129.
16. Kaewprayoon, W.; Suwannasom, N.; Kloypan, C.; Steffen, A.; Xiong, Y.; Schellenberger, E.; Pruß, A.; Georgieva, R.; Bäumler, H. Determination of methemoglobin in hemoglobin submicron particles using nmr relaxometry. *Int. J. Mol. Sci.* **2020**, *26*, 8978. [CrossRef]
17. Kloypan, C.; Suwannasom, N.; Chaiwaree, S.; Prapan, A.; Smuda, K.; Baisaeng, N.; Pruß, A.; Georgieva, R.; Bäumler, H. In-vitro haemocompatibility of dextran-protein submicron particles. *Artif. Cells Nanomed. Biotechnol.* **2019**, *47*, 241–249. [CrossRef]
18. Gienger, J.C. Determination of Optical and Geometrical Properties of Blood Cells and Microparticles from Light Scattering Measurements. Ph.D. Thesis, Technical University of Berlin, Berlin, Germany, 2019.
19. Nagasaka, M.; Yuzawa, H.; Horigome, T.; Kosugi, N. In operando observation system for electrochemical reaction by soft X-ray absorption spectroscopy with potential modulation method. *Rev. Sci. Instrum.* **2014**, *85*, 104105. [CrossRef] [PubMed]
20. Babick, F.; Mielke, J.; Wohlleben, W.; Weigel, S.; Hodoroaba, V.D. How reliably can a material be classified as a nanomaterial? Available particle-sizing techniques at work. *J. Nanopart. Res.* **2016**, *18*, 158. [CrossRef]

21. Hinghofer-Szalkay, H. Method of high-precision microsample blood and plasma mass densitometry. *J. Appl. Physiol.* **1986**, *60*, 1082–1088. [CrossRef] [PubMed]
22. Kratky, O.; Leopold, H.; Stabinger, H. Dichtemessungen an Flüssigkeiten und Gasen auf 10^{-6} g/cm^3 bei 0,6 cm^3 Präparatvolumen (Determination of Density of Liquids and Gases to an Accuracy of 10^{-6} g/cm^3, with a Sample Volume of only 0,6cm^3). *Z. Angew. Phys.* **1969**, *27*, 273–277.
23. Haldane, J. The ferricyanide method of determining the oxygen capacity of blood. *J. Physiol.* **1900**, *25*, 295–302. [CrossRef]
24. Cook, S.F. The action of potassium cyanide and potassium ferricyanide on certain respiratory pigments. *J. Gen. Physiol.* **1928**, *11*, 339–348. [CrossRef] [PubMed]
25. Tucker, V.A. Method for oxygen content and dissociation curves on microliter blood samples. *J. Appl. Physiol.* **1967**, *23*, 410–414. [CrossRef]
26. Zander, R.; Lang, W.; Wolf, H.U. Alkaline haematin D-575, a new tool for the determination of haemoglobin as an alternative to the cyanhaemiglobin method. I. description of the method. *Clin. Chim. Acta* **1984**, *136*, 83–93. [CrossRef]
27. Wolf, H.U.; Lang, W.; Zander, R. Alkaline haematin D-575, a new tool for the determination of haemoglobin as an alternative to the cyanhaemiglobin method. II. Standardisation of the method using pure chlorohaemin. *Clin. Chim. Acta* **1984**, *136*, 95–104. [CrossRef]
28. Haney, C.R.; Buehler, P.W.; Gulati, A. Purification and chemical modifications of hemoglobin in developing hemoglobin based oxygen carriers. *Adv. Drug Deliv. Rev.* **2000**, *40*, 153–169. [CrossRef]
29. Gienger, J.; Groß, H.; Neukammer, J.; Bär, M. Determining the refractive index of human hemoglobin solutions by Kramers–Kronig relations with an improved absorption model. *Appl. Opt.* **2016**, *55*, 8951–8961. [CrossRef] [PubMed]
30. Barer, R.; Joseph, S. Refractometry of Living Cells Part I Basic Principles. *Refract. Living Cells Part. I Basic Princ.* **1954**, *s3–95*, 399–423.
31. Friebel, M.; Meinke, M. Model function to calculate the refractive index of native hemoglobin in the wavelength range of 250–1100 nm dependent on concentration. *Appl. Opt.* **2006**, *45*, 2838–2842. [CrossRef]
32. Zijlstra, W.G.; Buursma, A.; Van, A. *Visible and Near Infrared Absorption Spectra of Human and Animal Haemoglobin: Determination and Application*; VSP International Science Publishers: Leiden, The Netherlands, 2000.
33. Daimon, M.; Masumura, A. Measurement of the refractive index of distilled water from the near-infrared region to the ultraviolet region. *Appl. Opt.* **2007**, *46*, 3811–3820. [CrossRef]
34. Senf, F.; Flechsig, U.; Eggenstein, F.; Gudat, W.; Klein, R.; Rabus, H.; Ulm, G. A plane-grating monochromator beamline for the PTB undulators at BESSY II. *J. Synchrotron Radiat.* **1998**, *5*, 780–782. [CrossRef]
35. Lubeck, J.; Beckhoff, B.; Fliegauf, R.; Holfelder, I.; Hönicke, P.; Müller, M.; Pollakowski, B.; Reinhardt, F.; Weser, J. A novel instrument for quantitative nanoanalytics involving complementary X-ray methodologies. *Rev. Sci. Instrum.* **2013**, *84*, 045106. [CrossRef] [PubMed]
36. Grötzsch, D.; Streeck, C.; Nietzold, C.; Malzer, W.; Mantouvalou, I.; Nutsch, A.; Dietrich, P.; Unger, W.; Beckhoff, B.; Kanngießer, B. A sealable ultrathin window sample cell for the study of liquids by means of soft X-ray spectroscopy. *Rev. Sci. Instrum.* **2017**, *88*, 123112. [CrossRef] [PubMed]
37. *DIN 58933-1—Haematology—Procedure for Determining the Volume Fraction of Erythrocytes (Packed Cell Volume) in Blood—Part. 1: Reference Method Based on Centrifugation*; Beuth Verlag: Berlin, Germany, 1995.
38. Bellmann, C.; Caspari, A.; Moitzi, C.B. *Dynamische und Elektrophoretische Lichtstreuung—Leitfaden zur Partikelgrößenbestimmung und Zetapotentialbestimmung*; Anton Paar GmbH: Graz, Austria, 2019; ISBN 978-3-200-04433-3.
39. Witt, K.; Wolf, H.U.; Heuck, C.; Kammel, M.; Kummrow, A.; Neukammer, J. Establishing traceability of photometric absorbance values for accurate measurements of the haemoglobin concentration in blood. *Metrologia* **2013**, *50*, 539. [CrossRef]
40. Martens, S.; Klauenberg, K.; Neukammer, J.; Cowen, S.; Ellison, S.L.R.; Elster, C. Quantifying Uncertainty When Comparing Measurement Methods–Haemoglobin Concentration as an Example of Correlation in Straight-Line Regression. Available online: https://zenodo.org/record/4282094#.YCNzgHmxVPY (accessed on 2 January 2021).
41. Adair, G.S.; Adair, M.E. The density increments of proteins. *Proc. R. Soc. Lond. A Math. Phys. Sci.* **1947**, *190*, 341–356. [CrossRef] [PubMed]

Publication 2 / Publikation 2

Kloypan C, Suwannasom N, Chaiwaree S, Prapan A, **Smuda K**, Baisaeng N, Pruß A, Georgieva R, Bäumler H.

In-vitro haemocompatibility of dextran-protein submicron particles.

In-vitro haemocompatibility of dextran-protein submicron particles

Chiraphat Kloypan, Nittiya Suwannasom, Saranya Chaiwaree, Ausanai Prapan, Kathrin Smuda, Nuttakorn Baisaeng, Axel Pruß, Radostina Georgieva & Hans Bäumler

Taylor & Francis
Taylor & Francis Group

ᵃ OPEN ACCESS   Check for updates

In-vitro haemocompatibility of dextran-protein submicron particles

Chiraphat Kloypan[a,b], Nittiya Suwannasom[a,c], Saranya Chaiwaree[d], Ausanai Prapan[e], Kathrin Smuda[a], Nuttakorn Baisaeng[f], Axel Pruß[a], Radostina Georgieva[a,g] and Hans Bäumler[a]

[a]Institute of Transfusion Medicine, Charité-Universitätsmedizin Berlin, Berlin, Germany; [b]Division of Clinical Immunology and Transfusion Sciences, School of Allied Health Sciences, University of Phayao, Phayao, Thailand; [c]Division of Biochemistry and Nutrition, School of Medical Sciences, University of Phayao, Phayao, Thailand; [d]Department of Radiological Technology, Faculty of Allied Health Sciences, Naresuan University, Phitsanulok, Thailand; [e]Department of Pharmaceutical Technology, Faculty of Pharmacy, Payap University, Chiang Mai, Thailand; [f]Division of Pharmaceutical Sciences, School of Pharmaceutical Sciences, University of Phayao, Phayao, Thailand; [g]Department of Medical Physics, Biophysics and Radiology, Faculty of Medicine, Trakia University, Stara Zagora, Bulgaria

ABSTRACT

Blood compatibility is a key requirement to fulfil for intravenous administration of drug and oxygen carrier system. Recently, we published the fabrication of oxidised-dextran (Odex)-crosslinked protein particles by one-pot formulation. In the current study we investigate the haemocompatibility of these Odex - particles including albumin particles (Odex-APs) and haemoglobin particles (Odex-HbMPs). Odex-APs and Odex-HbMPs have a submicron size ranged 800–1000 nm with peanut-like shape and a negative surface charge. In vitro haemocompatibility assays included haemolysis test, indirect phagocytosis test and platelet activation test in human blood. Odex-APs and Odex-HbMPs did not provoke any undesirable effects on the blood cells. Firstly, the ratio of haemolysis after contacted with Odex-crosslinked protein particles were less than 5% and therefore the particles may be considered non-haemolytic. Secondly, the incubation of leukocyte with Odex-APs/HbMPs did not influence the phagocytosis of leukocyte. We conclude that our particles are not recognized by monocytes or granulocytes. Finally, exposure of Odex-APs/HbMPs to platelets did not cause an activation of platelets. Additionally, Odex-HbMP/AP did not enhance or attenuate agonist-induced platelet activation. We conclude that Odex-crosslinked protein particles exhibit a very good haemocompatibility and represent highly promising carriers for drugs or oxygen.

Introduction

A major part of the micro- and nanometer size particles in clinical and preclinical investigations are biomolecule-based particles fabricated from polysaccharides, polyaminoacids, polypeptides, proteins or lipids. Among them, protein-based micro- and nanoparticles have been extensively investigated [1] as a site-specific drug carrier for cancer [2–7] as well as haemoglobin-based oxygen carriers (HBOCs) [8–16].

However, questions concerning the safety of prolonged use of nano- and micro-particles have been raised since most biomedical nanoparticles, for therapeutic and/or diagnostic purposes, are typically intravenously administrated and directly interact with the blood. Hence, the haemocompatibility of the nano- and micro- particles becomes important and critical. Materials are considered to be haemocompatible, if they are able to remain effectual after being exposed to blood but do not bring about any form of toxicity to the blood cells and do not cause any changes in composition and viscosity of the blood plasma [17]. For instance, the rupture of red blood cells (RBCs) and subsequent haemoglobin releasing can cause the symptoms haemoglobinuria or anuria followed by renal failure [18]. Additionally, platelets are critical to haemostasis by virtue of their ability to adhere, aggregate and release the contents of their granules as well as their capacity to alter their surface characteristics to support blood coagulation. Therefore, thrombotic and thromboembolic complications, as well as bleeding risks associated with the disseminated intravascular coagulopathy (DIC) remain of serious concern. Besides, the phagocytic cells (e.g. granulocytes and monocytes) can proficiently engulf particles in the blood which results in serious limitation of their blood circulation time and extravasation into target tissues [19]. Therefore, to avoid these events, the use of biocompatible and biodegradable materials are crucial factors for the fabrication of particles suitable for clinical applications.

The haemocompatibility of particles is mainly affected by their physicochemical characteristics such as chemical composition, size, shape, surface charge, hydrophobicity or hydrophilicity [20–22]. The fabrication techniques and selection of biomaterials are the fundamental steps, which can drastically impact the haemocompatibility of the particles as well as the efficacy of the proteins in the particles. Recently, we described a new promising formulation of protein submicron

particles called "One-Pot formulation" [23]. The new procedure is based on the coprecipitation-crosslinking-dissolution (CCD) method where the biopolymer particles are obtained in three main steps exploiting the ability of insoluble inorganic salts to incorporate macromolecules during precipitation in aqueous solutions. These macromolecules are subsequently crosslinked, and the inorganic precipitate is dissolved usually by complexation of the metal ions or pH change. With the one-pot procedure, coprecipitation and crosslinking were combined in one step due to the use of a biopolymer crosslinker, oxidised-dextran (Odex), which is coprecipitated together with a protein into a manganese carbonate ($MnCO_3$) template. Odex-HbMPs fabricated by one-pot demonstrated an improved oxygen storage capability. We hypothesized that dextran is able to improve not only the protein function and stability but also the haemocompatibility of the particles because of its protein-rejecting and cell repelling abilities [36,37]. In addition, the multivalent nature of dextran is advantageous for surface immobilization of biologically active molecules.

Therefore, the aim of this study is to investigate the haemocompatibility of Odex-APs and Odex-HbMPs using several methods including RBCs haemolysis, phagocytic activity of leukocytes and activation/aggregation of thrombocytes, in vitro.

Materials and methods

Materials

Dextran (M.W. 40,000 and 70,000 Da named as 40 T and 70 T, respectively) were purchased from AppliChem GmbH, Germany. Human serum albumin (HSA) solution for injection (200 g/L HSA, contains 16 mM sodium caprylate, 16 mM sodium N-acetyltryptophanate, 100–130 mM sodium chloride) was purchased from Baxalta Deutschland GmbH, Germany. Bovine haemoglobin solution (50 g/L in 0.9% NaCl) was obtained from Biophyll GmbH, Germany. Ethylenediaminetetraacetic acid disodium salt dihydrate (EDTA-Na_2), glycine, manganese chloride, sodium carbonate, sodium chloride, sodium hydroxide, and sodium (meta) periodate were purchased from Sigma-Aldrich, Germany. Phosphate buffered saline pH 7.4 (PBS, solutions contains 10 mM sodium phosphate dibasic, 1.9 mM potassium phosphate monobasic, 137 mM sodium chloride and 2.7 mM potassium chloride) was purchased from Fisher Scientific, USA. PHAGOTEST[TM] and PHAGOBURST[TM] kits were purchased from Glycotope Biotechnology GmbH, Germany.

Odex-crosslinked protein particles

50 mL of 10% dextran solutions (40 T and 70 T, 30.9 mmoL glucose subunits) were oxidised by sodium periodate (6.6 g, 30.9 mmoL) for 1 h at room temperature [24]. Then, the resulting oxidised dextran (Odex) was transferred to a cellulose dialysis tube (MWCO of 12,000: Carl Roth GmbH, Germany) and dialysed against water. The amount of aldehyde in Odex was quantified by hydroxylamine hydrochloride titration method with unmodified dextran as a reference [25].

Albumin particles (APs) and haemoglobin (HbMPs) were prepared by the one-pot procedure using 40T- and 70T-Odex as crosslinking as described earlier [23]. Briefly, equal volumes

of solution 1 consisting of 0.25 M of $MnCl_2$ and 50 mg/mL of HSA or Hb were rapidly mixed with solution 2 containing 0.25 M of Na_2CO_3 and 40 mg/mL of Odex (40 T or 70 T, individually) in the beaker under vigorous stirring at room temperature. After 30 s, 5 mg/mL of HSA was added to the suspension and incubated for 5 min under stirring to allow the HSA to absorb into particles surface. The resulting particle suspensions were then proceeded to the dissolution of the $MnCO_3$ template by 0.25 M EDTA/0.05 M Glycine for 30 min and the reduction by 0.4 mg/mL of $NaBH_4$. Finally, the obtained Odex cross-linked albumin particles (Odex-APs) or haemoglobin particles (Odex-HbMPs) were washed three times with PBS (6000 g for 5 min) and finally suspended in sterile PBS (final particle concentration 2×10^{11}/mL). APs and HbMPs crosslinked with 40T-Odex and 70T-Odex are named 40T-APs, 70T-APs, 40T-HbMPs and 70T-HbMPs, correspondingly.

For SEM imaging, samples were prepared by applying a drop of particles suspension onto glass slide followed by drying overnight. After sputtering with gold, measurements were conducted at an operation voltage of 3 keV using Gemini Leo 1550 instrument (Oberkochen, Germany) and ImageJ 1.44p software (Wayne Rasband, National Institute of Mental Health, Bethesda, MD, USA).

The hydrodynamic diameter and the zeta-potential of the Odex-APs and Odex-HbMPs were measured by dynamic light scattering using a Zetasizer Nano ZS instrument (Malvern Instruments Ltd., Malvern, UK) in PBS solution. Additionally, Odex-crosslinked particles were dispersed in PBS and analysed for autofluorescence using flow cytometry (BD FACSCanto II), FITC and PE channel were gated. BD FACSDIVA software (BD Biosciences, USA) was employed for data analysis.

Blood collection

Venous blood anticoagulated by lithium heparin or sodium citrate was collected from healthy volunteers. Informed consent was obtained from all donors in written form. The blood samples were withdrawn in accordance with the transfusion law of Germany. The use of donor blood samples for scientific purposes was approved by the ethics committee of the Charité – Universitätsmedizin Berlin (# EA1/137/14). Immediately after blood collection, tubes were slowly agitated to ensure an appropriate mixing of anticoagulant and blood and discarded if there was any evidence of clotting. The assays were performed within 2 h after blood collection.

Haemolysis test

The haemolytic test is based on the release of haemoglobin from damaged erythrocytes in vitro. Human heparinized erythrocytes were washed (3000 g, 5 min) in PBS until the supernatant was clear and colourless. RBCs were then to obtain a cell suspension with a volume concentration of 2% in PBS. 0.5 mL of 2% Odex-crosslinked particles suspension was mixed with 0.5 mL of the 2% washed human erythrocyte suspension. This ratio of particles to RBC corresponds to an exchange of 50% blood with particle suspension. 0.5 mL of

double distilled water and PBS were employed as the positive (PC) and negative (NC) control, respectively. After incubation at 37 °C for 3 h, the erythrocyte suspensions were centrifuged at 3000 g for 5 min, the supernatants were collected and pipetted into a 96-well plate. The haemolytic ratio was determined by measuring the absorbance of the supernatants at 545 nm using a microplate reader (Cytation™ 3 Cell Imaging Multi-Mode Reader, BioTek) and calculated according to the following equation:

$$\%Haemolytic\ ratio\ = \frac{(OD_{test}-OD_{NC})}{(OD_{PC}-OD_{NC})} \times 100 \qquad (1)$$

All results were estimated from the data of three individual experiments, and all data were expressed as the mean ± SD [26]. The value of the positive control (water) was set to 100% haemolysis.

Phagocytosis test

The activation of phagocytosis performance of granulocytes and monocytes in whole blood was investigated using an indirect method based on a modified PHAGOTEST. The method is suitable for non- fluorescing particles. The different particles (10 µL of 2×10^{11} per mL) were added to 50 µL of heparinized-whole blood and incubated at 37 °C for 0, 10, 30, 60, 120 min to allow uptake by the leucocytes. Samples with non-fluorescent *Escherichia coli* (2×10^9 bacteria per mL from PHAGOBURST kit) and PBS were used as a positive and negative control, respectively. After reaching the corresponding incubation time, the standard test for phagocytosis activity (PHAGOTEST) was performed with all samples. Briefly, 10 µL of fluorescein isothiocyanate labelled *E. coli* (FITC-*E. coli*, 2×10^9 bacteria per mL from Phagotest kit) were added to each sample and incubated at 37 °C for further 10 min. Afterwards, the fluorescence of non-phagocytosed *E. coli* was quenched, the RBCs were lysed and the leucocytes were fixed and DNA-stained by propidium iodide. Washing steps with PBS were performed between each preparation step. Finally, the leukocyte populations were analysed by flow cytometry (BD FACSCanto II) to obtain the percentage of granulocytes and monocytes which have phagocytosed FITC-*E. coli*. Leukocytes previously saturated with non-fluorescent bacteria or particles are not able to uptake the FITC-*E. coli*, and therefore decreased phagocytic activity to FITC-*E. coli* indicates phagocytic activity to the non-fluorescent bacteria or particles.

Platelet activation test

The influence of Odex-AP and Odex-HbMP on human platelets was investigated in platelet-rich plasma (PRP) samples. Citrated human whole blood was centrifuged at 150 g for 15 min at 20–25 °C, and the PRP fraction was collected. The platelet amount was detected before the test using a haematology analyser ABX Micros 60 (HORIBA Europe GmbH, Germany). 45 µL of PRP was gently mixed with 5 µL of particle suspensions (to a ratio of 10 = particles per 1 platelet). Platelets incubated with PBS were used as a control. The samples were incubated at 37 °C for 30 min with gently shaking. Then, the pre-incubated human platelets were activated with platelet agonists (0.5 mg/mL arachidonic acid (AA), 0.2 mg/mL collagen and 0.01 mM epinephrine (Epi): mõLab GmbH, Germany) to induce platelet activation and aggregation. The mixtures were incubated at 37 °C for further 30 min with shaking and the samples were then fixed by 0.5% formaldehyde in PBS. Finally, the platelets were stained by APC anti-human CD42b (GPIbα) antibody and Alexa Fluor® 488 anti-human CD62P (P-Selectin) antibody (BioLegend, San Diego, USA) and analysed by flow cytometry (BD FACSCanto II). Double-stained events were counted as activated platelets [27,28].

Statistical analysis

Data were presented as means ± standard deviation (SD), and statistical differences between groups were compared using ANOVA-like test. GraphPad Prism 6 software (GraphPad, La Jolla, CA, USA) was employed for graphs and statistical analyses. p Values <.05 was considered statistically significant.

Results

Particle characterisation

Odex-APs and Odex-HbMPs were successfully fabricated by the One-pot procedure. Like the CCD-technique using $MnCO_3$ as inorganic template, the morphology and the size of the obtained haemoglobin and albumin particles by the One-pot procedure were not significantly different as observed by SEM (Figure 1). The dynamic light scattering analysis of the particles is represented in Figure 2. The size of Odex-APs and Odex-HbMPs was about 800–1000 nm and the zeta-potential was approximately −13 mV and −9 mV as measured in PBS (conductivity 18–20 mS/cm) for Odex-APs and Odex-HbMPs,
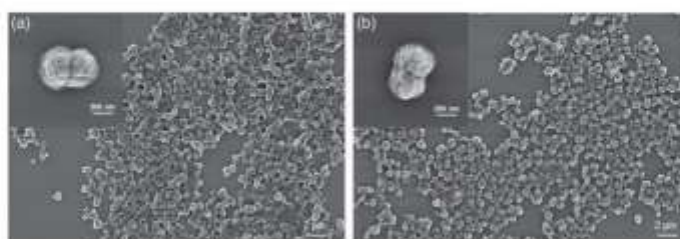

Figure 1. SEM images of Odex-AP (a) and Odex-HbMP (b) fabricated by One-pot formulation. The insets show peanut-like single particles.
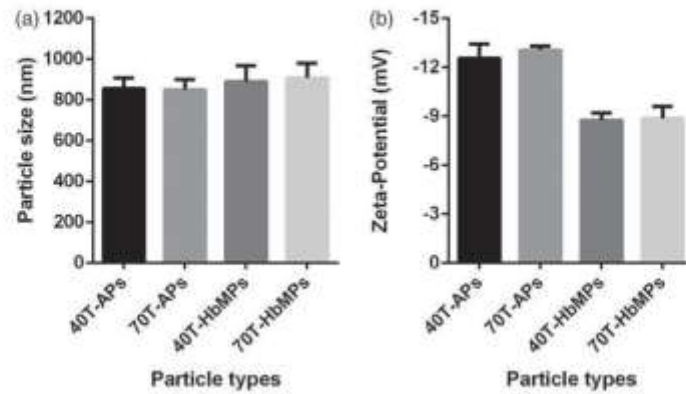
Figure 2. Characteristics of Odex-crosslinked protein particles. (a) Size and (b) Zeta-potential measured in 10 mM PBS (conductivity 18–20 mS/cm) at room temperature by Dynamic Light Scattering analysis. Data are presented as mean ± SD ($n = 5$).
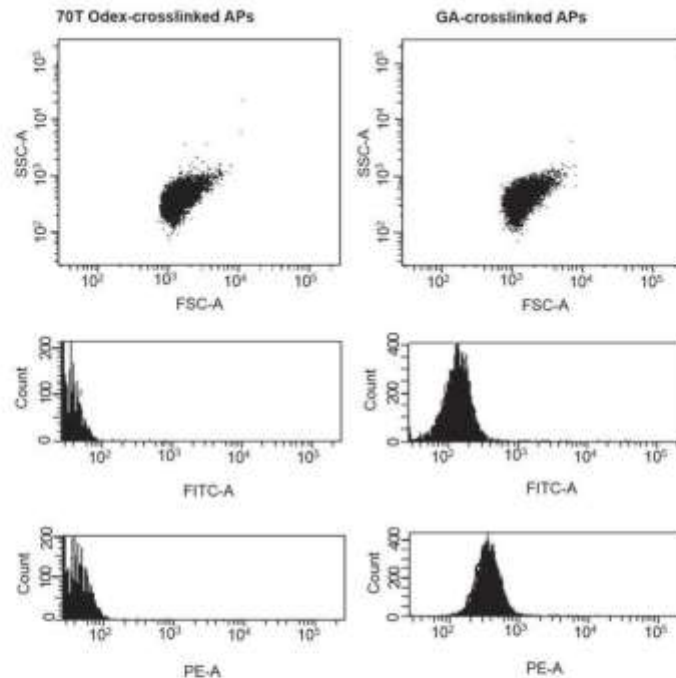

Figure 3. The side vs forward scatter dot plot of 70T-APs and GA-crosslinked APs (GA-APs). The stronger fluorescence intensity of GA-APs was observed compared to Odex-crosslinked particles. (APs and HbMPs crosslinked with both 40T and 70T Odex have the same phenomenon, figures were not shown).

respectively. No significant differences in size and zeta-potential could be detected for the particles prepared with 40T- and 70T-Odex.

The results of flow cytometry analysis in Figure 3 also demonstrated that Odex-particles had no auto-fluorescence in contrast to the protein particles prepared using the CCD technique and crosslinked by glutaraldehyde [8–10,29,30].

Haemolysis test

Haemolysis refers to the release of haemoglobin from RBCs due to damage of RBCs membrane, which is extensively applied to evaluate the biosafety of particles. A haemolytic ratio higher than 5% is considered as a significant damage of RBCs. The haemolytic ratio of the RBCs incubated with different Odex-crosslinked particles for 3 h at 37 °C is

demonstrated in Table 1. It can be seen clearly that the haemolysis ratio for the samples with Odex-APs and Odex-HbMPs was between 1% and 2% and so far, they obviously did not deteriorate significantly the RBCs.

Phagocytosis test

The commercial phagotest kit allows determinations of the percentage of phagocytes (in whole blood samples) which ingest FITC-labelled opsonized *E. coli* bacteria and is used as a diagnostic tool for functional testing of leukocytes. The test can be directly used to determine the phagocytosis of fluorescent particles by the phagocytes in the blood (mainly granulocytes and monocytes). However, in the case of the non-fluorescent particles, an additional fluorescent staining is needed which may alter their surface properties and influence the phagocytosis. Therefore, we employed an indirect method as described in the part Materials and Methods. Non-fluorescent E. coli, Odex-APs and Odex-HbMPs were

Table 1. Haemolytic ratio of odex-crosslinked particles.

Test sample	Haemolysis ratio (%)
40T-APs	1.14 ± 0.36
70T-APs	1.03 ± 0.16
40T-HbMPs	1.67 ± 0.58
70T-HbMPs	1.77 ± 0.52
PBS	0 ± 0.00
Water	100 ± 0.00

Data are presented as mean ± SD ($n = 3$).

added to the whole blood sample and incubated at 37 °C for 10–120 min in order to reach a saturated phagocytosis by the granulocytes and monocytes. Then, the standard test with FITC– labelled *E. coli* at 37 °C was performed with all samples. Results of the flow cytometry analysis of samples pre-incubated with non-stained *E. coli*, PBS, Odex-APs and Odex-HbMPs for 120 min is presented in Figure 4 as dot plots of granulocyte and monocyte populations detectable in the FITC channel. It can be seen that the distribution of the FITC-labelled cells is similar for the samples pre-incubated with PBS, 40T-APs and 40T-HbMPs. Only the positive control (pre-incubated with non-fluorescent E.coli) shows different behavior with an increased number of non-fluorescent cells.

The summarized results in dependency on the pre-incubation time are shown in Figure 5. The number of granulocytes and monocytes phagocytosing FITC-*E. coli* was not significantly different for Odex-crosslinked particles and PBS (negative control) over all pre-incubation times. In contrast, the positive control, *E. coli*, demonstrated a decrease in the percentage of the cells engulfing FITC-*E. coli* in a time-dependent manner, due to the phagocytosis of non-fluorescing *E. coli*.

Platelet activation test

To evaluate whether our Odex-APs and Odex-HbMPs alter the haemostasis system, their influence on the activation of
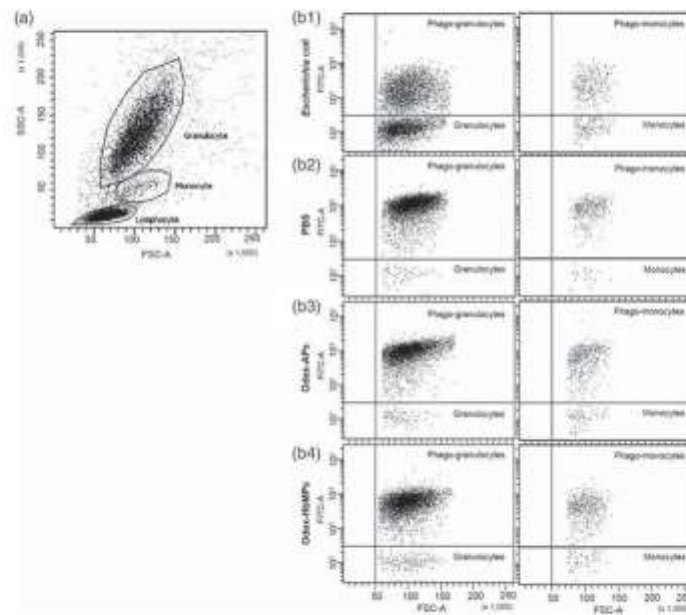

Figure 4. Flow cytometric dot plot of human peripheral blood leukocytes. (a) Sub-populations of leukocytes can be distinguished based on forward scatter (relative size) and side scatter (relative complexity). Granulocyte are large and complex; monocytes are slightly larger than lymphocytes and less complex than granulocyte, while lymphocytes are smaller and less complex. (b) Dot plots FITC/FSC demonstrate the phagocytic activity of granulocytes (left panel) and monocytes (right panel) detected with FITC-labelled *E. coli*. Preincubation with different particles was performed for 120 min. (b1) Preincubation of leukocytes with non-stained *E. coli* (positive control), (b2) Preincubation of leukocytes with PBS (negative control), (b3) Preincubation of leukocytes with Odex-APs, (b4) Preincubation of leukocytes with Odex-HbMPs.
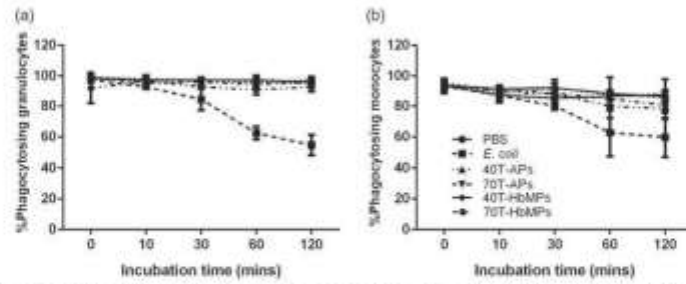
Figure 5. Percentage of phagocytic activity of (a) granulocyte and (b) monocyte on Odex-APs and Odex-HbMPs compared with PBS (negative control) and *E. coli* (positive control). On one hand, the fluorescence signal of detective FITC-*E. coli* decreased grammatically across incubation periods in positive control. On the other hand, leukocyte preincubated with PBS as well as Odex-APs and Odex-HbMPs showed a strong detective FITC-*E. coli* and there was no change over the incubation times. Data are presented as mean ± SD ($n = 3$).
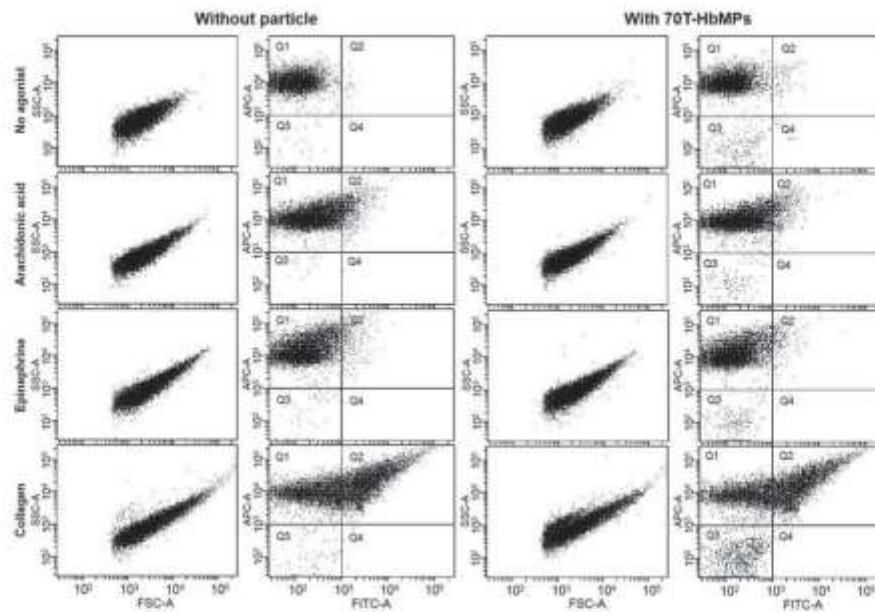

Figure 6. Flow cytometric analysis of the activation of platelets. Example of 70T-HbMPs compared to negative control. The events of the forward and side scatter as well as APC and FITC fluorescence channel are shown as dot plot. Platelets stained with APC-Antihuman CD42b (GPIbα) are enclosed in quadrant Q1. Double-stained with APC Anti-CD42ba and AlexaFlour 488 Antihuman-CD62P (P-selectin) events in quadrant Q2 represent activated-platelets. Non-stained particles were presented in Q3.

platelets was investigated. Figure 6 shows results of the flow cytometry analysis of platelets using the platelet-specific membrane receptor CD42b (GPIbα), and then distinguished those platelets that were activated using the activation marker CD62P. The results showed that the platelet activation assay was able to distinguish between platelets that are resting with high fluorescence level for CD42b and lower fluorescence levels for activation markers, CD62P, and those that have been activated by agonists with higher fluorescence levels for the two activation markers, CD42b and CD62P. Simultaneously, upon the stimulation of platelets by agonists, the aggregation of platelets was also observed as the shift of

forward scatter/side scatter positioning compared with the control.

Figure 7 summarizes the results of the flow cytometry analysis. Obviously, the Odex-APs or Odex-HbMPs did not cause activation of the platelets as compared to the control sample which was incubated with PBS. Additionally, platelet activation induced by agonists including arachidonic acid, collagen and epinephrine of pre-incubated PRP with particles was comparable to the control samples.

It can be concluded that Odex-APs or Odex-HbMPs do not influence the function of platelets and therefore no negative side effects on the haemostasis are expected.
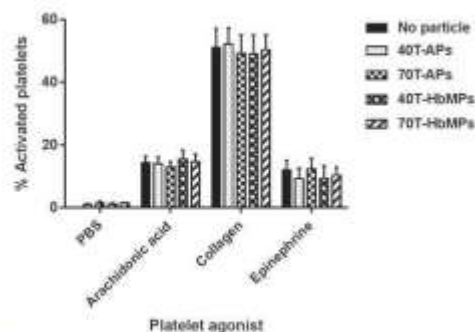
Figure 7. Platelet activation (as determined by %CD62P expression) is not influenced by Odex-APs and Odex-HbMPs. Fresh citrated PRP was treated with the different particles or PBS as a control. The presence of particles did not influence on arachidonic acid-, collagen- and epinephrine-induced platelet activation. Non-stimulated labelled platelets are shown as a baseline for spontaneous activation. Data are presented as mean ± SD (n = 3).

Discussion

Prior to all intravenous administration applications, the influence of particles on the blood cells needs to be evaluated. The haemocompatibility of particles is affected by their physical attributes, including size, shape, and flexibility, as well as their chemical composition, for instance, the incorporation of toxic compounds or active ligands for recognition and triggering of biological receptors. It has been well described that small particle size and positive charge caused thrombocyte and granulocyte activation, and haemolysis. Negatively charged particles larger than 60 nm hydrodynamic diameter appear to be considerably less haemotoxic than smaller ones [21]. Our new particles fit to these criteria. Additionally, a successful perfusion of isolated mouse glomeruli with concentrated HbMP suspensions of the same size in vitro without vasoconstriction of the afferent arterioles could be shown [10]. As the size of a particle decreases, its surface area per unit volume (or mass) increases and also allows a greater proportion of its atoms or molecules to be displayed on the surface rather than the interior of the material [31,32]. Therefore, it is very important to utilize procedures that allow preparation of particles with high degrees of uniformity, and with control over their physical and chemical characterisations.

Odex-APs and Odex-HbMPs fabricated by One-pot formulation have a size in the submicron range, uniform morphology and negative surface charge. The coating of the particles with human serum albumin improves significantly their blood compatibility by reducing the adsorption of other proteins as well the interaction with platelets and leukocytes [33]. Due to the covalent binding of albumin to haemoglobin the stability of the coating is sufficient to protect the particles during their circulation in the blood stream against non-specific adsorption of other plasma proteins.

Currently described in vitro assays for haemocompatibility testing of particulate materials are not standardized. We evaluated the haemocompatibility of the Odex-crosslinked particles by testing haemolysis (destruction of RBCs), phagocytosis by leucocytes and platelet activation in order to explore possible adverse effects of Odex-crosslinked protein particles to blood cells

RBCs are the most abundant compartment in the bloodstream and are an important component determining the haemocompatibility. Once they are lysed, they release not only haemoglobin but also procoagulant factors which can cause serious adverse effects [34]. According to the ISO 10993–4:2017, the haemolysis assays of Odex-AP and Odex-HbMP were considered to be non-haemolytic because these particles induced less than 5% haemolysis. Particle-induced haemolysis can be caused by the release of toxic substances from a biomaterial surface or from the interaction between particles and RBCs which result in the disruption and integrity of the RBC membrane and release of haemoglobin into the plasma. Additionally, it is generally agreed that surface properties (especially surface charge) are important, and there are several studies which have demonstrated this. For example, among a set of similar-sized fullerenes (C60-derivatives) bearing different numbers of anionic and cationic surface moieties, those with negative surface charge were not haemolytic, and haemolytic tendency increased in proportion to the number of attached cationic surface groups (positive surface charge) [18].

The charge of particles stemming from distinct surface chemistries influences opsonisation, circulation times and interaction with resident macrophages of organs comprising the phagocytic system. On the one hand, positively charged particles more prone to sequestration by macrophages in the lungs, liver and spleen. On the other hand, neutral and slightly negatively charged nanoparticles have longer circulation lifetimes and less accumulation in the aforementioned organs [35]. Our indirect phagotest assay showed that Odex-APs and Odex-HbMPs particles were not recognized by phagocytic cells including granulocytes and monocytes. As the adsorption of plasma proteins on the nanoparticle surface can have an important influence on the interactions between cells and the particles. Therefore, diminishing the susceptibility of particles to recognition by the phagocytes through coverage of their surface with hydrophilic polymers such as polyethylene glycol, dextrans or mimic the surface using human serum albumin is another strategy to prolong the residence time of particles in the circular system [22].

Activation of platelet plays a crucial role in the coagulation cascade. They are very sensitive to the presence of foreign materials that can enhance or attenuate the activity of platelets and further affect the blood coagulation.

It should also be considered that on the one dextran used as plasma expander influences the function of platelets due to its adsorption on platelets surface [36]. On the other hand, dextran forms not only a depletion layer around the blood cells and reduces the adsorption of proteins but can also be adsorbed to the cell surface. The dextran in the Odex-HbMP is covalently bound to haemoglobin and not free available for adsorption. But the moieties of dextran partially presented on the particle surface contribute to a repulsive force against other macromolecules [37].

Therefore, the interaction between platelets and particle is an important evaluation of biomaterials for blood

248 C. KLOYPAN ET AL.

compatibility. In this study, the presence of Odex-APs and Odex-HbMPs influenced neither the platelet activation/aggregation nor the agonist induced-platelet activation. The mechanisms through which particles induce platelet aggregation are largely unknown. Nevertheless, trends observed in studies of polymer-based nanoparticles are similar in their charge-dependence to those described above for haemolysis [18]. We assume that the negative surface charge as well as the albumin coating of Odex-APs and Odex-HbMPs prevent interaction between the particles and the platelets and therefore we do not expect negative effects on haemostasis.

Conclusions

In the current study, we demonstrated the *in vitro* evaluation of the compatibility of Odex-APs and Odex-HbMPs fabricated by "One-pot formulation" with human blood. The results of the haemolysis test, the direct phagocytosis test and of the platelet activation tests reflected good haemocompatibility. No biologically relevant alterations during blood contact were observed and therefore Odex-APs and Odex-HbMPs fabricated by "One-pot formulation" fulfill the requirements according to ISO 10993–4 for blood contacting materials. Therefore, their application potential is worthwhile to be further developed and explored.

Disclosure statement

No potential conflict of interest was reported by the authors.

Acknowledgements

References

[1] Jao D, Xue Y, Medina J, et al. Protein-based drug-delivery materials. Materials (Basel) 2017;10:1–24.

[2] Nitta SK, Numata K. Biopolymer-based nanoparticles for drug/gene delivery and tissue engineering. Int J Mol Sci. 2013;14:1629–1654.

[3] Elzoghby AO, Samy WM, Elgindy NA. Protein-based nanocarriers as promising drug and gene delivery systems. J Control Release. 2012;161:38–49.

[4] Elzoghby AO, Samy WM, Elgindy NA. Albumin-based nanoparticles as potential controlled release drug delivery systems. J Control Release. 2012;157:168–182.

[5] Lohcharoenkal W, Wang L, Chen YC, et al. Protein nanoparticles as drug delivery carriers for cancer therapy. Biomed Res Int. 2014:1.

[6] Hawkins MJ, Soon-Shiong P, Desai N. Protein nanoparticles as drug carriers in clinical medicine [Internet]. Adv Drug Deliv Rev. 2008;60:876–885.

[7] Kudarha RR, Sawant KK. Albumin based versatile multifunctional nanocarriers for cancer therapy: fabrication, surface modification, multimodal therapeutics and imaging approaches. Mater Sci Eng C. 2017;81:607–626.

[8] Xiong Y, Steffen A, Andreas K, et al. Hemoglobin-based oxygen carrier microparticles: synthesis, properties, and in vitro and in vivo investigations. Biomacromolecules. 2012;13:3292–3300.

[9] Bäumler H, Xiong Y, Liu ZZ, et al. Novel hemoglobin particles-promising new-generation hemoglobin-based oxygen carriers. Artif Organs. 2014;38:708–714.

[10] Xiong Y, Liu ZZ, Georgieva R, et al. Nonvasoconstrictive hemoglobin particles as oxygen carriers. ACS Nano. 2013;7:7454–7461.

[11] Jia Y, Duan L, Li J. Hemoglobin-based nanoarchitectonic assemblies as oxygen carriers. Adv Mater. 2016;28:1312–1318.

[12] Tao Z, Peter Ghoroghchian P. Microparticle, nanoparticle, and stem cell-based oxygen carriers as advanced blood substitutes. Trends Biotechnol. 2014;32:466–473.

[13] De Frates K, Markiewicz T, Gallo P, et al. Protein polymer-based nanoparticles: fabrication and medical applications. Int J Mol Sci. 2018;19:1–20.

[14] Duan L, Yan X, Wang A, et al. Highly loaded hemoglobin spheres as promising artificial oxygen carriers. ACS Nano. 2012;6:6897–6904.

[15] Tsuchida E, Sou K, Nakagawa A, et al. Artificial oxygen carriers, hemoglobin vesicles and albumin-hemes, based on bioconjugate chemistry. Bioconjugate Chem. 2009;20:1419–1440.

[16] Piras AM, Dessy A, Chiellini F, et al. Polymeric nanoparticles for hemoglobin-based oxygen carriers. Biochim Biophys Acta - Proteins Proteomics. 2008;1784:1454–1461.

[17] Naeye B, Deschout H, Röding M, et al. Hemocompatibility of siRNA loaded dextran nanogels. Biomaterials. 2011;32:9120–9127.

[18] Dobrovolskaia MA, Aggarwal P, Hall JB, et al. Preclinical studies to understand nanoparticle interaction with the immune system and its potential effects on nanoparticle biodistribution. Mol Pharm. 2008;5:487–495.

[19] Owens DE, Peppas NA. Opsonization, biodistribution, and pharmacokinetics of polymeric nanoparticles [Internet]. Int J Pharm. 2006;307:93–102.

[20] Albanese A, Tang PS, Chan WCW. The effect of nanoparticle size, shape, and surface chemistry on biological systems. Annu Rev Biomed Eng. 2012;14:1–16.

[21] Mayer A, Vadon M, Rinner B, et al. The role of nanoparticle size in hemocompatibility. Toxicology. 2009;258:139–147.

[22] Lundqvist M, Stigler J, Elia G, et al. Nanoparticle size and surface properties determine the protein corona with possible implications for biological impacts. Appl Phys Sci. 2008;105:14265–14270.

[23] Kloypan C, Prapan A, Suwannasom N, et al. Improved oxygen storage capacity of haemoglobin submicron particles by one-pot formulation. Artif Cells, Blood Substit Biotechnol. 2018; doi: 10.1080/21691401.2018.1521819

[24] Berillo D, Elowsson L, Kirsebom H. Oxidized dextran as crosslinker for chitosan cryogel scaffolds and formation of polyelectrolyte complexes between chitosan and gelatin. Macromol Biosci. 2012;12:1090–1099.

[25] Lisman A, Butruk B, Wasiak I, et al. Dextran/albumin hydrogel sealant for Dacron(R) vascular prosthesis. J Biomater Appl. 2014;28:1386–1396.

[26] Lu M, Zhao C, Wang Q, et al. Preparation, characterization and in vivo investigation of blood-compatible hemoglobin-loaded nanoparticles as oxygen carriers. Colloids Surf B Biointerfaces. 2016 ;1:171–179.

[27] Braune S, Walter M, Schulze F, et al. Changes in platelet morphology and function during 24 hours of storage. Clin Hemorheol Microcirc. 2014;58:159–170.

[28] Cuyper IMD, Meinders M, Vijver EVD, et al. A novel fl ow cytometry – based platelet aggregation assay. Blood. 2013;121:70–80.

[29] Bäumler H, Georgieva R. Coupled enzyme reactions in multicompartment microparticles. Biomacromolecules. 2010;11:1480–1487.

[30] Xiong Y, Georgieva R, Steffen A, et al. Structure and properties of hybrid biopolymer particles fabricated by co-precipitation cross-linking dissolution procedure. J Colloid Interface Sci. 2018;15:156–164.

[31] Nel A, Xia T, Mädler L, et al. Toxic potential of materials at the nanolevel [Internet]. Science. 2006;311:622–627.

[32] Blanco E, Shen H, Ferrari M. Principles of nanoparticle design for overcoming biological barriers to drug delivery. Nat Biotechnol. 2015;33:941–951.

[33] Tanzi MC. Bioactive technologies for hemocompatibility. Expert Rev Med Devices. 2005;2:473–492.

[34] Helms CC, Marvel M, Zhao W, et al. Mechanisms of hemolysis-associated platelet activation. J Thromb Haemost. 2013;11:2148–2154.

[35] Elci SG, Jiang Y, Yan B, et al. Surface charge controls the suborgan biodistributions of gold nanoparticles. ACS Nano. 2016;10: 5536–5542.

[36] Bäumler H, Donath E, Krabi A, et al. Electrophoresis of human red blood cells and platelets. Evidence for depletion of dextran. Biorheology. 1996; 33:333–351.

[37] Bäumler H, Neu B, Donath E, et al. Basic phenomena of red blood cell rouleaux formation. Biorheology. 1999; 36:439–442.

Publication 3 / Publikation 3

Xiong Y, Georgieva R, Steffen A, **Smuda K**, Bäumler H.

Structure and properties of hybrid biopolymer particles fabricated by co-precipitation cross-linking dissolution procedure.

https://doi.org/10.1016/j.jcis.2017.12.030

Curriculum Vitae

My curriculum vitae does not appear in the electronic version of my paper for reasons of data protection.

List of publications / Publikationsliste

Smuda K, Gienger J, Hönicke P, Neukammer.

Function of Hemoglobin-Based Oxygen Carriers: Determination of Methemoglobin Content by Spectral Extinction Measurements.

J. Int J Mol Sci. 2021 Feb 10;22(4):1753. doi: 10.3390/ijms22041753. PMID: 33578723, **IF-5.923 (2020)**

Kloypan C, Suwannasom N, Chaiwaree S, Prapan A, **Smuda K**, Baisaeng N, Pruß A, Georgieva R, Bäumler H.

In-vitro haemocompatibility of dextran-protein submicron particles.

Artif Cells Nanomed Biotechnol. 2019 Dec;47(1):241-249. doi:10.1080/21691401.2018.1548476. PMID: 30663396, **IF-3.343**

Gienger J, **Smuda K**, Müller R, Bär M, Neukammer J.

Refractive index of human red blood cells between 290 nm and 1100 nm determined by optical extinction measurements.

Sci Rep. 2019; 9: 4623. Published online 2019 Mar 15. doi: 10.1038/s41598-019-38767-5. PMCID: PMC6420646, **IF-3.998**

Suwannasom N, **Smuda K**, Kloypan C, Kaewprayoon W, Baisaeng N, Boonla C, Georgieva R, Bäumler H.

Detection of CD33 expression on monocyte surface is influenced by phagocytosis and temperature.

Gen Physiol Biophys. 2019 Sep;38(5):369-378. doi: 10.4149/gpb_2019021. Epub 2019 Aug 14. PMID: 31411573, **IF-1.070**

Suwannasom N, **Smuda K**, Kloypan C, Kaewprayoon W, Baisaeng N, Prapan A, Chaiwaree S, Georgieva R, Bäumler H.

Albumin Submicron Particles with Entrapped Riboflavin—Fabrication and Characterization

Nanomaterials (Basel) 2019 Mar; 9(3): 482. Published online 2019 Mar 25. doi: 10.3390/nano9030482. PMCID: PMC6474188, **IF-4.324**

Zhang Y, Du W, **Smuda K**, Georgieva R, Bäumler H, Gao C.

Inflammatory activation of human serum albumin- or ovalbumin-modified chitosan particles to macrophages and their immune response in human whole blood.

J Mater Chem B. 2018 May 21;6(19):3096-3106. doi: 10.1039/c7tb03096g. Epub 2018 Apr 27. PMID: 32254344, **IF-5.047**

Kao I, Xiong Y, Steffen A, **Smuda K**, Zhao L, Georgieva R, Pruss A, Bäumler H.

Preclinical In Vitro Safety Investigations of Submicron Sized Hemoglobin Based Oxygen Carrier HbMP-700.

Artif Organs. 2018 Mar 6. doi: 10.1111/aor.13071, **IF-2.379**

Xiong Y, Georgieva R, Steffen A, **Smuda K**, Bäumler H.

Structure and properties of hybrid biopolymer particles fabricated by co-precipitation cross-linking dissolution procedure.

J Colloid Interface Sci. 2018 Mar 15;514:156-164. doi: 10.1016/j.jcis.2017.12.030. Epub 2017 Dec 12, **IF-6.361**

Ivanov IT, Paarvanova BK, Ivanov V, **Smuda K**, Bäumler H, Georgieva R.

Effects of heat and freeze on isolated erythrocyte submembrane skeletons.

Gen Physiol Biophys. 2017 Apr;36(2):155-165. doi: 10.4149/gpb_2016046. Epub 2017 Feb 2. , **IF-1.479**

Severyukhina AN, Petrova NV, Yashchenok AM, Bratashov DN, **Smuda K**, Mamonova IA, Yurasov NA, Puchinyan DM, Georgieva R, Bäumler H, Lapanje A, Gorin DA.

Light-induced antibacterial activity of electrospun chitosan-based material containing photosensitizer.

Mater Sci Eng C Mater Biol Appl. 2017 Jan 1;70(Pt 1):311-316. doi: 10.1016/j.msec.2016.09.005, **IF-5.080**

Severyukhina AN, Petrova NV, **Smuda K**, Terentyuk GS, Klebtsov BN, Georgieva R, Bäumler H, Gorin DA.

Photosensitizer-loaded electrospun chitosan-based scaffolds for photodynamic therapy and tissue engineering.

Colloids Surf B Biointerfaces. 2016 Aug 1;144:57-64. doi: 10.1016/j.colsurfb.2016.03.081. Epub 2016 Mar 29, **IF-3.887**

Koziol MJ, Sievers TK, **Smuda K**, Yu Xiong, Muller A, Wojcik F, Steffen A, Dathe M, Georgieva R, Baeumler H.

Kinetics and Efficiency of a Methyl-Carboxylated 5-Fluorouracil - Bovine Serum Albumin Adduct for Targeted Delivery.

Macromol Bioscience. 11/2013; DOI:10.1002 /mabi.201300363, **IF-3.650**

Xiong Y, Liu ZZ, Georgieva R, **Smuda K**, Steffen A, Sendeski M, Voigt A, Patzak A, Bäumler H.

Nonvasoconstrictive hemoglobin particles as oxygen carriers.

ACS Nano. 2013 Sep 24;7(9):7454-61. doi: 10.1021/nn402073n. Epub 2013 Aug 7, **IF-12.033**

Acknowledgements / Danksagung